SPRINGER BRIEFS IN MOLECULAR SCIENCE
ELECTRICAL AND MAGNETIC PROPERTIES OF ATOMS, MOLECULES, AND CLUSTERS

Yuriko Aoki
Yuuichi Orimoto
Akira Imamura

Quantum Chemical Approach for Organic Ferromagnetic Material Design

Springer

SpringerBriefs in Molecular Science

Electrical and Magnetic Properties of Atoms, Molecules, and Clusters

Series editor

George Maroulis, Patras, Greece

More information about this series at http://www.springer.com/series/11647

Yuriko Aoki · Yuuichi Orimoto
Akira Imamura

Quantum Chemical Approach for Organic Ferromagnetic Material Design

Springer

Yuriko Aoki
Department of Material Sciences,
Faculty of Engineering Sciences
Kyushu University
Kasuga, Fukuoka
Japan

Akira Imamura
Department of Chemistry,
Faculty of Sciences
Hiroshima University
Higashihiroshima, Hiroshima
Japan

Yuuichi Orimoto
Department of Material Sciences,
Faculty of Engineering Sciences
Kyushu University
Kasuga, Fukuoka
Japan

ISSN 2191-5407 ISSN 2191-5415 (electronic)
SpringerBriefs in Molecular Science
ISSN 2191-5407 ISSN 2191-5415 (electronic)
SpringerBriefs in Electrical and Magnetic Properties of Atoms, Molecules, and Clusters
ISBN 978-3-319-49827-0 ISBN 978-3-319-49829-4 (eBook)
DOI 10.1007/978-3-319-49829-4

Library of Congress Control Number: 2016957504

Printed on acid-free paper

This Springer imprint is published by Springer Nature
The registered company is Springer International Publishing AG
The registered company address is: Gewerbestrasse 11, 6330 Cham, Switzerland

Knowing without seeing is at the heart of chemistry.

—Roald Hoffmann
(The Nobel Prize in Chemistry 1981)

自分のやりたい学問と距離のある学問であればあるほど、
後になって創造的な仕事をする上で重要な意味をもってくる。

－『学問の創造』より

—Kenichi Fukui
(The Nobel Prize in Chemistry 1981)

Two quotes from Prof. Hoffmann and Prof. Fukui, who were awarded the Nobel prize in chemistry in 1981, are written above. Both the great scientists were supervisors of AI (last author), who was the supervisor of YA (first author) and YO (second author). Professor Fukui's Japanese quote, from his Japanese book, roughly means that "the more you conduct a study in areas distant from your own academic field, the more creative your later work will be". Additionally, when

AI was Prof. Fukui's student, he distinctly remembers the unforgettable words from him —"there is no need to read a lot of papers, but it is essential to read a few important papers in detail between the lines and extract some important concepts from there". The treatments introduced in this monograph are not intended for general use as a text book but are definitely original and more or less affected by the thinking of these two great scientists. Although highly efficient advanced supercomputers are now available, we still believe that the concepts pursued in the early quantum chemistry period (1930s) must be of permanent importance in the cultivation of new fields or the further development of an existing field.

August 2016

Yuriko Aoki
Yuuichi Orimoto
Akira Imamura

Preface

This monograph aims to summarize an overview of theoretical research in organic material design by means of quantum chemical approaches based on the molecular orbital theory from primary Hückel to ab initio levels of theory. Most of the contents are based on our own approach to identify simple and efficient guidelines for magnetic design, which have not been described in other books.

There has been long-term interest in magnetic. The magnetic properties of some metals have been known and utilized since ancient times, while organic- and molecule-based magnets have been investigated as replacements for metallic magnets in charge transfer complexes, organic radical magnets, ferri-magnets, and so on, since the early 1980s. From an economic point of view, newly synthesized organic polymer magnets must display advantages over traditional inorganic metal or metal oxide magnets in functional flexibility, substantial weight savings, and facile processibility over their life cycle.

This monograph comprises five chapters. In Chap. 1, we survey the historical aspects of various current and potential applications of magnetic properties. In Chaps. 2 and 3, we describe a quantum chemistry approach, together with its mathematical background, that may be used to find hydrocarbon systems with degenerate non-bonding molecular orbitals (NBMOs) that interact with each other (Chap. 2) and identify high-spin-preferred systems using an analytical index that allows the simple design of high-spin systems while considering correlation effects (Chap. 3). In Chap. 4, we show our own method, used to analyze the effect of high-spin stability (the dominant contribution to this stability comes from exchange terms) through orbital interactions. For this purpose, we develop our own treatment called the through-space (TS)/through-bond (TB) interaction analysis method, to understand how high-spin stability may be realized by considering the interaction between NBMO radicals through bonds (within a molecule) or through space (within a molecule or between molecules). Finally, in Chap. 5, we show how to extend the methods discussed in Chaps. 2–4 to large systems. The elongation (ELG) method, which we have been developing since early the 1990s, is a very efficient finite cluster approach that is available for both the Hartree-Fock (HF) and post-HF levels of theory. This method follows to the procedures for building up a

large system at a time by adding small units to an appropriate size of cluster and growing the cluster with order-N ($O(N)$) computational time. In Chap. 5, we present some applications that are utilized for modeling solvation effect using the polarizable continuum model (PCM) method and, particularly, the minimized mixing molecular orbital (MMMO) localization process for non-bonding molecular orbitals. The MMMO localization, a unique and simple method, can be applied very efficiently to open-shell part of organic polyradicals with great reliability and stable convergence in the self-consistent field (SCF) calculations during the ELG process under the PCM, called the MMELG-PCM method. Some applications that show the efficiency with $O(N)$ and accuracy of the ELG approach are presented by implementing it to various open-shell polymers and dendrimers. Although the ELG method has been continuously developed in our laboratory since the first publish in 1991 by AI et al., there is still room for further development and improvement to utilize it for magnetism. Future prospects are given in Chap. 6 together with a concluding summary. The content of this monograph is a very basic and fundamental, and so we hope it would be a help for the study of young researchers who are going to learn quantum chemistry related to magnetic property.

There are thousands of papers published on organic magnetism, both experimental and theoretical, but we have cited only part of them in the references as the result of space limitations. In addition, this monograph is a type of magnetic version of a previously published SpringerBriefs on NLO properties for large systems entitled "Calculations on Nonlinear Optical Properties for Large Systems: The Elongation Method," where YA is a common author; in this manuscript, the fundamental concepts of the ELG method are described with some applications. The interested reader is therefore referred to the above-mentioned SpringerBriefs to discover further details about other applications of the ELG method in NLO functionals.

August 15, 2016
(82nd Birthday of AI)

Kasuga, Japan

Yuriko Aoki

Kasuga, Japan

Yuuichi Orimoto

Hiroshima, Japan

Akira Imamura

Acknowledgments

We would express our great acknowledgments to Japan Science and Technology Agency (JST)—Strategic Basic Research Programs both of PRESTO and CREST. Besides JST, this work was partly supported by a grant-in-aid from the Ministry of Education, Culture, Sports, Science and Technology (MEXT) of Japan (No. 04205104, 04453016, 07554087, 08454183, 08740548, 09740525, 14340185, 16655009, 19350012, 21655007, 23245005) and the Japan Society for the Promotion of Science (JSPS). The authors are also grateful to the researchers involved in the development of the elongation method described in Chap. 5: Feng Long Gu, Jacek Korchowiec, Marcin Makowski, Yanliang Ren, Kai Liu, Xun Zhu, Peng Xie, Shohei Onitsuka, Shinichi Abe, Ryota Tsutsui, Daisuke Konishi, and other students, for their elaborating research on this project. We also very much appreciate Bernard Kirtman, Michael Springborg, and Benoît Champagne for their stimulating discussion on the development of the elongation method and its application to the determination of functional properties, especially nonlinear optical (NLO) properties. YA also thanks George Maroulis very much for his continuous encouragement of our research on the topics described in this monograph. The release of the elongation method in the GAMESS program package was facilitated by the great support of Michael Schmidt at Iowa State University. We thank Ikuko Okawa for preparing some figures, supporting data and reference reduction. The calculations were mainly performed on the Linux clusters of the laboratories provided by JST-PRESTO, JST-CREST, and MEXT in Aoki's group at Kyushu University, as well as the high-performance computing system in Research Institute for Information Technology at Kyushu University.

Contents

Acronyms

2e	Two-Electron
2L, 3L, …	Two-line, Three-line, …
AO	Atomic Orbital
AP	Analytically Prediction
AR	Allyl Radical
BR	Benzyl Radical
CI	Configuration Interaction
CONV	Conventional Method
DC	Divide and Conquer
DFT	Density Functional Theory
DMRG	Density Matrix Renormalization Group
ELG	Elongation Method
ER	Edmiston-Rüdenberg
FC	Frozen Core
FF	Finite Field
FMO	Fragment Molecular Orbital
FULL	Full Interaction
HB model	Heisenberg Model
HC	Hydrocarbon
HF	Hartree-Fock
HHC	Heteroatom-included Hydrocarbon
HMO	Hückel Molecular Orbital
HOMO	Highest Occupied Molecular Orbital
HS (or H)	Highest-Spin/High-Spin
LCAO	Linear Combination of Atomic Orbitals
LCI	Local Configuration Interaction
LMP2	Local Møller–Plesset Second-order Perturbation Theory
LS (or L)	Lowest-Spin/Low-Spin
LUMO	Lowest Unoccupied Molecular Orbital

MMELG	Minimized Mixing Elongation Method
MMMO	Minimized Mixing Molecular Orbital
MO	Molecular Orbital
MP	Møller–Plesset
MR	Methylene/Methylidyne Radical
NBMO	Non-bonding Molecular Orbital
NBO	Natural Bond Orbital
NLO	Nonlinear Optical
NN	Nitronyl Nitroxide
O(*N*)	Order-*N*
OR1, OR2, …, OR*n*	Open-Ring 1, Open-Ring 2, … Open-Ring *n*
ORB	Organic Radical Battery
PCM	Polarizable Continuum Model
PMO	Perturbational Molecular Orbital
post-HF	post-Hartree-Fock
PTMA	Poly(2,2,6,6-tetramethylpiperidinyloxy methacrylate)
QC	Quantum Chemistry
RLMO	Regional Localized Molecular Orbital
RO (ROHF, ROMP, etc.)	Restricted Open-shell
ROB3LYP	Restricted Open-shell Becke's Three-parameter, Lee–Yang–Parr exchange-correlation functional
S, D, T, Q, …	Singlet, Doublet, Triplet, Quartet, …
SCF	Self-consistent Field
SOMO	Singly Occupied Molecular Orbital
SR, DR, TR	Single Ring, Double Rings, Triple Rings
SRE	Self-repulsion Energy
TB	Through-Bond
TEMPO	2,2,6,6-tetramethyl piperidinyloxyl
TS	Through-Space
UB3LYP	Unrestricted B3LYP
UHF	Unrestricted Hartree-Fock
VB	Valence-Bond

Chapter 1
Survey of Organic Magnetism

Abstract In this chapter, we initially give an overview of magnetism and briefly discuss the advantages of "organic ferromagnetism." Next, we review the many rules and indices used for predicting ferromagnetism that are proposed in the frameworks of molecular orbital methods and valence-bond theory. We introduce two types of strategies for designing ferromagnetic systems: "*inter*-molecular spin alignment (molecular magnets)" and "*intra*-molecular spin alignment (high-spin polymers)." Finally, we mention the theoretical approaches used to understand and predict magnetism in larger systems, namely, statistical treatment using the Ising model and quantum chemistry calculations for large systems.

1.1 Overview

Magnetism exists in three general types: ferromagnetism, paramagnetism, and diamagnetism. In this section, these types of magnetism are briefly introduced. The effect of temperature on magnetism is also mentioned.

1.1.1 Ferromagnetism

Figure 1.1 illustrates *ferromagnetism* (a) and its relatives anti-ferromagnetism (b) and ferrimagnetism (c, d). In systems exhibiting these types of magnetism, the electron spins interact with each other. As a result, electron spin alignment occurs, even in weak external magnetic fields. With the exception of anti-ferromagnetic compounds, these species exhibit spontaneous magnetization. In other words, magnetic materials of these types have intrinsic magnetic moments. These types of magnetism can be described as follows:

- **Ferromagnetism** (Fig. 1.1a): the electrons' spins align parallel because an exchange interaction causes neighboring electrons' spins to be in the same direction. Ferromagnetism is further divided into two types: hard and soft

Y. Aoki et al., *Quantum Chemical Approach for Organic Ferromagnetic Material Design*,
SpringerBriefs in Electrical and Magnetic Properties of Atoms, Molecules, and Clusters,
DOI 10.1007/978-3-319-49829-4_1

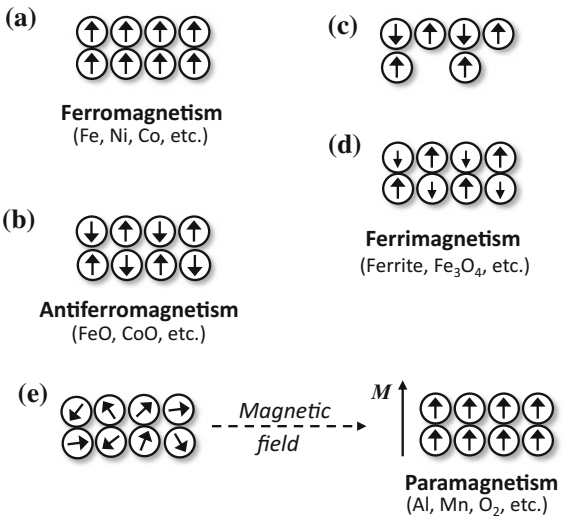

Fig. 1.1 Types of magnetism: **a** ferromagnetism, **b** antiferromagnetism, **c**, **d** ferrimagnetism, and **e** paramagnetism

ferromagnetism, which are associated with the presence of impurities in the system. A hard magnetic material contains impurities, while a soft one does not. The presence of impurities prevents the electron spins from flipping their spin direction. As a result, a hard magnetic material can maintain its magnetism for an extended period after removal of the external magnetic field (this feature is called *residual magnetization*), while a soft magnetic material demagnetizes quickly after removal of the external magnetic field.

- **Antiferromagnetism** (Fig. 1.1b): the electrons' spins align anti-parallel because an exchange interaction causes neighboring electrons' spins to be directed opposite to each other. The up- and down-spins cancel, resulting in zero magnetism (i.e., no spontaneous magnetization).
- **Ferrimagnetism** (Fig. 1.1c, d): the electrons' spins align anti-parallel for the same reason as described for antiferromagnetism. However, the number (Fig. 1.1c) or magnitude (Fig. 1.1d) of up-spins is different from that of down-spins. The imbalance of up- and down-spins leads to spontaneous magnetization.

1.1.2 Paramagnetism and Diamagnetism

- **Paramagnetism**: in a paramagnetic material, the electrons' spins do not interact with each other. As the result, electron spin alignment generally occurs only in the presence of a strong external magnetic field (Fig. 1.1e). Each spin in the system aligns parallel to the magnetic field.

- **Diamagnetism**: in a diamagnetic material, a small magnetic moment occurs anti-parallel to an applied external magnetic field because of electromagnetic induction. Diamagnetism is an inherent property of all materials, and it doesn't be related to the presence of free-radical electron spins.

1.1.3 *Effect of Temperature on Magnetism*

Temperature dependence is a basic feature of magnetism. With increasing temperature, thermal fluctuations in the spin direction increase. In a paramagnetic material, the magnetic moment of the system M is proportional to the external magnetic field H:

$$M = \chi H. \tag{1.1}$$

In this equation, χ denotes the magnetic susceptibility, which follows *Curie's law* at around room temperature:

$$\chi = \frac{const.}{T}, \tag{1.2}$$

where the T is the absolute temperature.

In a ferromagnetic material, the relationship between temperature and magnetism is complicated by the involvement of inter-spin interactions. Figure 1.2 shows the temperature dependence of spontaneous magnetization in a ferromagnetic system. When the temperature is low, large spontaneous magnetization is present because the exchange interactions are dominant compared to the temperature effects. At higher temperatures, the electron spins become disordered and overcome the exchange interactions, which eventually results in paramagnetism. The temperature at which the spontaneous magnetization of a ferromagnetic material disappears is called the *Curie* temperature T_C. At temperatures above T_C, the magnetic susceptibility χ follows the *Curie–Weiss law*, which can be expressed as

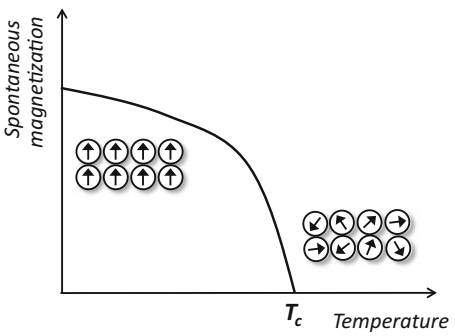

Fig. 1.2 Temperature dependence of spontaneous magnetization in ferromagnetic systems. T_c indicates Curie temperature

$$\chi = \frac{const.}{T - T_C}. \tag{1.3}$$

1.2 Why Organic Ferromagnetism?

The main focus of this book is "organic" ferromagnetism. Why organic ferromagnetism? To answer this question, we begin by discussing the features of inorganic ferromagnetism. We then describe the advantages of organic ferromagnetism compared with inorganic ferromagnetism and highlight the potential applications of organic ferromagnetic materials in the development of new high-performance innovative materials. Moreover, organic–inorganic hybrid systems, including supramolecular systems, are briefly mentioned.

1.2.1 Inorganic Magnets

In inorganic magnets containing transition-metal atoms, the presence of unpaired internal *d*- or *f*-type electrons plays an important role in magnetism (Fig. 1.3a). In general, strong magnetism and high transition temperatures are expected in such inorganic materials. The main weak points of inorganic magnets are (1) their heaviness, and (2) the use of rare (earth) metals.

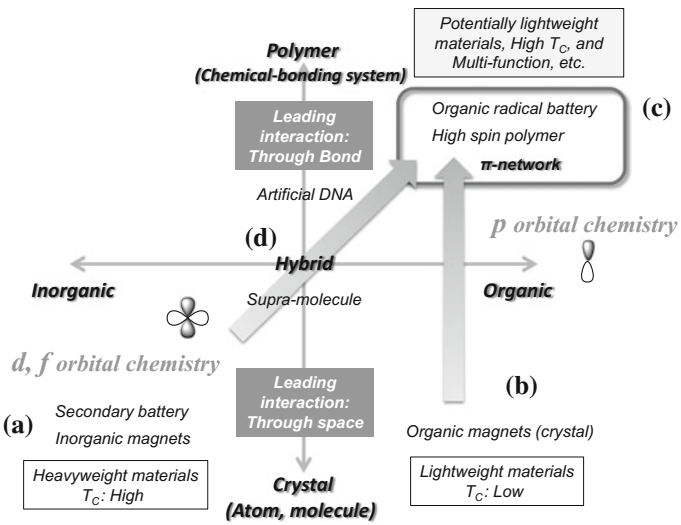

Fig. 1.3 Overview of magnetism and its applications: **a** inorganic and **b** organic magnetic crystals; **c** organic magnetic polymer; **d** organic-inorganic hybrid system

1.2.2 Advantages and Potential Applications of Organic Magnets

Organic magnets are expected to have potential as new innovative materials because: (1) they are generally lightweight, (2) they exhibit the properties of plastic, (3) they are prepared from abundant raw materials (i.e., they are free of rare metal(s)), (4) their magnetic properties are tunable, and (5) their magnetism may be coupled with other properties. In general, however, radical electrons in organic systems are highly reactive (i.e., unstable) and easily form chemical bonds. Thus, the realization of organic magnets remains a challenge.

The transition temperatures (T_C) of magnetic crystals based on small organic molecules (Fig. 1.3b) are generally too low to permit practical use because the through-space (TS) exchange interactions between molecules are generally weak.

In addition to molecular crystals, many efforts have been made to align the electron spins in polymers (Fig. 1.3c). The main driving force for this alignment is an intramolecular exchange interaction through bonds using the π-network. As the result of strong through-bond (TB) exchange interactions, a high-spin polymer is expected to show ferromagnetism at higher temperatures. For example, Rajca et al. synthesized a ladder-type high-spin polymer, which showed very high spin multiplicity (Fig. 1.4) [1–4]. High-spin polymers have the potential to show both coupled- and multi-functions induced by their π-networks, for example, "magnetism + conductivity" [5, 6]. One of the applications of high-spin polymers is in organic radical batteries (ORBs) (Fig. 1.3c) [7–10]. An ORB in which (2,2,6,6-tetramethylpiperidin-1-yl)oxyl (TEMPO) (Fig. 1.5a), poly(2,2,6,6-tetramethylpiperidinyloxy methacrylate) (PTMA) (Fig. 1.5b), and Li were used as the radical source, cathode active material, and anode active material, respectively, was proposed [7]. As another example, an *all*-organic radical battery has been proposed [8–10]. Figure 1.5c (charging), d (discharging) show schematic illustrations of the reactions in an ORB; at each electrode, the reduction/oxidation

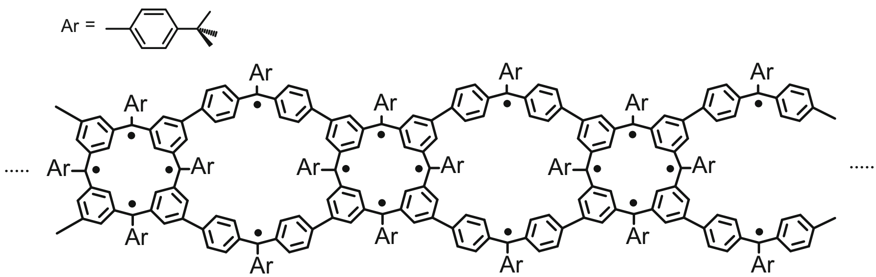

Fig. 1.4 High-spin polymer synthesized by Rajca et al.

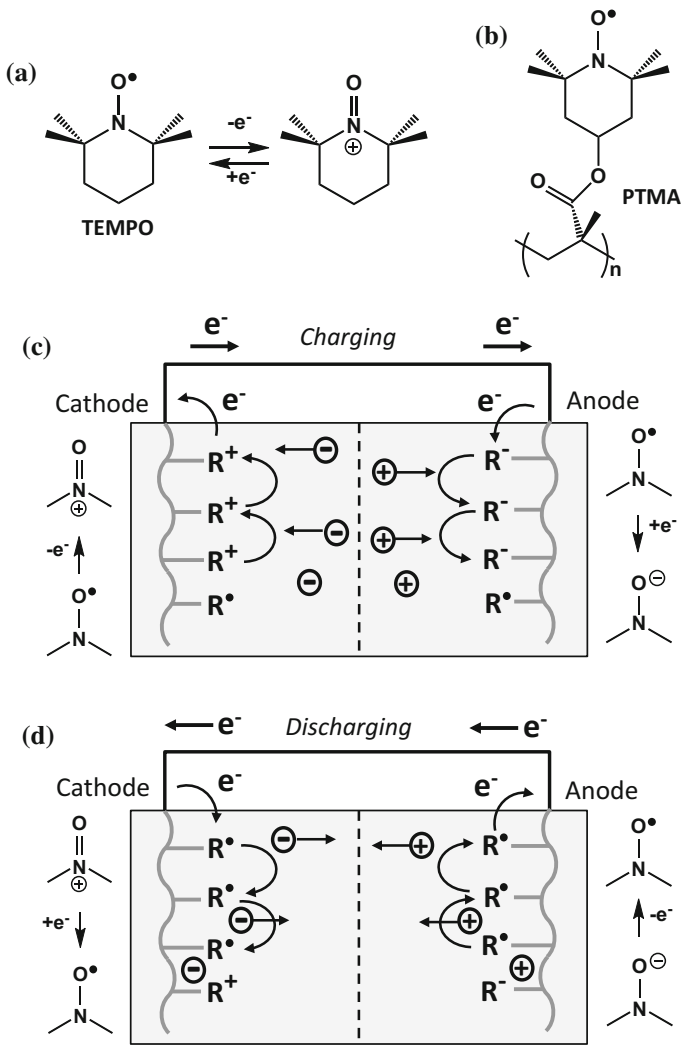

Fig. 1.5 Organic radical batteries. **a** Redox reactions of TEMPO and **b** PTMA. Schematic illustrations of **c** charging and **d** discharging reactions in the battery

reaction of the nitroxide radical controls the charge/discharge process. As a molecular stacking system, a molecular spin battery was proposed [11].

Organic–inorganic hybrid systems (Fig. 1.3d) are also recognized as potential magnetic materials. Metal complexes (for example, [12–14]) and supramolecules (for example, [15–17]) have been actively investigated for the purpose. Various types of artificial DNA have also attracted interest for their numerous potential properties including magnetism (for example, [18, 19]).

1.3 Development of the Disjoint and Non-disjoint Concepts in Organic Systems

The field of organic- and molecule-based magnetism began in Japan almost five decades ago [20, 21]. Around four decades ago, Itoh predicted that polycarbenes should have high-spin ground states [22]. Qualitative theoretical approaches based on Hückel theory were reported to describe the multiplicity of the ground states of large alternant organic molecules with conjugated bonds [23] and the band structures of nonclassical polymers [24]. In the last three decades, Iwamura et al. designed a molecular assembly of diphenylcarbenes having intermolecular ferromagnetic interactions [25]. They also discussed the potential use of polycarbenes as microdomains in macroscopic ferromagnets and investigated the magnetic behavior of a nonet tetracarbene as a model for one-dimensional organic ferromagnets [26, 27]. This area has become one of the most important fields of material science in Japan (for example, [27–33]) and internationally (for example, [34–41]).

In the last two decades, many experimental and theoretical reports relating the design of new magnetic materials based on organic, inorganic, and hybrid molecules to their functional properties have appeared (for example, [42–57]). Furthermore, Rajca [2, 3, 58–62], Nishide [63–80], and other experimentalists and theoreticians (for example, [81–85]) have extended hydrocarbon-based magnetic compounds to include one- and two-dimensional systems, ladder-type structures, and systems containing hetero-atom radical centers. One can get more references in some review books (for example, [86]) and more historical information on the long term development by both theoretical and experimental ways in magnetic properties of organic materials. Recently, highly accurate ab initio molecular orbital (MO) calculations, together with remarkable developments in supercomputer technology, have resulted in an increase in the use of theoretical techniques in the molecular design of organic ferromagnets.

The synthesis of novel organic materials based on the theoretical design of magnetic property is emerging as an advanced approach of modern organic chemistry. Magnetism resulting from the interactions of electron spins requires a large number of unpaired electrons. Ferromagnetism caused by the coupling of electron spins is essential to produce magnetic materials. In practice, however, keeping a high-spin state permanently is not as easy as in theory. In recent years, many studies of high-spin organic molecules (those with $S = 1$ (triplet) or greater) have provided valuable insights into the spin-coupling mechanisms available to organic structures as well as several general approaches for the preparation of high-spin materials. Nowadays, a hybrid experimental–computational approach is popular to find stable organic high-spin systems as cited in the top of this section, not only for ferromagnets, but also for potential applications in spin batteries, magnetic storage devices, and optical and conducting materials. In particular, there is a desire to manipulate the interrelationships between optical, conducting, and magnetic properties.

The molecular design of organic ferromagnets requires the construction of organic molecules with high spin multiplicities and the introduction of intermolecular ferromagnetic interactions. At the Hückel level, we developed a simple rule that states that the combination of two molecules that contain special sites where one molecule has no MO coefficient and the other molecule has no or some MO coefficients (a so-called 0–* combination, explained in Chap. 2) maintains the original degenerate MO energy levels, even after the combination, if the two energies are the same [87]. We were then inspired by the work of Borden and Davidson (B&D) [88] and noted that if two carbon sites belonging to different molecules both have no MO coefficients, the system should be classified as "disjoint"; if one of the two sites has nonzero MO coefficients, the system should be classified as "non-disjoint". The "disjoint" and "non-disjoint" concept has been confirmed using variational principles in MO calculations without any approximation in the framework of the Hückel method (see Chap. 2). B&D explained that, if the Hückel non-bonding MOs (NBMOs) cannot be localized to disjoint groups of atoms, the energy of the triplet lies well below that of the corresponding open-shell singlet at the Self-consistent field (SCF) level. The system then corresponds to a "non-disjoint" system. Additionally, the fact that a 0–* combination between two molecules produces a "non-disjoint" organic molecule leads to the stabilization of the triplet state.

The treatment proposed in this chapter provides one method of solving the problem of how to make "disjoint" or "nondisjoint" organic ferromagnets by combining two or more molecules. The results obtained seem consistent with those obtained using the spin polarization mechanism, i.e., the "spin up and down rule," which has been used widely by experimentalists to judge whether molecules show triplet or singlet states, although we have so far been unable to find any report that provides a mathematical proof. We show in Chap. 2 the mathematical basis of our approach developed for the prediction of organic high-spin systems. Before that, in this chapter, we describe some of the basic general features of π-conjugated molecules.

1.3.1 Alternant and Non-alternant Hydrocarbons

Conjugated hydrocarbons are classified as alternant or non-alternant. Alternant means that stars (*) can be put on alternating carbon atoms with no two stars adjacent. Alternant hydrocarbons can be further sub-classified as even alternant or odd alternant. In even-alternant hydrocarbons, the numbers of starred (*) and unstarred (unmarked) carbon atoms are equal in principle; the numbers of starred and unstarred carbon atoms are not equal in odd-alternant hydrocarbons. Since the number of stars in an odd-alternant or non-alternant hydrocarbon is always maximized, the numbers of starred carbon atoms in these systems must be greater than their numbers of unstarred carbon atoms by at least one. The left-hand side of Fig. 1.6 shows examples of even-alternant hydrocarbons (first two lines) and

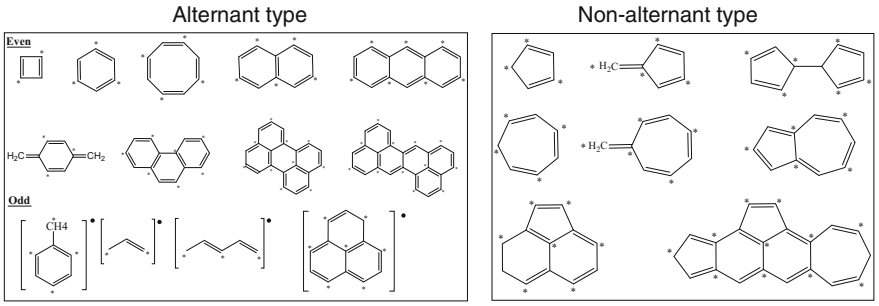

Fig. 1.6 Examples of alternant and non-alternant hydrocarbons

odd-alternant hydrocarbons where one unpaired electron remains (last line). The right side of Fig. 1.6 shows non-alternant hydrocarbons, in which it is not possible to star alternating carbon atoms without marking two adjacent centers. If a system includes a ring with an odd number of carbon atoms, it must, in principle, be classified as non-alternant.

1.3.2 Kekulé and Non-Kekulé Molecules

Since the predictions of qualitative resonance theory of unsaturated hydrocarbons we reanalyzed in terms of LCAO MO theory [89], numerous theoretical analyses of the electronic states and physical properties of unsaturated hydrocarbons have been reported in conjunction with experimental data (for example, [90–94]).

Before discussing the high-spin ground states of hydrocarbons, we describe Kekulé and non-Kekulé forms. Kekulé suggested the structure of benzene in which the carbon atoms are arranged in a hexagon with alternating double and single carbon–carbon bonds [95]. Based on this suggestion, there are two bonding arrangements (two alternation patterns) possible for benzene; however, the true structure is considered to be in between the two Kekulé forms as a result of resonance. Similar Kekulé-type conjugated molecules are depicted in the left-hand side of Fig. 1.7.

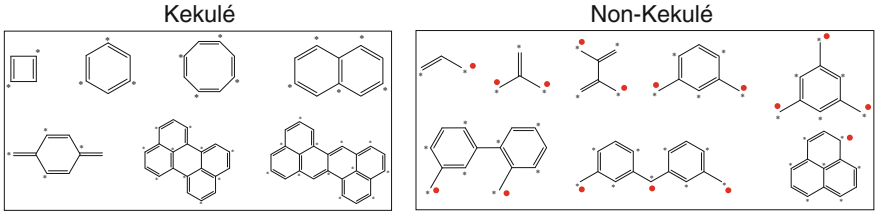

Fig. 1.7 Kekulé and non-Kekulé forms of conjugated molecules

A well-known approach for the development of high-spin organic molecules is the control of TB exchange in a conjugated molecule, which should be related to the non-Kekulé forms illustrated in the right-hand side of Fig. 1.7. Non-Kekulé conjugated molecules have two or more formal radical centers and are traditionally believed to be stable in high-spin states. However, several non-Kekulé hydrocarbon structures were found that did not conform to this belief, being addressed as "violations of Hund's rule in non-Kekulé hydrocarbons" [96]. Disjoint NBMOs in B&D's classification mentioned above can explain these exceptional non-Kekulé molecules.

Theoretical approaches such as Hückel theory were developed beginning in the 1950s and seem outdated. However, highly accurate treatment of large open-shell systems at ab initio levels is also still demanding, even with the most advanced recent supercomputers, and so, for many complicated problems related to electron correlation effects, a qualitative discussion is therefore inevitable. In this context, these old and simple treatments are still useful to predict the possibility of high-spin stability without or before performing heavy calculations. Therefore, a hybrid approach involving a combination of the old concepts and high performance ab initio computations must be employed to design open-shell functional materials and may be helpful for the synthesis of new organic ferromagnets or related functional compounds. There are many recent theoretical reports describing high-level calculations related tonon-Kekulé molecules (for example, [97–99]). We are attempting to develop a theory based on hybrid Hückel level–ab initio level calculations for the efficient treatment of large open-shell non-Kekulé systems. We introduce the mathematical evidence behind our simple concept to find disjoint and non-disjoint systems at the Hückel level in Chap. 2 and then present a novel treatment extended to ab initio levels of theory in Chap. 5.

1.4 Index for Finding High-Spin State

Many rules and indices have been proposed for predicting low-spin or high-spin state. These are mainly classified into two types, that is, MO-based approaches and approaches based on valence bond (VB) theory [100].

1.4.1 Molecular-Orbital-Based Index

Hund's rule [101, 102] states that when a system has energetically degenerate NBMOs the electrons tend to occupy each NBMO with a parallel spin configuration (see Fig. 1.8). Thus, when designing a high-spin molecule, it is important to generate as many degenerate NBMOs as possible. On the other hand, it should be noted

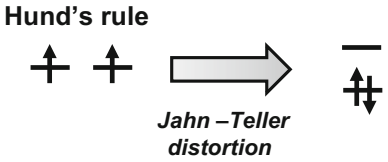

Fig. 1.8 Hund's rule concerning electron-spin arrangement in degenerate MOs, and Jahn–Teller effect leading to MO degeneracy breaking

that Jahn–Teller distortion (for example, [103]) often breaks the MO degeneracy, resulting in a low-spin ground state.

In 1950, Longuet-Higgins proposed a MO approach to count the number of NBMOs (N^{NBMO}) in alternant hydrocarbons by [89]

$$N^{NBMO} = N - 2T, \tag{1.4}$$

where the N is the number of carbon atoms and the T is the maximum possible number of double bonds. Then, the spin angular momentum s can be obtained by

$$s = \frac{1}{2}N^{NBMO} = \frac{1}{2}(N - 2T). \tag{1.5}$$

For example, as shown in Fig. 1.9a, *meta*-phenylenedimethane is expected to have two NBMOs (s = 1), whereas the *para*- and *ortho*-isomers have no NBMOs (s = 0).

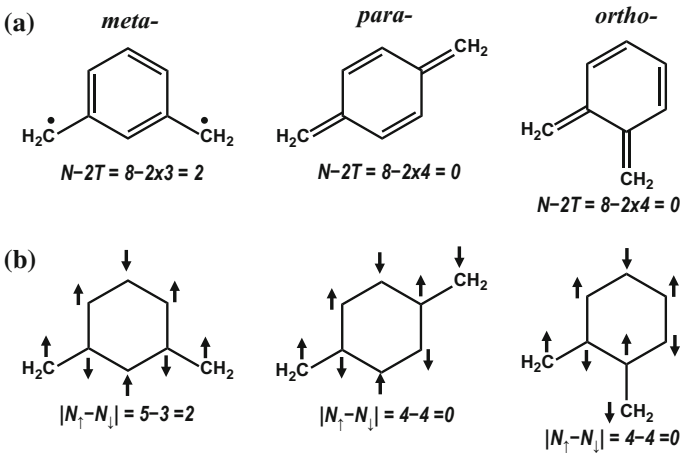

Fig. 1.9 Rules for counting radical electrons using **a** MO approach based on numbers of carbon atoms and double bonds and **b** VB (≡HB) approach based on numbers of up- and down-spins. Phenylenedimethane isomers are selected as examples. See main text for details

1.4.2 Valence-Bond-Theory-Based Index

In 1978, Ovchinnikov proposed a VB-based rule for predicting s by the simple formula [23]

$$s = \frac{1}{2}\left|N_{\uparrow} - N_{\downarrow}\right|, \tag{1.6}$$

where $N_{\uparrow}$ and $N_{\downarrow}$ indicate the numbers of up- and down-spins, respectively. In this rule, adjacent carbon atoms are alternatively assigned $\uparrow$ and $\downarrow$ spins (see Fig. 1.9b). Then, Eq. (1.6) provides s by counting the numbers of up- and down-spins. This technique gave the same conclusions for phenylenedimethane isomers as the MO-based method.

In the Heisenberg (HB) model [104], the spin Hamiltonian among more than two sites is expressed as

$$\hat{H}_{HB} = -2\sum_{a,b} J_{ab}\hat{\mathbf{S}}_a \cdot \hat{\mathbf{S}}_b, \tag{1.7}$$

where the $\hat{\mathbf{S}}_a$ indicates the spin angular momentum operator on the spin site a, and J_{ab} is an effective exchange integral between sites a and b; in the VB approach, a and b indicate atomic orbitals. J_{ab} can be described using an exchange integral K_{ab} and an overlap integral S_{ab} by (for example, [105])

$$J_{ab} = K_{ab} - cS_{ab}^2, \tag{1.8}$$

where c is a positive constant.

At the ab initio MO level, J can be expressed in terms of the total energy and the expectation value $\langle S^2 \rangle$ after approximate spin projection as follows [106]:

$$J = \left(E^{LS} - E^{HS}\right) \Big/ \left(\left\langle \hat{S}^2 \right\rangle^{HS} - \left\langle \hat{S}^2 \right\rangle^{LS}\right), \tag{1.9}$$

where HS and LS denote high- and low-spin states, respectively, and this treatment has been developed (for example, [107–113]).

Finally, in addition to the indices introduced here, many other rules and criteria have been proposed for judging ferromagnetism (for example, [114–117]).

1.5 Strategy for Ferromagnetism

Exchange interactions between radical electrons play an essential part in the ferromagnetism of a system. To obtain ferromagnetic systems, we have to arrange radical spins by controlling the exchange interactions. There are two main types of

strategies used for the design of ferromagnetic systems while taking into account the exchange interactions: the first is aimed at the development of radical crystals using TS intermolecular interactions, and the second focuses on the preparation of radical polymers using intramolecular interactions, in which the leading interaction occurs through bonds (see Fig. 1.10). The concept of TS and TB interactions was originally proposed by Hoffmann et al. in 1968 [118]. The concept divides various interactions into two categories: those that occur through space and those that occur through bonds. The concept of TS/TB interactions has been widely used to explain various experimental phenomena (for example, [119–122]).

1.5.1 Approach to Radical Crystals

In the design of radical crystals by stacking small radical molecules (Fig. 1.10a) (for example, [115, 123, 124]), the TS exchange interactions between the molecules are the dominant contributors to the ferromagnetic properties of the whole system. Many magnetic systems based on the stacked molecule approach have been investigated from both theoretical and experimental standpoints, and various organic molecule-based radical crystals [49, 125–134], including nitronyl nitroxide (NN)-based crystals (for example, [135, 136]) and charge-transfer salt crystals [33, 137], have been proposed. As a special case, radical crystals designed to merge magnetic and conduction properties have been investigated using this approach [5, 6].

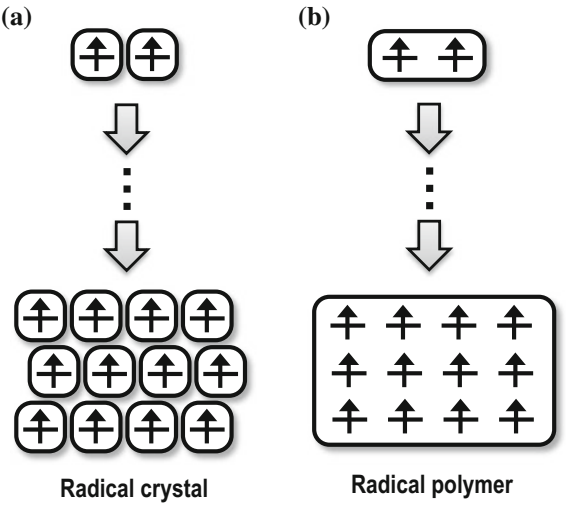

Fig. 1.10 Strategies of producing **a** radical crystals and **b** radical polymers

1.5.2 Approach to Radical Polymers

In the design of radical polymers by arranging as many radical spins as possible in a system (Fig. 1.10b) (for example, [21, 22, 138]), intramolecular TB exchange interactions such as π-conjugation are the essential factors for defining magnetic properties. In general, TB-type exchange interactions are stronger than TS-type interactions. Thus, radical polymers are expected to have T_C values much higher than those of radical crystals. In practice, polymers with very high spin multiplicities, such as those shown in Fig. 1.4, have been reported by Rajca [2] and Rajca and Rajca [1, 3, 4]. In addition, a hybrid strategy that fits between the TS and TB approaches has also been proposed (for example, [30]).

Various systems based on the radical polymer approach have been investigated both theoretically and experimentally. In particular, magnetic systems that use π- or mixed π/σ-networks have been actively studied [35, 139–147]. We can roughly classify the systems from the viewpoint of the system dimensionality. For (quasi-) one-dimensional systems [148–160], disjoint/non-disjoint composite bands [161] and finite-fused-azulene chains [162] have been proposed, among others for example. In the case of two-dimensional systems [163–169], graphene-based systems [170, 171] such as graphene-nanodots [172] and graphene-nanoribbons [173] have been investigated, for example. Using the TS–TB mixed approach, spin alignment through hydrogen bonds [174–176] and inter-chain (inter-layer) interactions between (quasi-)one-dimensional (two-dimensional) magnetic polymers [177, 178] have been investigated, among others [179].

1.6 Ising Model: Theoretical Approaches to Large High-Spin Systems (I)

Magnetism is strongly related to temperature and is often described using statistical mechanics. Here, we review the statistical treatment of magnetics called the *Ising* model [180–182]. Figure 1.11a shows a typical Ising model. In a system, *N*-spins are placed on the lattice one-by-one. Each spin has a magnetic moment μ and has one of only two possible states, i.e., the up-spin state (+1) or the down-spin state (−1). For simplicity, each spin interacts only with the nearest neighboring spin(s) in the two-dimensional space. In the Ising model, the Hamiltonian of a system in an external magnetic field H can be described by

$$\mathrm{H} = -J \sum_{i,j} \sigma_i \sigma_j - \mu H \sum_i \sigma_i, \tag{1.10}$$

where the coupling constant J defines the features of the magnetic interaction between electron spins, and $J > 0$ and $J < 0$ indicate ferromagnetic and antiferromagnetic interactions, respectively.

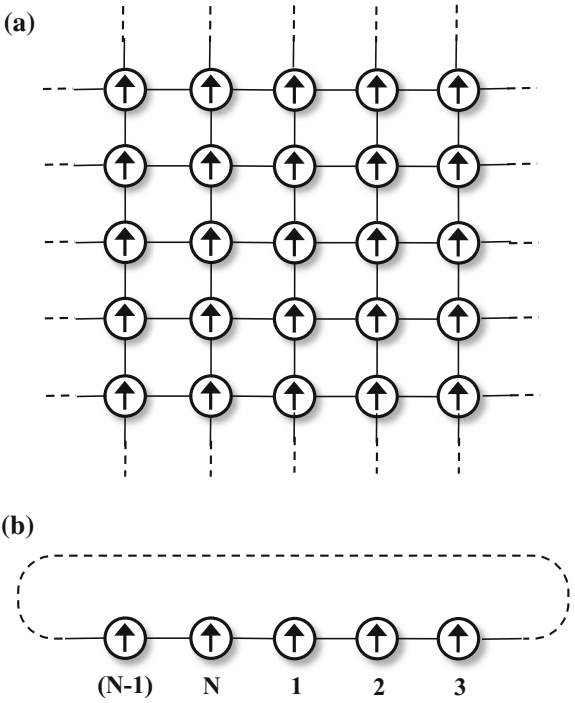

Fig. 1.11 Ising models for **a** two-dimensional system and **b** one-dimensional system with periodic boundary conditions

By means of the mean field approximation, we can assume that Eq. 1.10 can be rewritten as the sum of the Hamiltonian for each spin site, H_i:

$$H \cong \sum_i H_i = \sum_i (-Jz\langle\sigma\rangle\sigma_i - \mu H\sigma_i), \tag{1.11}$$

where z and $\langle\sigma\rangle$ indicate the number of nearest-neighboring spins and the thermal mean field of the spins, respectively. By considering the sum of states and Helmholtz free energy, the mean value of the magnetization of the system can be expressed as [183]

$$Magnetization = \left\langle \sum_i \sigma_i \right\rangle = N \tanh(k_B T)^{-1}(Jz\langle\sigma\rangle + \mu H), \tag{1.12}$$

where k_B is the Boltzmann constant. As another example, Fig. 1.11b shows the Ising model for a one-dimensional N-spin system with periodic boundary conditions. The Hamiltonian for the system can be expressed using the boundary conditions as

$$\mathrm{H} = -J \sum_{i=1} \sigma_i \sigma_{i+1}, \quad \text{where} \quad \sigma_{N+1} = \sigma_1. \tag{1.13}$$

Finally, it should be noted that a quantum-chemistry (QC)-based treatment (for example, [184]) beyond the classical Ising model has been developed in this field.

1.7 Quantum Chemistry Approach: Theoretical Approaches to Large High-Spin Systems (II)

An understanding of inter-radical exchange interactions is an important factor in the design of ferromagnetic systems. Furthermore, to achieve accurate designs, a quantitative examination of the interactions should be required. QC calculations that obviously treat electrons and their spin are candidates for analyzing the exchange interactions (for example, [105, 110, 126, 130, 134, 136, 137, 144, 174, 176, 184–188]).

Ab initio QC was rapidly developed for the elucidation of reactions mechanism, especially since the Nobel prize in chemistry was awarded to R. Hoffmann and K. Fukui on 1981, concerning the course of chemical reactions by role of frontier orbitals [189, 190]. Owing to recent remarkable progress of high performance supercomputer, QC treatment is much more being developed to be applicable to large systems. In this subsection, we introduce various QC techniques for describing larger high-spin systems. There are several QC methods such as (semi-) empirical MO, ab initio MO, and density functional theory (DFT) methods. In this book, we focus on ab initio MO methods; the ab initio MO method is a non-empirical theory, and the computational cost of a calculation is $O(N^{3-4})$, where N indicates the system size. Electron correlation effects can be included by performing post-HF calculations (such as Møller–Plesset (MP) perturbation theory and configuration interaction (CI) calculations); the cost of the post-HF treatment is $O(N^{5-7})$. Because ab initio calculations are very time consuming, they are normally only useful for small molecules.

Recently, many fragmentation methods for closed-shell systems have been developed in which the required computational time scales linearly with system size. However, efficient and accurate methods for open-shell systems have rarely been reported in QC, because the rapid increase in the active space of a large open-shell system makes it difficult to treat large-scale CIs. Nevertheless, a precise description that includes electron-correlation effects, at least for the open-shell part, is necessary to predict the magnetic properties and temperature effects. Spin multiplicity is, in fact, very important in predicting T_C. Unfortunately, however, it is difficult to obtain reliable T_C values that include electron-correlation effects except in the case of some qualitative prediction techniques that use pseudo-potentials.

1.7.1 *Open-Shell Ab Initio Molecular Orbital Methods for Larger Systems*

We review several methods beyond the conventional method that can be employed to perform calculations for larger open-shell systems efficiently.

Open-shell elongation method. The elongation (ELG) method [191, 192], developed in this author's group, is a linear-scaling method that mimics the polymerization reaction using a computer. Figure 1.12 shows a schematic illustration of the open-shell ELG method procedures [193, 194]. First, a starting cluster is computed as an open-shell system to obtain its canonical MOs (CMOs). The CMOs then undergo a unitary transformation into two regional localized MOs (RLMOs), i.e., active and frozen RLMOs localized to active (reaction terminal side) and frozen (remaining) regions, respectively; this procedure is called the localization step. A new monomer then attacks the active RLMO of the starting cluster. Here, it is assumed that the frozen RLMOs to be far from the attacking monomer

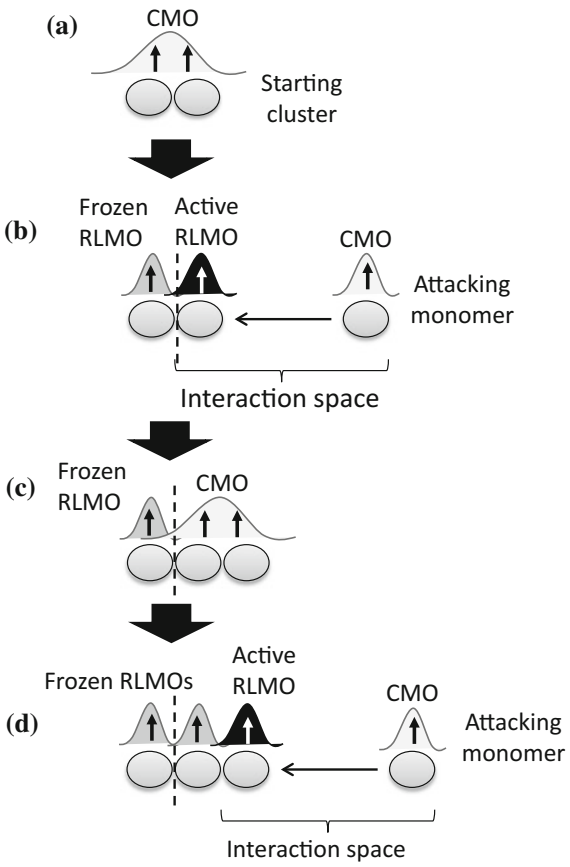

Fig. 1.12 Open-shell ELG method procedures

and that there is no interaction between them. The eigenvalue problem is solved within the open-shell scheme only for the interaction space consisting of the active RLMOs and CMOs of the monomer to obtain the new CMOs for the limited space; this procedure is called the ELG step. By repeating the localization and ELG steps, the electronic structures of the system can be elongated step by step while keeping the electron spins (spin multiplicity) in the frozen region. The computational accuracy of the ELG method is on the order of 10^{-8} hartrees per atom. A detailed description of the open-shell ELG method is provided in Chap. 5.

Open-shell fragment molecular orbital method. The fragment MO (FMO) method has been proposed [195–197] and developed [198–205] for calculating large systems. In this method, properties such as the total energy of the system can be obtained from the energies of each fragment and fragment pair. For example, the two-body FMO energy of N fragments is described by

$$E^{FMO2} = \sum_{I}^{N} E_I + \sum_{I>J}^{N} (E_{IJ} - E_I - E_J), \tag{1.14}$$

where E_I and E_{IJ} represent the total energies of the single fragment and fragment pair, respectively. These energies are calculated under the static electric field generated by the other fragments. The method has been extended to include calculations for open-shell systems (FMO-ROHF, FMO-ROMP2, and FMO-ROCC) [206].

Open-shell divide-and-conquer method. The divide-and-conquer (DC) method has been proposed [207–209] and developed [210–216] for the calculation of large systems. In the DC method, the whole system is initially divided into subsystems. Each subsystem (central region) is surrounded by a buffer region, which is made up of subsystems adjacent to the central region. The CMOs for the localization region consisting of the central and buffer regions are obtained from conventional calculations under the static electric field generated by the other parts of the system. The density matrix for the whole system is constructed from those corresponding to the localization regions while controlling the Fermi level. The static electric field is recalculated using the new density matrix, and each localization region is recalculated in the field. These processes are repeated self-consistently. The spin-unrestricted open-shell scheme has been proposed at the HF and DFT levels (DC-UHF/UDFT) [217] and for a MP-based method (DC-UMP2) [218, 219].

Density matrix renormalization group method. The density matrix renormalization group (DMRG) methods are among the most actively developing ab initio QC techniques used to predict magnetic properties, even though these methods were not originally formulated from a wavefunction perspective, but rather using renormalizatioin group language [220]. The DMRG algorithm was originally introduced by White [221, 222] to treat properties of large quantum lattice models and was later extended to ab initio Hamiltonians [223–227]. Yanai et al. implemented orbital optimization with the DMRG to enable the self-consistent improvement of the active orbitals, as is done in the complete active space

self-consistent field (CASSCF) method, creating what is known as the DMRG-CASSCF method [228, 229]. Furthermore, they presented a novel parallelized implementation of the DMRG algorithm that is oriented toward applications for polynuclear transition metal compounds [230]. Recently, these methods have been further developed to encompass complete active space second-order perturbation theory (DMRG-CASPT2) [231, 232] and multireference CI (DMRG-MRCI) techniques [233]. Associated dynamic correlation methods, which can handle large active spaces, are also known [234].

References

1. Rajca, A., Wongsriratanakul, J., Rajca, S.: Magnetic ordering in an organic polymer. Science **294**, 1503–1505 (2001)
2. Rajca, A.: From high-spin organic molecules to organic polymers with magnetic ordering. Chem. Eur. J. **8**, 4834–4841 (2002)
3. Rajca, A., Wongsriratanakul, J., Rajca, S.: Organic spin clusters: macrocyclic-macrocyclic polyarylmethyl polyradicals with very high spin S = 5-13. J. Am. Chem. Soc. **126**, 6608–6626 (2004)
4. Rajca, S., Rajca, A., Wongsriratanakul, J., Butler, P., Choi, S.-M.: Organic spin clusters. A dendritic-macrocyclic poly(arylmethyl) polyradical with very high spin of S = 10 and Its derivatives: synthesis, magnetic studies, and small-angle neutron scattering. J. Am. Chem. Soc. **126**, 6972–6986 (2004)
5. Matsushita, M.M., Kawakami, H., Sugawara, T., Ogata, M.: Molecule-based system with coexisting conductivity and magnetism and without magnetic inorganic ions. Phys. Rev. B **77**, 195208 (2008)
6. Komatsu, H., Matsushita, M.M., Yamamura, S., Sugawara, Y., Suzuki, K., Sugawara, T.: Influence of magnetic field upon the conductance of a unicomponent crystal of a tetrathiafulvalene-based nitronyl nitroxide. J. Am. Chem. Soc. **132**, 4528–4529 (2010)
7. Nakahara, K., Iwasa, S., Satoh, M., Morioka, Y., Iriyama, J., Suguro, M., Hasegawa, E.: Rechargeable batteries with organic radical cathodes. Chem. Phys. Lett. **359**, 351–354 (2002)
8. Suga, T., Pu, Y.-J., Kasatori, S., Nishide, H.: Cathode- and anode-active poly(nitroxylstyrene)s for rechargeable batteries: p- and n-type redox switching via substituent effects. Macromolecules **40**, 3167–3173 (2007)
9. Nishide, H., Oyaizu, K.: Toward flexible batteries. Science **319**, 737–738 (2008)
10. Janoschka, T., Hager, M.D., Schubert, U.S.: Powering up the future: radical polymers for battery applications. Adv. Mater. **24**, 6397–6409 (2012)
11. Morita, Y., Nishida, S., Murata, T., Moriguchi, M., Ueda, A., Satoh, M., Arifuku, K., Sato, K., Takui, T.: Organic tailored batteries materials using stable open-shell molecules with degenerate frontier orbitals. Nat. Mater. **10**, 947–951 (2011)
12. Ferlay, S., Mallah, T., Ouahes, R., Veillet, P., Verdaguer, M.: A room-temperature organometallic magnet based on Prussian blue. Nature **378**, 701–703 (1995)
13. Ishikawa, N., Sugita, M., Ishikawa, T., Koshihara, S.-Y., Kaizu, Y.: Lanthanide double-decker complexes functioning as magnets at the single-molecular level. J. Am. Chem. Soc. **125**, 8694–8695 (2003)
14. Osa, S., Kido, T., Matsumoto, N., Re, N., Pochaba, A., Mrozinski, J.: A tetranuclear 3d-4f single molecule magnet:$[Cu^{II}LTb^{III}(hfac)_2]_2$. J. Am. Chem. Soc. **126**, 420–421 (2004)
15. Michaut, C., Ouahab, L., Bergerat, P., Kahn, O., Bousseksou, A.: Structure and ferromagnetic interactions in open-shell supramolecular assemblies constructed from radical cations and hexacyanometallate anions. J. Am. Chem. Soc. **118**, 3610–3616 (1996)

16. Kahn, O.: Chemistry and physics of supramolecular magnetic materials. Acc. Chem. Res. **33**, 647–657 (2000)
17. Akutagawa, T., Shitagami, K., Aonuma, M., Noro, S.-I., Nakamura, T.: Ferromagnetic and antiferromagnetic coupling of $[Ni(dmit)_2]^-$ anion layers induced by Cs_2^+ (benzo[18] crown-6)$_3$ supramolecule. Inorg. Chem. **48**, 4454–4461 (2009)
18. Tanaka, K., Tengeiji, A., Kato, T., Toyama, N., Shionoya, M.: A discrete self-assembled metal array in artificial DNA. Science **299**, 1212–1213 (2003)
19. Matsui, T., Miyachi, H., Sato, T., Shigeta, Y., Hirao, K.: Structural origin of copper ion containing artificial DNA: a density functional study. J. Phys. Chem. B **112**, 16960–16965 (2008)
20. Itoh, K.: Electron spin resonance of an aromatic hydrocarbon in its quintet ground state. Chem. Phys. Lett. **1**, 235–238 (1967)
21. Mataga, N.: Possible "ferromagnetic states" of some hypothetical hydrocarbons. Theoret. Chim. Acta (Berl.) **10**, 372–376 (1968)
22. Itoh, K.: Electronic structures of aromatic hydrocarbons with high spin multiplicities in the electronic ground state. Pure Appl. Chem. **50**, 1251–1259 (1978)
23. Ovchinnikov, A.A.: Multiplicity of the ground state of large alternant organic molecules with conjugated bonds (Do organic ferromagnetics exist?). Theoret. Chim. Acta (Berl.) **47**, 297–304 (1978)
24. Tyutyulkov, N., Schuster, P., Polansky, O.: Band structure of nonclassical polymers. Theoret. Chim. Acta (Berl.) **63**, 291–304 (1983)
25. Sugawara, T., Murata, S., Kimura, K., Iwamura, H., Sugawara, Y., Iwasaki, H.: Design of molecular assembly of diphenylcarbenes having ferromagnetic intermolecular interactions. J. Am. Chem. Soc. **107**, 5293–5294 (1985)
26. Sugawara, T., Bandow, S., Kimura, K., Iwamura, H., Itoh, K.: Magnetic behavior of nonet tetracarbene, *m*-phenylenebis((diphenylmethylen-3-yl)methylene). J. Am. Chem. Soc. **106**, 6449–6450 (1984)
27. Sugawara, T., Bandow, S., Kimura, K., Iwamura, H., Itoh, K.: Magnetic behavior of nonet tetracarbene as a model for one-dimensional organic ferromagnets. J. Am. Chem. Soc. **108**, 368–371 (1986)
28. Teki, Y., Takui, T., Itoh, K., Iwamura, H., Kobayashi, K.: Preparation and ESR detection of a ground-state nonet hydrocarbon as a model for one-dimensional organic ferromagnets. J. Am. Chem. Soc. **108**, 2147–2156 (1986)
29. Izuoka, A., Murata, S., Sugawara, T., Iwamura, H.: Molecular design and model experiments of ferromagnetic intermolecular interaction in the assembly of high-spin organic molecules. Generation and characterization of the spin states of isomeric bis (phenylmethylenyl)[2.2]paracyclophanes. J. Am. Chem. Soc. **109**, 2631–2639 (1987)
30. Yamaguchi, K., Toyoda, Y., Fueno, T.: A generalized MO (GMO) approach to unstable molecules with quasi-degenerate electronic states: ab initio GMO calculations of intramolecular effective exchange integrals and designing of organic magnetic polymers. Synth. Met. **19**, 81–86 (1987)
31. Yamaguchi, K., Toyoda, Y., Nakano, M., Fueno, T.: Ab initio and semiempirical MO calculations of intermolecular effective exchange integrals between organic radicals. Designing of organic ferromagnet, ferrimagnet and ferromagnetic conductors. Synth. Met. **19**, 87–92 (1987)
32. Fujita, I., Teki, Y., Takui, T., Kinoshita, T., Itoh, K., Miko, F., Sawaki, Y., Iwamura, H., Izuoka, A., Sugawara, T.: Design, preparation, and electron spin resonance detection of a ground-state undecet ($S = 5$) hydrocarbon. J. Am. Chem. Soc. **112**, 4074–4075 (1990)
33. Yamaguchi, K., Namimoto, H., Fueno, T., Nogami, T., Shirota, Y.: Possibilities of organic ferromagnets and ferrimagnets by the use of charge-transfer (CT) complexes with radical substituents. Ab initio MO studies. Chem. Phys. Lett. **166**, 408–414 (1990)
34. Korshak, Y.V., Medvedeva, T.V., Ovchinnikov, A.A., Spector, V.N.: Organic polymer ferromagnet. Nature **326**, 370–372 (1987)

35. Torrance, J.B., Oostra, S., Nazzal, A.: A new, simple model for organic ferromagnetism and the first organic ferromagnet. Synth. Met. **19**, 709–714 (1987)
36. Miller, J.S., Epstein, A.J., Reiff, W.M.: Molecular/organic ferromagnets. Science **240**, 40–47 (1988)
37. Miller, J.S., Epstein, A.J., Reiff, W.M.: Molecular ferromagnets. Acc. Chem. Res. **21**, 114–120 (1988)
38. Miller, J.S., Epstein, A.J., Reiff, W.M.: Ferromagnetic molecular charge-transfer complexes. Chem. Rev. **88**, 201–220 (1988)
39. Ovchinnikov, A.A., Spector, V.N.: Organic ferromagnets. New results. Synth. Met. **27**, 615–624 (1988)
40. Decurtins, S., Gutlich, P., Hasselbach, K., Hauser, A., Spiering, H.: Light-induced excited-spin-state trapping in iron (II) spin-crossover systems. Optical spectroscopic and magnetic susceptibility study. Inorg. Chem. **24**, 2174–2178 (1985)
41. Miller, T.J.E.: Brushless Permanent-Magnet and Reluctance Motor Drives. Oxford University Press, New York (1989)
42. Matsushita, M., Nakamura, T., Momose, T., Shida, T., Teki, Y., Takui, T., Kinoshita, T., Itoh, K.: Novel organic ions of high-spin state. 2. Determination of the spin multiplicity of the ground state and ^{1}H-ENDOR study of the monoanion of *m*-phenylenebis (phenylmethylene). J. Am. Chem. Soc. **114**, 7470–7475 (1992)
43. Teki, Y., Fujita, I., Takui, T., Kinoshita, T., Itoh, K.: Topology and spin alignment in a novel organic high-spin molecule, 3, 4′-Bis (phenylmethylene) biphenyl, as studied by ESR and a generalized UHF Hubbard calculation. J. Am. Chem. Soc. **116**, 11499–11505 (1994)
44. Mitani, M., Takano, Y., Yoshioka, Y., Yamaguchi, K.: Density functional study of intramolecular ferromagnetic interaction through m-phenylene coupling unit. III. Possibility of high-spin polymer. J. Chem. Phys. **111**, 1309 (1999)
45. Dietz, F., Tyutyulkov, N.: Photoswitching of the magnetic properties of one-dimensional π-electron systems. Part II. Conjugated polymers with di-hetarylethene and benzylidene-anthrone fragments in the elementary units. Phys. Chem. Chem. Phys. **3**, 4600–4605 (2001)
46. Dietz, F., Tyutyulkov, N.: Organic polymers with indirect magnetic interaction caused by the molecular topology of the elementary units. Chem. Phys. **264**, 37–51 (2001)
47. Matsuoka, F., Yamashita, Y., Kawakami, T., Kitagawa, Y., Yoshioka, Y., Yamaguchi, K.: Theoretical investigation on the magnetic interaction of the tetrathiafulvalene–nitronyl nitroxide stacking model: possibility of organic magnetic metals and magnetic superconductors. Polyhedron **20**, 1169–1176 (2001)
48. Teki, Y., Miyamoto, S., Nakatsuji, M., Miura, Y.: π-Topology and spin alignment utilizing the excited molecular field: Observation of the excited high-spin quartet (S = 3/2) and quintet (S = 2) states on purely organic π-conjugated spin systems. J. Am. Chem. Soc. **123**, 294–305 (2001)
49. Tyutyulkov, N., Staneva, M., Stoyanova, A., Alaminova, D., Olbrich, G., Dietz, F.: Structure and magnetic interaction in organic radical crystals. 6. Spin-transfer crystals: a theoretical study. J. Phys. Chem. B **106**, 2901–2909 (2002)
50. Nakano, M., Kishi, R., Nakagawa, N., Ohta, S., Takahashi, H., Furukawa, S.-I., Kamada, K., Ohta, K., Champagne, B., Botek, E.: Second hyperpolarizabilities (γ) of bisimidazole and bistriazole benzenes: diradical character, charged state, and spin state dependences. J. Phys. Chem. A **110**, 4238–4243 (2006)
51. Minami, T., Ito, S., Nakano, M.: Signature of singlet open-shell character on the optically allowed singlet excitation energy and singlet-triplet energy gap. J. Phys. Chem. A **117**, 2000–2006 (2013)
52. Miller, J.S., Calabrese, J.C., McLean, R.S., Epstein, A.J.: meso-(Tetraphenylporphinato) manganese (III)-tetracyanoethenide, $[Mn^{III}TPP]^{\cdot\oplus}[TCNE]^{\cdot\ominus}$. A new structure-type linear-chain magnet with a T_c of 18K. Adv. Mater. **4**, 498–501 (1992)
53. Stumpf, H.O., Ouahab, L., Pei, Y., Grandjean, D., Kahn, O.: A molecular-based magnet with a fully interlocked three-dimensional structure. Science **261**, 447–447 (1993)

54. Decurtins, S., Schmalle, H.W., Oswald, H.R., Linden, A., Ensling, J., Gütlich, P., Hauser, A.: A polymeric two-dimensional mixed-metal network. Crystal structure and magnetic properties of $\{[P(Ph)_4][MnCr(ox)_3]\}$. Inorg. Chim. Acta **216**, 65–73 (1994)
55. Matsuda, K., Nakamura, N., Inoue, K., Koga, N., Iwamura, H.: Toward dendritic two-dimensional polycarbenes: syntheses of 'Starburst'-type nona-and dodecadiazo compounds and magnetic study of their photoproducts. Bull. Chem. Soc. Jpn. **69**, 1483–1494 (1996)
56. Hatlevik, Ø., Buschmann, W.E., Zhang, J., Manson, J.L., Miller, J.S.: Enhancement of the magnetic ordering temperature and air stability of a mixed valent vanadium hexacyanochromate (III) magnet to 99 C (372 K). Adv. Mater. **11**, 914–918 (1999)
57. Boldog, I., Gaspar, A.B., Martinez, V., Pardo-Ibanez, P., Ksenofontov, V., Bhattacharjee, A., Gutlich, P., Real, J.A.: Spin-crossover nanocrystals with magnetic, optical, and structural bistability near room temperature. Angew. Chem. Int. Ed. Engl. **120**, 6533–6537 (2008)
58. Rajca, A.: Organic diradicals and polyradicals: from spin coupling to magnetism? Chem. Rev. **94**, 871–893 (1994)
59. Rajca, A., Rajca, S., Wongsriratanakul, J.: Very high-spin organic polymer: π-conjugated hydrocarbon network with average spin of $S \geq 40$. J. Am. Chem. Soc. **121**, 6308–6309 (1999)
60. Rajca, A., Olankitwanit, A., Wang, Y., Boratynski, P.J., Pink, M., Rajca, S.: High-spin $S = 2$ ground state aminyl tetraradicals. J. Am. Chem. Soc. **135**, 18205–18215 (2013)
61. Gallagher, N.M., Olankitwanit, A., Rajca, A.: High-spin organic molecules. J. Org. Chem. **80**, 1291–1298 (2015)
62. Ciccullo, F., Gallagher, N.M., Geladari, O., Chasse, T., Rajca, A., Casu, M.B.: A derivative of the blatter radical as a potential metal-free magnet for stable thin films and interfaces. ACS Appl. Mater. Interfaces **8**, 1805–1812 (2016)
63. Nishide, H., Kaneko, T., Igarashi, M., Tsuchida, E., Yoshioka, N., Lahti, P.M.: Magnetic characterization and computational modeling of poly (phenylacetylenes) bearing stable radical groups. Macromolecules **27**, 3082–3086 (1994)
64. Nishide, H.: High-spin alignment in π-conjugated polyradicals: a magnetic polymer. Adv. Mater. **7**, 937–941 (1995)
65. Nishide, H., Kaneko, T., Nii, T., Katoh, K., Tsuchida, E., Yamaguchi, K.: Through-bond and long-range ferromagnetic spin alignment in a π-conjugated polyradical with a poly (phenylenevinylene) skeleton. J. Am. Chem. Soc. **117**, 548–549 (1995)
66. Nishide, H., Kaneko, T., Nii, T., Katoh, K., Tsuchida, E., Lahti, P.M.: Poly (phenylenevinylene)-attached phenoxyl radicals: ferromagnetic interaction through planarized and π-conjugated skeletons. J. Am. Chem. Soc. **118**, 9695–9704 (1996)
67. Nishide, H., Miyasaka, M., Tsuchida, E.: Average octet radical polymer: a stable polyphenoxyl with star-shaped π conjugation. Angew. Chem. Int. Ed. **37**, 2400–2402 (1998)
68. Nishide, H., Ozawa, T., Miyasaka, M., Tsuchida, E.: A nanometer-sized high-spin polyradical: Poly (4-phenoxyl-1, 2-phenylenevinylene) planarily extended in a non-Kekulé fashion and its magnetic force microscopic images. J. Am. Chem. Soc. **123**, 5942–5946 (2001)
69. Kaneko, T., Makino, T., Miyaji, H., Teraguchi, M., Aoki, T., Miyasaka, M., Nishide, H.: Ladderlike ferromagnetic spin coupling network on a π-conjugated pendant polyradical. J. Am. Chem. Soc. **125**, 3554–3557 (2003)
70. Michinobu, T., Inui, J., Nishide, H.: *m*-Phenylene-linked aromatic poly (aminium cationic radical) s: persistent high-spin organic polyradicals. Org. Lett. **5**, 2165–2168 (2003)
71. Nishide, H., Iwasa, S., Pu, Y.-J., Suga, T., Nakahara, K., Satoh, M.: Organic radical battery: nitroxide polymers as a cathode-active material. Electrochim. Acta **50**, 827–831 (2004)
72. Fukuzaki, E., Nishide, H.: Room-temperature high-spin organic single molecule: nanometer-sized and hyperbranched poly [1, 2, (4)-phenylenevinyleneanisylaminium]. J. Am. Chem. Soc. **128**, 996–1001 (2006)
73. Kurata, T., Koshika, K., Kato, F., Kido, J., Nishide, H.: An unpaired electron-based hole-transporting molecule: triarylamine-combined nitroxide radicals. Chem. Commun. 2986–2988 (2007)

74. Oyaizu, K., Ando, Y., Konishi, H., Nishide, H.: Nernstian adsorbate-like bulk layer of organic radical polymers for high-density charge storage purposes. J. Am. Chem. Soc. **130**, 14459–14461 (2008)
75. Oyaizu, K., Suga, T., Yoshimura, K., Nishide, H.: Synthesis and characterization of radical-bearing polyethers as an electrode-active material for organic secondary batteries. Macromolecules **41**, 6646–6652 (2008)
76. Oyaizu, K., Nishide, H.: Radical polymers for organic electronic devices: a radical departure from conjugated polymers? Adv. Mater. **21**, 2339–2344 (2009)
77. Suga, T., Ohshiro, H., Sugita, S., Oyaizu, K., Nishide, H.: Emerging N-type redox-active radical polymer for a totally organic polymer-based rechargeable battery. Adv. Mater. **21**, 1627–1630 (2009)
78. Suga, T., Sugita, S., Ohshiro, H., Oyaizu, K., Nishide, H.: p- and n-type bipolar redox-active radical polymer: toward totally organic polymer-based rechargeable devices with variable configuration. Adv. Mater. **23**, 751–754 (2011)
79. Fukuzaki, E., Nishide, H.: 2, 6, 10-Tris (dianisylaminium)-3, 7, 11-tris (hexyloxy) triphenylene: a robust quartet molecule at room temperature. Org. Lett. **8**, 1835–1838 (2006)
80. Murata, H., Miyajima, D., Nishide, H.: A high-spin and helical organic polymer: Poly {[4-(dianisylaminium) phenyl] acetylene}. Macromolecules **39**, 6331–6335 (2006)
81. Iwamura, H.: What role has organic chemistry played in the development of molecule-based magnets? Polyhedron **66**, 3–14 (2013)
82. Mayhall, N.J., Head-Gordon, M.: Computational quantum chemistry for multiple-site heisenberg spin couplings made simple: still only one spin-flip required. J. Phys. Chem. Lett. **6**, 1982–1988 (2015)
83. Dotti, N., Heintze, E., Slota, M., Hübner, R., Wang, F., Nuss, J., Dressel, M., Bogani, L.: Conduction mechanism of nitronyl-nitroxide molecular magnetic compounds. Phys. Rev. B **93**, 165201 (2016)
84. Mañeru, D.R., de Moreira, I.P.R., Illas, F.: Helical folding-induced stabilization of ferromagnetic polyradicals based on triarylmethyl radical derivatives. J. Am. Chem. Soc. **138**, 5271–5275 (2016)
85. Nam, Y., Cho, D., Lee, J.Y.: Doping effect on edge-terminated ferromagnetic graphene nanoribbons. J. Phys. Chem. C **120**, 11237–11244 (2016)
86. Lahti, P.M.: Magnetic properties of organic materials. Marcel Dekker Inc, New York (1999)
87. Aoki, Y., Imamura, A.: A simple rule to find nondisjoint NBMO degenerate systems for designing high-spin organic molecules. Int. J. Quant. Chem. **74**, 491–502 (1999)
88. Borden, W.T., Davidson, E.R.: Effects of electron repulsion in conjugated hydrocarbon diradicals. J. Am. Chem. Soc. **99**, 4587–4594 (1977)
89. Longuet-Higgins, H.C.: Some studies in molecular orbital theory I. Resonance structures and molecular orbitals in unsaturated hydrocarbons. J. Chem. Phys. **18**, 265–274 (1950)
90. Greenwood, H.H.: Molecular orbital theory of reactivity in aromatic hydrocarbons. J. Chem. Phys. **20**, 1653 (1952)
91. Potts, R.B.: Molecular orbital theory of alternant hydrocarbons. J. Chem. Phys. **21**, 758 (1953)
92. Crowe, R.W., Devins, J.C.: Sparking potential and molecular structure of unsaturated hydrocarbon gases. J. Chem. Phys. **33**, 413–418 (1960)
93. Sovers, O., Kauzmann, W.: Role of *d*-hybridization in the Pi molecular orbitals of unsaturated hydrocarbons. J. Chem. Phys. **38**, 813–824 (1963)
94. Ferguson, A.F., Pople, J.A.: Molecular orbital theory of diamagnetism. V. Anisotropies of some aromatic hydrocarbon molecules. J. Chem. Phys. **42**, 1560–1562 (1965)
95. Kekulé, A.: Untersuchungen über aromatische Verbindungen Ueber die Constitution der aromatischen Verbindungen. I. Ueber die Constitution der aromatischen Verbindungen. Justus Liebigs Annalen der Chemie **137**, 129–196 (1866)
96. Borden, W.T., Iwamura, H., Berson, J.A.: Violations of Hund's rule in non-Kekulé hydrocarbons: theoretical prediction and experimental verification. Acc. Chem. Res. **27**, 109–116 (1994)

97. Cui, Z.H., Gupta, A., Lischka, H., Kertesz, M.: Concave or convex π-dimers: the role of the pancake bond in substituted phenalenyl radical dimers. Phys. Chem. Chem. Phys. **17**, 23963–23969 (2015)
98. Ito, S., Nakano, M.: Theoretical molecular design of heteroacenes for singlet fission: tuning the diradical character by modifying π-conjugation length and aromaticity. J. Phys. Chem. C **119**, 148–157 (2015)
99. Das, A., Müller, T., Plasser, F., Lischka, H.: Polyradical character of triangular Non-Kekulé structures, Zethrenes, *p*-Quinodimethane-Linked Bisphenalenyl, and the Clar Goblet in comparison: an extended multireference study. J. Phys. Chem. A **120**, 1625–1636 (2016)
100. Heitler, W., London, F.: Wechselwirkung neutraler Atome und homöopolare Bindung nach der Quantenmechanik. Zeitschrift für Physik **44**, 455–472 (1927)
101. Hund, F.: Linienspektren und Periodisches System der Elemente. Springer, Berlin (1927)
102. Hund, F.: Zur Deutung der Molekelspektren. IV. Zeitschrift für Physik **51**, 759–795 (1928)
103. Miller, J.S., Dixon, D.A., Calabrese, J.C.: Crystal structure of Hexaazaoctadecahydrocoronene Dication $[HAOC]^{2+}$ a singlet benzene dication. Science **240**, 1185–1188 (1988)
104. Heisenberg, W.: Mehrkörperproblem und Resonanz in der Quantenmechanik. Zeitschrift für Physik **38**, 411–426 (1926)
105. Kawakami, T., Yamanaka, S., Mori, W., Yamaguchi, K., Kajiwara, A., Kamachi, M.: No-overlap and orientation principle for ferromagnetic interactions between nitroxide groups. Chem. Phys. Lett. **235**, 414–421 (1995)
106. Yamaguchi, K., Fukui, H., Fueno, T.: Molecular orbital (MO) theory for magnetically interacting organic compounds. Ab-initio MO calculations of the effective exchange integrals for cyclophane-type carbene dimers. Chem. Lett. **15**, 625–628 (1986)
107. Yamaguchi, K., Takahara, Y., Fueno, T.: Ab-initio molecular orbital studies of structure and reactivity of transition metal-oxo compounds. In: Applied Quantum Chemistry, pp. 155–184. Springer, New York (1986)
108. Yamaguchi, K., Takahara, Y., Fueno, T., Nasu, K.: Ab initio MO calculations of effective exchange integrals between transition-metal ions via oxygen dianions: nature of the copper-oxygen bonds and superconductivity. Jpn. J. Appl. Phys. **26**, L1362 (1987)
109. Yamaguchi, K., Jensen, F., Dorigo, A., Houk, K.: A spin correction procedure for unrestricted Hartree-Fock and Møller-Plesset wavefunctions for singlet diradicals and polyradicals. Chem. Phys. Lett. **149**, 537–542 (1988)
110. Yamaguchi, K., Toyoda, Y., Fueno, T.: Ab initio calculations of effective exchange integrals for triplet carbene clusters. Importance of stacking modes for ferromagnetic interactions. Chem. Phys. Lett. **159**, 459–464 (1989)
111. Yamaguchi, K., Okumura, M., Mori, W., Maki, J., Takada, K., Noro, T., Tanaka, K.: Comparison between spin restricted and unrestricted post-Hartree—Fock calculations of effective exchange integrals in Ising and Heisenberg models. Chem. Phys. Lett. **210**, 201–210 (1993)
112. Nishino, M., Yamanaka, S., Yoshioka, Y., Yamaguchi, K.: Theoretical approaches to direct exchange couplings between divalent chromium ions in naked dimers, tetramers, and clusters. J. Phys. Chem. A **101**, 705–712 (1997)
113. Kitagawa, Y., Saito, T., Nakanishi, Y., Kataoka, Y., Matsui, T., Kawakami, T., Okumura, M., Yamaguchi, K.: Spin contamination error in optimized geometry of singlet Carbene ($^1A_1$) by broken-symmetry method. J. Phys. Chem. A **113**, 15041–15046 (2009)
114. McConnell, H.M.: Ferromagnetism in solid free radicals. J. Chem. Phys. **39**, 1910 (1963)
115. McConnell, H.M.: Proceedings of the Robert A. Welch Foundation. Conf. Chem. Res. **11**, 144 (1967)
116. Misra, A., Schmalz, T.G., Klein, D.J.: Clar theory for radical benzenoids. J. Chem. Inf. Model. **49**, 2670–2676 (2009)
117. Hatanaka, M.: Stability criterion for organic ferromagnetism. Theor. Chem. Acc. **129**, 151–160 (2011)

118. Hoffmann, R., Imamura, A., Hehre, W.J.: Benzynes, dehydroconjugated molecules, and the interaction of orbitals separated by a number of intervening σ bonds. J. Am. Chem. Soc. **90**, 1499–1509 (1968)
119. Bischof, P., Gleiter, R., Haider, R.: Through-bond interaction of two mutually perpendicular π systems. A comparison with spiroconjugation. J. Am. Chem. Soc. **100**, 1036–1042 (1978)
120. Post, A.J., Nash, J.J., Love, D.E., Jordan, K.D., Morrison, H.: Organic photochemistry. 107. Photochemical activation of distal functional groups in polyfunctional molecules. Photochemistry and photophysics of the *syn*-7- and *anti*-7-chlorobenzonorbornenes. J. Am. Chem. Soc. **117**, 4930–4935 (1995)
121. Lomas, J.S.: ^{1}H NMR study of through-bond and through-space effects in the hetero-association of pyridine with alkane diols. J. Phys. Org. Chem. **24**, 129–139 (2011)
122. Oka, Y., Inoue, K., Kumagai, H., Kurmoo, M.: Long-range magnetic ordering at 5.5 K for cobalt(II)-hydroxide diamond chains isolated by 17 Å with α-phenylcinnamate. Inorg. Chem. **52**, 2142–2149 (2013)
123. Breslow, R.: Stable 4n PI electron triplet molecules. Pure Appl. Chem. **54**, 927–938 (1982)
124. Awaga, K., Sugano, T., Kinoshita, M.: Ferromagnetic intermolecular interaction in the galvinoxyl radical: cooperation of spin polarization and charge-transfer interaction. Chem. Phys. Lett. **141**, 540–544 (1987)
125. Sugawara, T., Tukada, H., Izuoka, A., Murata, S., Iwamura, H.: Magnetic interaction among diphenylmethylene molecules generated in crystals of some diazodiphenylmethanes. J. Am. Ceram. Soc. **108**, 4272–4278 (1986)
126. Takano, Y., Taniguchi, T., Isobe, H., Kubo, T., Morita, Y., Yamamoto, K., Nakasuji, K., Takui, T., Yamaguchi, K.: Hybrid density functional theory studies on the magnetic interactions and the weak covalent bonding for the phenalenyl radical dimeric pair. J. Am. Chem. Soc. **124**, 11122–11130 (2002)
127. Soriano, M.R., Tsobnang, F., Méhauté, A.L., Wimmer, E.: Study of ferromagnetic properties of molecular magnets based on aminonaphthalenesulfonic acid and aniline. Synth. Met. **76**, 317–321 (1996)
128. Alberola, A., Less, R.J., Pask, C.M., Rawson, J.M., Palacio, F., Oliete, P., Paulsen, C., Yamaguchi, A., Farley, R.D., Murphy, D.M.: A thiazyl-based organic ferromagnet. Angew. Chem. Int. Ed. Engl. **42**, 4782–4785 (2003)
129. Ivanova, A., Baumgarten, M., Karabunarliev, S., Tyutyulkov, N.: Design of ferromagnetic alternating stacks of neutral and ion-radical hydrocarbons. Phys. Chem. Chem. Phys. **5**, 4932–4937 (2003)
130. Takeda, R., Takano, Y., Kitagawa, Y., Kawakami, T., Yamashita, Y., Matsuoka, F., Yamaguchi, K.: Theoretical studies on contributions of SOMO–SOMO and other couplings to the magnetic interaction in radical clusters. Synth. Met. **133–134**, 593–595 (2003)
131. Fujita, W., Awaga, K.: Crystal structure and magnetic properties of a thiazyl organic ferromagnet, BBDTA GaCl4 with Tc = 7.0 K. Chem. Phys. Lett. **388**, 186–189 (2004)
132. Minkov, I., Tadjer, A.: Magnetic interactions in nonalternant mixed molecular radical crystals and mixed ion radical crystals. Int. J. Quant. Chem. **99**, 667–676 (2004)
133. Zhu, L., Yao, K.L., Liu, Z.L.: The electronic structure and the ferromagnetic intermolecular interactions in the crystal of TEMPO radicals. J. Magn. Magn. Mater. **301**, 301–307 (2006)
134. Deumal, M., LeRoux, S., Rawson, J.M., Robb, M.A., Novoa, J.J.: A theoretical study of the magnetism of the α-*p*-cyano-tetrafluorophenyl-dithiadiazolyl radical using a first principles *bottom-up* procedure. Polyhedron **26**, 1949–1958 (2007)
135. Kinoshita, M., Turek, P., Tamura, M., Nozawa, K., Shiomi, D., Nakazawa, Y., Ishikawa, M., Takahashi, M., Awaga, K., Inabe, T., Maruyama, Y.: An organic radical ferromagnet. Chem. Lett. **20**, 1225–1228 (1991)
136. Okumura, M., Kitagawa, Y., Kawakami, T., Yamaguchi, K.: Theoretical calculations of the pressure effect for the β-phase of *p*-NPNN. Polyhedron **28**, 1898–1902 (2009)
137. Kawakami, T., Taniguchi, T., Nakano, S., Kitagawa, Y., Yamaguchi, K.: Theoretical studies on magnetic interactions in many types of organic donor salts: BEDT-TTF, BETS. TMTTF TMTSF. Polyhedron **22**, 2051–2065 (2003)

138. Fukutome, H., Takahashi, A., Ozaki, M.-A.: Design of conjugated polymers with polaronic ferromagnetism. Chem. Phys. Lett. **133**, 34–38 (1987)
139. Klein, D.J., Nelin, C.J., Alexander, S., Matsen, F.A.: High-spin hydrocarbons. J. Chem. Phys. **77**, 3101–3108 (1982)
140. Teki, Y., Takui, T., Itoh, K., Iwamura, H., Kobayashi, K.: Design, preparation and ESR detection of a ground-state nonet hydrocarbon as a model for one-dimensional organic ferromagnets. J. Am. Chem. Soc. **105**, 3722–3723 (1983)
141. Ishida, T., Iwamura, H.: Bis[3-*tert*-butyl-5-(*N*-oxy-*tert*-butylamino)phenyl] nitroxide in a quartet ground state: a prototype for persistent high-spin poly[(oxyimino)-1,3-phenylenes]. J. Am. Chem. Soc. **113**, 4238–4241 (1991)
142. Lahti, P.M., Ichimura, A.S.: Semiempirical study of electron exchange interaction in organic high-spin π-systems. Classifying structural effects in organic magnetic molecules. J. Org. Chem. **56**, 3030–3042 (1991)
143. Pranata, J.: Spin preferences of conjugated polyradicals: the disjoint NBMO analysis. J. Am. Chem. Soc. **114**, 10537–10541 (1992)
144. Yoshizawa, K., Tanaka, K., Yamabe, T.: Ferromagnetic coupling through *m*-phenylene. Molecular and crystal orbital study. J. Phys. Chem. **98**, 1851–1855 (1994)
145. Li, S., Ma, J., Jiang, Y.: Electron correlation and magnetism: a simple molecular orbital approach for predicting ground-state spins of conjugated hydrocarbons. J. Phys. Chem. A **101**, 5587–5592 (1997)
146. Tukada, H., Mochizuki, K.: Long-range magnetic interactions in *trans*-1,4-Cyclohexylene- and 1,3-Adamantylene-bis(*p*-nitrenylbenzene) by π-σ-π hyperconjugation. Org. Lett. **3**, 3305–3308 (2001)
147. Shil, S., Misra, A.: Photoinduced antiferromagnetic to ferromagnetic crossover in organic systems. J. Phys. Chem. A **114**, 2022–2027 (2010)
148. Ivanov, C.I., Olbrich, G., Barentzen, H., Polansky, O.E.: Magnetic properties of alternate nonclassical polymers: the elementary excitation spectrum. Phys. Rev. B **36**, 8712–8718 (1987)
149. Li, J., Tang, A.: Ab initio UHF crystal-orbital studies on ferromagnetic polymers. Chem. Phys. Lett. **170**, 359–363 (1990)
150. Matsumoto, T., Ishida, T., Koga, N., Iwamura, H.: Intramolecular magnetic coupling between two nitrene or two nitroxide units through 1,1-diphenylethylene chromophores. Isomeric dinitrenes and dinitroxides related in connectivity to trimethylenemethane, tetramethyleneethane, and pentamethylenepropane. J. Am. Chem. Soc. **114**, 9952–9959 (1992)
151. Miura, Y., Matsumoto, M., Ushitani, Y., Teki, Y., Takui, T., Itoh, K.: Magnetic and optical characterization of poly(ethynylbenzene) with pendant nitroxide radicals. Macromolecules **26**, 6673–6675 (1993)
152. Yamaguchi, K., Okumura, M., Maki, J., Noro, T.: High-spin ion radicals of polyenes and polyamines. A MO theoretical study. Chem. Phys. Lett. **207**, 9–14 (1993)
153. Tanaka, H.: Magnetism of spin polymers prepared by the oxidative polyrecombination of captodative compounds. Macromol. Symp. **84**, 137–143 (1994)
154. Tanaka, K., Ago, H., Yamabe, T.: Design of ferromagnetic polymers involving organosilicon moieties. Synth. Met. **72**, 225–229 (1995)
155. Dannenberg, J.J., Liotard, D., Halvick, P., Rayez, J.C.: Theoretical studies of high-spin organic molecules. 1. Enhanced coupling between multiple unpaired electrons. J. Phys. Chem. **100**, 9631–9637 (1996)
156. Tyutyulkov, N., Baumgarten, M., Dietz, F.: Polaronic high-spin π-conjugated 1-D polymers with polymethine radicals within the elementary units. Chem. Phys. Lett. **353**, 231–238 (2002)
157. Kaneko, T., Makino, T., Miyaji, H., Teraguchi, M., Aoki, T., Miyasaka, M., Nishide, H.: Ladderlike ferromagnetic spin coupling network on a π-conjugated pendant polyradical. J. Am. Chem. Soc. **125**, 3554–3557 (2003)

158. Zaidi, N.A., Giblin, S.R., Terry, I., Monkman, A.P.: Room temperature magnetic order in an organic magnet derived from polyaniline. Polymer **45**, 5683–5689 (2004)
159. Ma, H., Liu, C., Zhang, C., Jiang, Y.: Theoretical study of very high spin organic π-conjugated polyradicals. J. Phys. Chem. A **111**, 9471–9478 (2007)
160. Fu, H.H., Yao, K.L., Liu, Z.L.: Magnetic properties of very-high-spin organic π-conjugated polymers based on Green's function theory. J. Chem. Phys. **129**, 134706 (2008)
161. Hatanaka, M.: Magnetism in disjoint/non-disjoint composite bands. Chem. Phys. **392**, 90–95 (2012)
162. Qu, Z., Zhang, S., Liu, C., Malrieu, J.P.: Communication: a dramatic transition from nonferromagnet to ferromagnet in finite fused-azulene chain. J. Chem. Phys. **134**, 021101 (2011)
163. Zhanga, J., Wang, R., Wang, L., Baumgarten, M.: Using triazine as coupling unit for intramolecular ferromagnetic coupling of multiradicals. Chem. Phys. **246**, 209–215 (1999)
164. Dias, J.R.: Disjoint molecular orbitals in nonalternant conjugated diradical hydrocarbons. J. Chem. Inf. Comput. Sci. **43**, 1494–1501 (2003)
165. Miyasaka, M., Saito, Y., Nishide, H.: Magnetic force microscopy images of a nanometer-sized, purely organic high-spin polyradical. Adv. Funct. Mater. **13**, 113–117 (2003)
166. Hirai, K., Kamiya, E., Itoh, T., Tomioka, H.: A dendrimer approach to high-spin polycarbenes. Conversion of connectivity from disjoint to non-disjoint by perturbation of nonbonding molecular orbital coefficients. Org. Lett. **8**, 1847–1850 (2006)
167. Álvarez Collado, J.R.: Calculation of the atomic spin densities and energy band gaps of carbon high-spin aromatic (pi) large macromolecular systems. J. Chem. Phys. **129**, 154703 (2008)
168. Ito, A., Ino, H., Tanaka, K.: Electronic structures of newly designed two-dimensional high-spin organic polymers. Polyhedron **28**, 2080–2086 (2009)
169. Li, X., Wang, Q., Jena, P.: Ferromagnetism in two-dimensional carbon chains linked by 1,3,5-benzenetriyl units. J. Phys. Chem. C **115**, 19621–19625 (2011)
170. Hatanaka, M.: Wannier analysis of magnetic graphenes. Chem. Phys. Lett. **484**, 276–282 (2010)
171. Wang, M., Li, C.M.: Magnetic properties of all-carbon graphene-fullerene nanobuds. Phys. Chem. Chem. Phys. **13**, 5945–5951 (2011)
172. Philpott, M.R., Kawazoe, Y.: Graphene nanodots with intrinsically magnetic protrusions. J. Chem. Phys. **136**, 064706 (2012)
173. San-Fabiín, E., Moscardó, F.: Polarized-unpolarized ground state of small polycyclic aromatic hydrocarbons. Int. J. Quant. Chem. **113**, 815–819 (2013)
174. Kawakami, T., Takeda, S., Mori, W., Yamaguchi, K.: Theoretical study of the effective exchange interactions between nitroxides via hydrogen atoms. Chem. Phys. Lett. **261**, 129–137 (1996)
175. Maruta, G., Takeda, S., Imachi, R., Ishida, T., Nogami, T., Yamaguchi, K.: Solid-state high-resolution ^{1}H and ^{2}D NMR study of the electron spin density distribution of the hydrogen-bonded organic ferromagnetic compound 4-hydroxyimino-TEMPO. J. Am. Chem. Soc. **121**, 424–431 (1999)
176. Daigoku, K., Okada, A., Nakada, K.: Theoretical study of intermolecular spin alignments through hydrogen bonding of the carboxy group. Chem. Phys. Lett. **430**, 221–226 (2006)
177. Mishima, A., Nasu, K.: Ferromagnetism in a new type of organic polymer based on benzene rings bridged by carbons. Synth. Met. **22**, 23–33 (1987)
178. Wang, W.Z., Liu, Z.L., Yao, K.L.: Interchain coupling model for quasi-one-dimensional π-conjugated organic ferromagnets. Phys. Rev. B **55**, 12989–12994 (1997)
179. Yoshizawa, K., Kuga, T., Sato, T., Hatanaka, M., Tanaka, K., Yamabe, T.: Through-bond and through-space interactions of organic radicals coupled by *m*-phenylene. Bull. Chem. Soc. Jpn. **69**, 3443–3450 (1996)
180. Ising, E.: Beitrag zur Theorie des Ferromagnetismus. Zeitschrift für Physik **31**, 253–258 (1924)

181. Onsager, L.: Crystal statistics. I. A two-dimensional model with an order-disorder transition. Phys. Rev. **65**, 117–149 (1944)
182. Yang, C.N.: The spontaneous magnetization of a two-dimensional Ising model. Phys. Rev. **85**, 808–816 (1952)
183. Okabe, Y.: Statistical Mechanics, 3rd edn. Shokado, Tokyo (2003)
184. Hansda, S., Pal, A.K., Datta, S.N.: Ferromagnetic nature of silicon-substituted *meta*-xylylene polyradicals. J. Phys. Chem. C **119**, 3754–3761 (2015)
185. Datta, S.N., Pal, A.K., Hansda, S., Latif, I.A.: On the photomagnetism of nitronyl nitroxide, imino nitroxide, and verdazyl-substituted azobenzene. J. Phys. Chem. A **116**, 3304–3311 (2012)
186. Saito, T., Ito, A., Watanabe, T., Kawakami, T., Okumura, M., Yamaguchi, K.: Performance of the coupled cluster and DFT methods for through-space magnetic interactions of nitroxide dimer. Chem. Phys. Lett. **542**, 19–25 (2012)
187. Nishizawa, S., Hasegawa, J.-Y., Matsuda, K.: Theoretical investigation of the β value of the π-conjugated molecular wires by evaluating exchange interaction between organic radicals. J. Phys. Chem. C **117**, 26280–26286 (2013)
188. Bhattacharya, D., Shil, S., Goswami, T., Misra, A., Panda, A., Klein, D.J.: A theoretical study on magnetic properties of bis-TEMPO diradicals with possible application. Comp. Theor. Chem. **1024**, 15–23 (2013)
189. Fukui, K., Yonezawa, T., Shingu, H.: A molecular orbital theory of reactivity in aromatic hydrocarbons. J. Chem. Phys. **20**, 722 (1952)
190. Fukui, K., Yonezawa, T., Nagata, C., Shingu, H.: Molecular orbital theory of orientation in aromatic, heteroaromatic, and other conjugated molecules. J. Chem. Phys. **22**, 1433–1442 (1954)
191. Imamura, A., Aoki, Y., Maekawa, K.: A theoretical synthesis of polymers by using uniform localization of molecular orbitals: proposal of an elongation method. J. Chem. Phys. **95**, 5419–5431 (1991)
192. Aoki, Y., Gu, F.L.: An elongation method for large systems toward bio-systems. Phys. Chem. Chem. Phys. **14**, 7640–7668 (2012)
193. Korchowiec, J., Gu, F.L., Aoki, Y.: Elongation method at restricted open-shell Hartree-Fock level of theory. Int. J. Quant. Chem. **105**, 875–882 (2005)
194. Zhu, X., Aoki, Y.: Development of minimized mixing molecular orbital method for designing organic ferromagnets. J. Comput. Chem. **36**, 1232–1239 (2015)
195. Kitaura, K., Ikeo, E., Asada, T., Nakano, T., Uebayasi, M.: Fragment molecular orbital method: an approximate computational method for large molecules. Chem. Phys. Lett. **313**, 701–706 (1999)
196. Fedorov, D.G., Kitaura, K.: Extending the power of quantum chemistry to large systems with the fragment molecular orbital method. J. Phys. Chem. A **111**, 6904–6914 (2007)
197. Fedorov, D.G., Nagata, T., Kitaura, K.: Exploring chemistry with the fragment molecular orbital method. Phys. Chem. Chem. Phys. **14**, 7562–7577 (2012)
198. Nakano, T., Kaminuma, T., Sato, T., Fukuzawa, K., Akiyama, Y., Uebayasi, M., Kitaura, K.: Fragment molecular orbital method: use of approximate electrostatic potential. Chem. Phys. Lett. **351**, 475–480 (2002)
199. Mochizuki, Y., Koikegami, S., Amari, S., Segawa, K., Kitaura, K., Nakano, T.: Configuration interaction singles method with multilayer fragment molecular orbital scheme. Chem. Phys. Lett. **406**, 283–288 (2005)
200. Chiba, M., Fedorov, D.G., Kitaura, K.: Time-dependent density functional theory with the multilayer fragment molecular orbital method. Chem. Phys. Lett. **444**, 346–350 (2007)
201. Chiba, M., Fedorov, D.G., Kitaura, K.: Time-dependent density functional theory based upon the fragment molecular orbital method. J. Chem. Phys. **127**, 104108 (2007)
202. Mochizuki, Y., Tanaka, K., Yamashita, K., Ishikawa, T., Nakano, T., Amari, S., Segawa, K., Murase, T., Tokiwa, H., Sakurai, M.: Parallelized integral-direct CIS(D) calculations with multilayer fragment molecular orbital scheme. Theor. Chem. Acc. **117**, 541–553 (2007)

203. Chiba, M., Fedorov, D.G., Kitaura, K.: Polarizable continuum model with the fragment molecular orbital-based time-dependent density functional theory. J. Comput. Chem. **29**, 2667–2676 (2008)
204. Chiba, M., Fedorov, D.G., Nagata, T., Kitaura, K.: Excited state geometry optimizations by time-dependent density functional theory based on the fragment molecular orbital method. Chem. Phys. Lett. **474**, 227–232 (2009)
205. Chiba, M., Koido, T.: Electronic excitation energy calculation by the fragment molecular orbital method with three-body effects. J. Chem. Phys. **133**, 044113 (2010)
206. Pruitt, S.R., Fedorov, D.G., Kitaura, K., Gordon, M.S.: Open-shell formulation of the fragment molecular orbital method. J. Chem. Theory Comput. **6**, 1–5 (2010)
207. Yang, W.: Direct calculation of electron density in density-functional theory: implementation for benzene and a tetrapeptide. Phys. Rev. A **44**, 7823–7826 (1991)
208. Yang, W.: Direct calculation of electron density in density-functional theory. Phys. Rev. Lett. **66**, 1438–1441 (1991)
209. Zhao, Q., Yang, W.: Analytical energy gradients and geometry optimization in the divide-and-conquer method for large molecules. J. Chem. Phys. **102**, 9598–9603 (1995)
210. Yang, W., Lee, T.-S.: A density-matrix divide-and-conquer approach for electronic structure calculations of large molecules. J. Chem. Phys. **103**, 5674–5678 (1995)
211. Kobayashi, M., Akama, T., Nakai, H.: Second-order Møller-Plesset perturbation energy obtained from divide-and-conquer Hartree-Fock density matrix. J. Chem. Phys. **125**, 204106 (2006)
212. Kobayashi, M., Imamura, Y., Nakai, H.: Alternative linear-scaling methodology for the second-order Møller-Plesset perturbation calculation based on the divide-and-conquer method. J. Chem. Phys. **127**, 074103 (2007)
213. Kobayashi, M., Nakai, H.: Extension of linear-scaling divide-and-conquer-based correlation method to coupled cluster theory with singles and doubles excitations. J. Chem. Phys. **129**, 044103 (2008)
214. Kobayashi, M., Nakai, H.: Dual-level hierarchical scheme for linear-scaling divide-and-conquer correlation theory. Int. J. Quant. Chem. **109**, 2227–2237 (2009)
215. Kobayashi, M., Nakai, H.: Divide-and-conquer-based linear-scaling approach for traditional and renormalized coupled cluster methods with single, double, and noniterative triple excitations. J. Chem. Phys. **131**, 114108 (2009)
216. Kobayashi, M., Nakai, H.: How does it become possible to treat delocalized and/or open-shell systems in fragmentation-based linear-scaling electronic structure calculations? The case of the divide-and-conquer method. Phys. Chem. Chem. Phys. **14**, 7629–7639 (2012)
217. Kobayashi, M., Yoshikawa, T., Nakai, H.: Divide-and-conquer self-consistent field calculation for open-shell systems: implementation and application. Chem. Phys. Lett. **500**, 172–177 (2010)
218. Nakai, H., Kobayashi, M.: Linear-scaling electronic structure calculation program based on divide-and-conquer method. Procedia Comput. Sci. **4**, 1145–1150 (2011)
219. Yoshikawa, T., Kobayashi, M., Nakai, H.: Linear-scaling divide-and-conquer second-order Møller-Plesset perturbation calculation for open-shell systems: implementation and application. Theor. Chem. Acc. **130**, 411–417 (2011)
220. Chan, G.K.-L., Dorando, J.J., Ghosh, D., Hachmann, J., Neuscamman, E., Wang, H., Yanai, T.: An introduction to the Density Matrix Renormalization Group Ansatz in quantum chemistry. In: Frontiers in quantum systems in chemistry and physics, vol. 18, pp. 49–65. Springer, New York (2008)
221. White, S.R.: Density matrix formulation for quantum renormalization groups. Phys. Rev. Lett. **69**, 2863–2866 (1992)
222. White, S.R.: Density-matrix algorithms for quantum renormalization groups. Phys. Rev. B **48**, 10345 (1993)
223. Mitrushenkov, A.O., Fano, G., Ortolani, F., Linguerri, R., Palmieri, P.: Quantum chemistry using the density matrix renormalization group. J. Chem. Phys. **115**, 6815 (2001)

224. Chan, G.K.-L., Head-Gordon, M.: Highly correlated calculations with a polynomial cost algorithm: a study of the density matrix renormalization group. J. Chem. Phys. **116**, 4462 (2002)
225. Legeza, Ö., Röder, J., Hess, B.: Controlling the accuracy of the density-matrix renormalization-group method: the dynamical block state selection approach. Phys. Rev. B **67**, 125114 (2003)
226. Moritz, G., Reiher, M.: Decomposition of density matrix renormalization group states into a Slater determinant basis. J. Chem. Phys. **126**, 244109 (2007)
227. Zgid, D., Nooijen, M.: On the spin and symmetry adaptation of the density matrix renormalization group method. J. Chem. Phys. **128**, 014107 (2008)
228. Ghosh, D., Hachmann, J., Yanai, T., Chan, G.K.: Orbital optimization in the density matrix renormalization group, with applications to polyenes and β-carotene. J. Chem. Phys. **128**, 144117 (2008)
229. Mizukami, W., Kurashige, Y., Yanai, T.: Communication: Novel quantum states of electron spins in polycarbenes from ab initio density matrix renormalization group calculations. J. Chem. Phys. **133**, 091101 (2010)
230. Kurashige, Y., Yanai, T.: High-performance ab initio density matrix renormalization group method: applicability to large-scale multireference problems for metal compounds. J. Chem. Phys. **130**, 234114 (2009)
231. Kurashige, Y., Yanai, T.: Second-order perturbation theory with a density matrix renormalization group self-consistent field reference function: theory and application to the study of chromium dimer. J. Chem. Phys. **135**, 094104 (2011)
232. Kurashige, Y., Chalupsky, J., Lan, T.N., Yanai, T.: Complete active space second-order perturbation theory with cumulant approximation for extended active-space wavefunction from density matrix renormalization group. J. Chem. Phys. **141**, 174111 (2014)
233. Saitow, M., Kurashige, Y., Yanai, T.: Multireference configuration interaction theory using cumulant reconstruction with internal contraction of density matrix renormalization group wave function. J. Chem. Phys. **139**, 044118 (2013)
234. Yanai, T., Kurashige, Y., Mizukami, W., Chalupský, J., Lan, T.N., Saitow, M.: Density matrix renormalization group for *ab initio* Calculations and associated dynamic correlation methods: a review of theory and applications. Int. J. Quant. Chem. **115**, 283–299 (2015)

Chapter 2
Nonbonding Molecular Orbital Method and Mathematical Proof for Disjoint/Non-disjoint Molecules

Abstract In this chapter, we introduce our own technique, which was developed to design non-disjoint systems with high-spin states more stable than those of disjoint systems, as mentioned in Chap. 1. Pure hydrocarbon (HC) systems are addressed first, because high-spin organic molecules are accessible when non-bonding molecular orbitals (NBMOs) are present as a result of the symmetry of the alternant HC skeleton. This description is then followed by a discussion of heteroatom-included HC (HHC) systems. We explain the basic idea of making non-disjoint combinations between molecules feasible when designing large organic non-disjoint systems with high-spin ground states.

2.1 Introduction

The explanation below is based on mathematics using linear algebra because disjoint or non-disjoint combinations can be defined at a simple Hückel level.

In odd-alternant HCs, all of the carbon atoms can be either starred (*) or unstarred (0) in such a way that two atoms of the same type are not directly joined by a bond. The atoms of one set (*) are numbered from 1 to h and the atoms of the other set (0) are numbered from (h + 1) to n. We define active carbon atoms as "*" and inactive carbon atoms as (0). The equations to be solved for each group can be expressed as follows:

$$\begin{cases} -\varepsilon C_r + \sum_{s=h+1}^{n} \beta_{rs} C_s = 0 & (r = 1, 2, \ldots, h) \\ -\varepsilon C_r + \sum_{s=1}^{h} \beta_{rs} C_s = 0 & (r = h+1, h+2, \ldots, n) \end{cases}. \tag{2.1}$$

Y. Aoki et al., *Quantum Chemical Approach for Organic Ferromagnetic Material Design*, SpringerBriefs in Electrical and Magnetic Properties of Atoms, Molecules, and Clusters,
DOI 10.1007/978-3-319-49829-4_2

The NBMO method [1] is useful to elucidate the nature of radicals and the interactions between them in super-molecules. In alternant HCs, the NBMOs can easily be defined by hand (without a computer), and the NBMO coefficients easily be obtained without the need for computational calculations. Even for non-alternant HCs, most of which are composed of odd-numbered rings, the NBMO levels with $\lambda = 0$ can be found using some special techniques [2]. That is, the carbon atoms that have non-zero coefficients and those with zero coefficients can be recognized by hand for both alternant and non-alternant HCs. Using this method, we can obtain insight into how to combine radical molecules in such a way as to maintain the degeneracy of the levels in the combined super-molecule. In other words, based on their NBMO coefficients, we can determine a means of combining radical molecules so that the energy levels of the NBMOs in the original molecules are retained. This simple treatment would be a first step to satisfy the minimum condition that the system should possess degenerate energy levels, before discussing if the system shows low spin or high spin.

We can prove mathematically that there are two combination methods that maintain two NBMOs even after the intermolecular interaction. One is the formation of linkages between the carbon atoms that have zero NBMO coefficients; this method is shown in Fig. 2.1a. Molecules A and B each have their own single NBMO, and the linkage between the two molecules must occur between the two carbon atoms with zero coefficients in order to maintain the two original NBMO levels. Molecules A and B may be either alternant or non-alternant HCs.

The second method is the formation of a linkage between the two atoms, one of which has a no coefficient in molecule A and another on which has a non-zero coefficient in molecule B. This method is depicted in Fig. 2.1b. Molecule A must be an alternant HC, and molecule B may be either an alternant HC or a non-alternant HC in order to satisfy the condition that the two original NBMOs keep their original energy levels. The former (Fig. 2.1a) corresponds to a "disjoint" linkage, and the latter (Fig. 2.1b) corresponds to a "non-disjoint" linkage. As explained below, both types of linkages can maintain the original NBMO levels "completely (not approximately)" even after the linkage is formed.

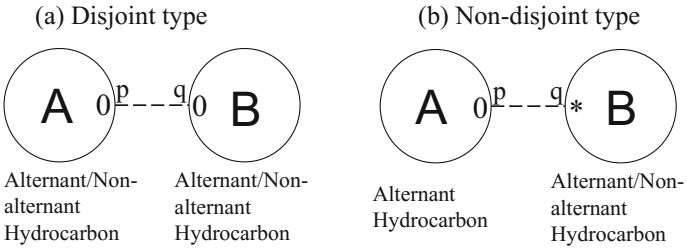

Fig. 2.1 General rule for producing super-molecule that possesses two degenerate NBMOs: **a** disjoint and **b** non-disjoint linkages

The most important difference between the two types of super-molecules is the interaction between the two NBMOs. Disjoint super-molecules have no interactions between their NBMOs, so the electron spins are not induced to produce a high-spin state, while non-disjoint super-molecules are characterized by small interactions induced through exchange integrals, leading to high-spin states due to Hund's rule. This simple concept is not a rule of thumb but can be logically proven using linear algebra without introducing any approximations except those inherent in the Hückel method. First, we present the derivations of the NBMO degeneracy for both disjoint and non-disjoint systems using an atomic-orbital (AO)-based Hamiltonian [3] and then using a molecular-orbital (MO)-based Hamiltonian.

2.2 Atomic-Orbital-Based Proof for Disjoint and Non-disjoint Hydrocarbons

In this section, the derivation of a rule to obtain two degenerate NBMOs in a super-molecule composed of two HC radicals is presented for systems based on pure HCs. In odd-alternant HCs, we can number alternating active carbon atoms, denoted by a star "*", from 1 to h, while avoiding the labelling the neighboring carbon atoms and the other atoms are numbered from (h + 1) to n. The equations for the above two sets can be expressed for molecule A as follows:

$$\begin{cases} -\varepsilon C_r + \sum_{s=h_A+1}^{n_A} \beta_{rs} C_s = 0 & (r = 1, 2, \ldots, h_A) \\ -\varepsilon C_r + \sum_{s=1}^{h_A} \beta_{rs} C_s = 0 & (r = h_A + 1, h_A + 2, \ldots, n_A) \end{cases}, \tag{2.2}$$

where h_{A} represents the number of active (starred) carbons and n_{A} represents the total number of carbon atoms in molecule A. In the same way, the secular equation for molecule B can be expressed using h_{B} as follows:

$$\begin{cases} -\varepsilon C_r + \sum_{s=n_A+h_B+1}^{n} \beta_{rs} C_s = 0 & (r = n_A + 1, \ldots, n_A + h_B) \\ -\varepsilon C_r + \sum_{s=n_A+1}^{n_A+h_B} \beta_{rs} C_s = 0 & (r = n_A + h_B + 1, \ldots, n) \end{cases} \tag{2.3}$$

where the numbering of the carbon atoms in molecule B is from (n_{A} + 1) to n, the total number of carbon atoms. The secular determinant of the two isolated systems (before being linked) is written as

$$\Delta(\varepsilon) = \begin{array}{c|cccc} & \text{* -part of A} & \text{0 - part of A} & \text{* -part of B} & \text{0 - part of B} \\ \hline \text{* -part of A} & -\varepsilon I & \beta_1 & 0 & 0 \\ \text{0 - part of A} & \beta_1^T & -\varepsilon I & 0 & 0 \\ \text{* -part of B} & 0 & 0 & -\varepsilon I & \beta_2 \\ \text{0 - part of B} & 0 & 0 & \beta_2^T & -\varepsilon I \end{array}, \tag{2.4}$$

where $-\varepsilon I$ in the diagonal blocks indicates that the matrix is completely diagonalized, because starred active carbons (or unstarred inactive carbons) cannot be directly combined within a molecule. Off-diagonal blocks are indicated by

$$\beta_1 = \begin{pmatrix} \beta_{1,h_A+1} & \beta_{1,h_A+2} & \cdots & \\ \beta_{2,h_A+1} & \beta_{2,h_A+2} & & \\ \vdots & & \ddots & \\ & & & \beta_{h_A,n_A} \end{pmatrix} \tag{2.5}$$

and

$$\beta_2 = \begin{pmatrix} b_{n_A+1,n_A+h_B+1} & b_{n_A+1,n_A+h_B+2} & \cdots & \\ b_{n_A+2,n_A+h_B+1} & b_{n_A+2,n_A+h_B+2} & & \\ \vdots & & \ddots & \\ & & & b_{n,n} \end{pmatrix}. \tag{2.6}$$

Equations (2.5) and (2.6) provide the interaction terms between the active and inactive carbon atoms within molecules A and B, respectively. Whether an matrix element has value or not depends on bonding information at the Hückel level. That is, off-diagonal block matrices β_1 and β_2 indicate intramolecular bonding information between active and inactive carbon atoms in each molecule.

2.2.1 Hydrocarbons Disjoint (HC-AO-D)

We now consider disjoint combinations. If a link is created between inactive atoms (0) of both molecule A and molecule B, the secular determinant can be written as

$$\Delta(\varepsilon) = \left|\begin{array}{c|c|c|c} -\varepsilon I & \beta_1 & 0 & 0 \\ \hline \beta_1^T & -\varepsilon I & 0 & P \\ \hline 0 & 0 & -\varepsilon I & \beta_2 \\ \hline 0 & P^T & \beta_2^T & -\varepsilon I \end{array}\right|, \tag{2.7}$$

where $P(P^T)$ in the off-diagonal block is added to Eq. (2.4). The $P(P^T)$ matrix includes only one non-zero element because one bond is formed between molecules A and B.

The rank of the matrix can now be reduced using mathematical techniques in linear algebra. That is, the first h columns (the columns corresponding to the *-part of A) and the columns from $(n_A + 1)$ to $(n_A + h_B)$ (the columns corresponding to the *-part of B) of Eq. (2.7) are multiplied times $1/(-\varepsilon)$. Additionally, the rows from $(h_A + 1)$ to n_A (the rows corresponding to the 0-part of A) and the last $n_B - h_B$ rows (the rows corresponding to the 0-part of B) are multiplied times-ε, so that Eq. (2.7) can finally be expressed as

$$\Delta(\varepsilon) = (-\varepsilon)^{2h_A - n_A + 2h_B - n_B} |H_{0-0}| = \varepsilon^2 |H_{0-0}|, \tag{2.8}$$

where

$$|H_{0-0}| = \left|\begin{array}{c|c|c|c} I & \beta_1 & 0 & 0 \\ \hline \beta_1^T & \varepsilon^2 I & 0 & -\varepsilon P \\ \hline 0 & 0 & I & \beta_2 \\ \hline 0 & -\varepsilon P^T & \beta_2^T & \varepsilon^2 I \end{array}\right|. \tag{2.9}$$

In Eq. (2.8), it is assumed that the number of active carbon atoms is greater than the number of inactive carbon atoms by one. Therefore, $2h_A - n_A + 2h_B - n_B$ becomes 1 + 1 and as such, $\Delta(\varepsilon) = 0$ possesses the double solution with $\varepsilon = 0$. This means that no interaction occurs between the original two NBMOs, resulting in so-called “disjoint” molecules.

2.2.2 *Non-disjoint Hydrocarbons Non-disjoint (HC-AO-N)*

Next, we consider non-disjoint combinations. If a link is formed between the inactive atom (0) of molecule A and the active atom (*) of molecule B, the secular determinant can be written as

$$\Delta(\varepsilon)=\begin{vmatrix} -\varepsilon I & \beta_1 & 0 & 0 \\ \beta_1^T & -\varepsilon I & P & 0 \\ 0 & P^T & -\varepsilon I & \beta_2 \\ 0 & 0 & \beta_2^T & -\varepsilon I \end{vmatrix}, \tag{2.10}$$

where the position of the off-diagonal block is different from that in Eq. (2.7) because the link between two molecules is assumed to occur between an inactive carbon atom in molecule A and an active carbon atom in molecule B. After reducing the rank of the matrix using a procedure similar to that applies for Eqs. (2.7) and (2.8), Eq. (2.10) can finally be expressed as

$$\Delta(\varepsilon) = \varepsilon^2 |H_{0-*}|, \tag{2.11}$$

where

$$|H_{0-*}|=\begin{vmatrix} I & \beta_1 & 0 & 0 \\ \beta_1^T & \varepsilon^2 I & P & 0 \\ 0 & P^T & I & \beta_2 \\ 0 & 0 & \beta_2^T & \varepsilon^2 I \end{vmatrix}. \tag{2.12}$$

The presence of $\Delta(\varepsilon) = 0$ in Eq. (2.12) again provides two solutions with $\varepsilon = 0$. It was not immediately obvious whether the *–0 linkage could also cause exactly two solutions with $\varepsilon = 0$, as in the case of a 0–0 linkage, but it became clear by mathematical derivation. The existing of degenerate $\varepsilon = 0$ means that the original

NBMOs are completely reserved, even though some interaction occurs between the two NBMOs; thus, these systems are called "non-disjoint," as will be shown later.

We can conclude that the formation of either 0–0 or 0–* linkages between two molecules that already have NBMOs can maintain the original NBMO levels after linking. The mathematical prove is possible similarly for the case in which a system has more than one NBMO in its isolated molecules because the positions of the starred and unstarred carbons remain unchanged, even though several degenerate NBMOs are mixed with each other. Some applications to several models of organic conjugates systems are presented in the previous paper [3] where the reliability of the indices shown in the next Sect. 2.3 is examined by using both the density functional theory (DFT) with functional methods and the complete active space SCF (CASSCF) calculations.

The above AO-based proof simply addresses whether or not an $\varepsilon = 0$ solution exists after link formation; however, the interaction mechanism on the NBMO reservation are still not clarified. In the next section, an MO-based proof will be provided that permits a more detailed understanding of the reason why the NBMOs remain unchanged, even in a super-molecule, particularly in non-disjoint molecules.

2.3 Molecular-Orbital-Based Proof for Disjoint and Non-disjoint Hydrocarbons

As explained above, we can prove that the two types of linkages formed between two radical molecules can still preserve the original NBMO level in each isolated molecule after the intermolecular interaction. However, the AO-based treatment does not provide any insight into the mixing pattern between the MOs, which is important when trying to predict a high-spin ground state. Therefore, we present a proof of the same results as above using an approach based on the MOs of the two isolated molecules instead of their AOs [4]. The objective of this technique is to enable perturbation calculations to be performed for the newly created bond based on the isolated molecules. However, in fact, we treat the additional term arising from a new bond by a "variational method" using zeroth-order terms before the interaction. Therefore, the results obtained are not just from the lower-order terms of perturbation theory (unlike perturbational MO (PMO) analysis [5]) but provide exactly the same results a using full conventional diagonalization.

In general, the determinant of the secular equation based on the MOs can be expressed as

$$\left| H_{ij} - S_{ij}\,\varepsilon \right| = 0, \tag{2.13}$$

where H_{ij} and S_{ij} are Hamiltonian and overlap matrix elements, respectively, based on the ith and jth MOs. If the MOs used here are already solved for the whole system, H_{ij} corresponds to a diagonal matrix whose diagonal elements are ε_{ii}, and

S_{ij} becomes δ_{ij} for the orthonormal condition, then Eq. (2.13) is already satisfied. However, we can use any kind of basis for i and j because the original Hamiltonian and overlap matrices in the AO basis are unique for the whole system after linkage. The eigenvalues obtained after diagonalization are invariant if the transformations of the matrices are unitary. We suppose here that H_{ij} is the interaction matrix whose basis MOs arise from two isolated molecules before their combination.

For simplicity, considered at the Hückel level, the secular equation for solving a supermolecule from isolated MOs can be written as

$$\left|H_{ij} - \delta_{ij}\,\varepsilon\right| = 0, \tag{2.14}$$

where H_{ij} is a resonance matrix element between particular MOs, i and j, in each isolated molecule, which is given by

$$H_{ij} = \sum_{r}^{n}\sum_{s}^{n} C_{ir}^{(0)} C_{js}^{(0)} \left(H_{rs}^{(0)} + \Delta H_{rs}\right) = \varepsilon_{i}^{(0)}\delta_{ij} + \Delta H \tag{2.15}$$

where the $C_{ri}^{(0)}$ is defined as zeroth-order terms composed of MO coefficients of isolated molecules A and B as

$$\Psi_i(A) = \sum_{r=1}^{n_A} C_{ir}^{(0)}(A)\chi_r, \tag{2.16}$$

$$\Psi_i(B) = \sum_{s=1}^{n_B} C_{is}^{(0)}(B)\chi_s. \tag{2.17}$$

$H_{rs}^{(0)}$ represents the resonance integrals in the isolated molecules before linkage, and ΔH_{rs} represents the resonance matrix elements resulting from the linkage, which, in general, is β_{rs} at the Hückel level, between the rth and sth AOs, each of which belongs to a different molecule. ΔH_{rs} yields non-zero values when $r = p$ and $s = q$ according to the linkage definition shown in Fig. 2.1. We can treat the interaction using perturbation theory to estimate the linkage effect between the two molecules, where ΔH_{rs} is defined as a perturbation applied to the zeroth-order wavefunctions given in Eqs. (2.16) and (2.17). To reach the correct solution, however, perturbation theory enables terms beyond the second-order perturbation energy to be obtained. Therefore, we apply here a variational treatment using the secular equation to solve the interaction directly, not in the AO basis as for the conventional method, but in a zeroth-order MO basis. The results thus obtained by solving the zeroth-order MO-based secular determinant must be completely identical to those obtained by solving the whole system directly by conventional AO-based secular determinants. Therefore, we can discuss and analyze the results by supposing a completely correct solution in the framework of a given equation. This point is the advantage of the MO-based variational method compared to a perturbation method.

2.3.1 Hydrocarbons Disjoint (HC-MO-D)

We consider the linkage between two unstarred carbon atoms, one of which belongs to molecule A and the other to molecule B, regardless of whether the molecule is alternant or non-alternant hydrocarbon. The secular equation corresponding to Eq. (2.14) in the disjoint combination can be expressed as

$$\Delta_n^{Dis}(\varepsilon) = \begin{array}{c|cccc|cccc|} & & & N_A & & & & N_B & \\ & & & \downarrow & & & & \downarrow & \\ & \varepsilon_1^{(A)}-\varepsilon & & & & H_{11} & \cdots\cdots & & H_{1n_B} \\ & & \varepsilon_2^{(A)}-\varepsilon & 0 & 0 & & & 0 & \\ N_A \rightarrow & 0 & & -\varepsilon & 0 & 0 & & 0 & 0 \\ & 0 & & 0 & & & & 0 & \\ & & \ddots & & \varepsilon_{n_A}^{(A)}-\varepsilon & H_{n_A1} & \cdots\cdots & & H_{n_An_B} \\ & H_{11} & \cdots\cdots & & H_{1n_A} & \varepsilon_1^{(B)}-\varepsilon & & & \\ & & & 0 & & & \ddots & 0 & 0 \\ N_B \rightarrow & 0 & 0 & 0 & & 0 & & -\varepsilon & 0 \\ & & & 0 & & 0 & & 0 & \\ & H_{n_B1} & \cdots\cdots & & H_{n_Bn_A} & & & & \varepsilon_{n_B}^{(B)}-\varepsilon \end{array}, \tag{2.18}$$

where n_A and n_B represent the numbers of MOs of molecules A and B, respectively, and N_A and N_B indicate the NBMO levels of molecules A and B, respectively. $\varepsilon_i^{(A)}$ and $\varepsilon_i^{(B)}$ correspond to the orbital energies of molecules A and B, respectively, which are already solved in the isolated molecule and therefore fully diagonalized within each subspace. The NBMO level in each molecule with one radical has zero orbital energy if the Coulomb integral α is supposed to be 0 in the Hückel method; then, the central element in each diagonal element related to N_A or N_B is given by $(0 - \varepsilon)$. The most significant feature of this expression can be seen in off-diagonal sub-blocks, where all the matrix elements related to N_A or N_B in the two molecules are given by zero, as described below.

For a disjoint combination, the secular equation corresponding to Eq. (2.18) can be expressed as

$$\begin{aligned} \Delta H_{iN_A} &= \left(\sum_r^{\text{on A}} + \sum_r^{\text{on B}}\right)\left(\sum_s^{\text{on A}} + \sum_s^{\text{on B}}\right) C_{ir}^{(0)} C_{N_As}^{(0)} \Delta H_{rs} \\ &= \sum_r^{\text{on B}} \sum_s^{\text{on A}} C_{ir}^{(0)} C_{N_As}^{(0)} \Delta H_{rs} = 0 \quad (i = 1, 2, \ldots, n) \end{aligned} \tag{2.19}$$

$$\begin{aligned}\Delta H_{N_A j} &= \left(\sum_{r}^{\text{on A}} + \sum_{r}^{\text{on B}}\right)\left(\sum_{s}^{\text{onA}} + \sum_{s}^{\text{onB}}\right) C_{N_A r}^{(0)} C_{js}^{(0)} \Delta H_{rs} \\ &= \sum_{r}^{\text{on A}} \sum_{s}^{\text{on B}} C_{N_A r}^{(0)} C_{js}^{(0)} \Delta H_{rs} = 0 \quad (j = 1, 2, \ldots, n)\end{aligned} \tag{2.20}$$

$$\begin{aligned}\Delta H_{i N_B} &= \left(\sum_{r}^{\text{on A}} + \sum_{r}^{\text{on B}}\right)\left(\sum_{s}^{\text{on A}} + \sum_{s}^{\text{on B}}\right) C_{ir}^{(0)} C_{N_B s}^{(0)} \Delta H_{rs} \\ &= \sum_{r}^{\text{on A}} \sum_{s}^{\text{on B}} C_{ir}^{(0)} C_{N_B s}^{(0)} \Delta H_{rs} = 0 \quad (i = 1, 2, \ldots, n)\end{aligned} \tag{2.21}$$

$$\begin{aligned}\Delta H_{N_B j} &= \left(\sum_{r}^{\text{on A}} + \sum_{r}^{\text{on B}}\right)\left(\sum_{s}^{\text{on A}} + \sum_{s}^{\text{on B}}\right) C_{N_B r}^{(0)} C_{js}^{(0)} \Delta H_{rs} \\ &= \sum_{r}^{\text{on A}} \sum_{s}^{\text{on B}} C_{N_B r}^{(0)} C_{js}^{(0)} \Delta H_{rs} = 0 \quad (j = 1, 2, \ldots, n),\end{aligned} \tag{2.22}$$

where it is evident that at least one coefficient, either the rth or the sth, is zero because the coefficients under discussion are related to N_A or N_B even though $\Delta H_{rs}(=\Delta H_{pq})$ is non-zero at the linkage position. On the other hand, $\Delta H_{rs} = 0$ when both of the coefficients in each equation are non-zero, because the linkage is done only between the pth and qth AOs. Finally, Eqs. (2.19)–(2.22) must be zero. Therefore, two NBMOs with $\varepsilon = 0$ in the isolated molecules are not mixed at all with any other elements; that is, they are block-diagonalized for the two elements, thus keeping the original NBMO levels unchanged even after solving the secular equation. This type of mathematical proof is not easy to obtain using the perturbation method, since the full higher-order perturbation series must be successively calculated to achieve complete convergence. Therefore, using MO-based determinants, two clear solutions of Eq. (2.18) can be obtained:

$$\Delta_n^{Dis}(\varepsilon) = (-\varepsilon)^2 \Delta_{n-2}^{Dis}(\varepsilon). \tag{2.23}$$

It was demonstrated that two NBMO levels are maintained even after the formation of an intermolecular linkage between two carbon atoms with zero coefficients.

2.3.2 *Hydrocarbons Non-disjoint (HC-MO-N)*

We now consider the case of a non-disjoint linkage where an unstarred carbon in molecule A is combined with a starred carbon in molecule B. To maintain the two

NBMO levels after the linkage is formed, we found that molecule A, in which an unstarred carbon atom joins with molecule B, should be an alternant HC that obeys the pairing theorem. That is, the orbital energy should have a relationship between the $(n_A - i + 1)$th and ith energy levels that corresponds to

$$\varepsilon_{n_A - i + 1} = \varepsilon_i. \tag{2.24}$$

In addition, the coefficients in molecule A must fulfill the condition so that the $(n_A - i + 1)$th MO coefficient is given by a constant multiple of the ith MO coefficient:

$$C^{(A)}_{n_A - i + 1, r} = k_{ir} C^{(A)}_{ir}, \tag{2.25}$$

where $k_{ir} = -1$ for unstarred atoms when $k_{ir} = 1$ for starred atoms, and vice versa. For molecule B, no restriction is imposed on the coefficients to maintain the energy of the NBMO. Using the relationship described by Eq. (2.25), the matrix element between the $(n_A - i + 1)$th and its paired ith MO can be expressed as

$$H^{(AB)}_{n_A - i + 1, j} = \sum_r^{n_A} \sum_s^{n_B} C^{(A)}_{n_A - i + 1, r} C^{(B)}_{js} H^{(AB)}_{rs} = \sum_r^{n_A} \sum_s^{n_B} k_{ir} C^{(A)}_{ir} C^{(B)}_{js} H^{(AB)}_{rs} = k_{ip} H^{(AB)}_{ij}, \tag{2.26}$$

where $k_{ip} = \pm 1$. Mathematical proof that the two NBMOs keep their NBMO levels even after the formation of a linkage between starred and unstarred atoms is shown below.

In this case, the secular equation corresponding to the disjoint combination (i.e., Eq. (2.18)) can instead be expressed using Eqs. (2.24)–(2.26) as

$$\Delta_n^{Non\text{-}dis}(\varepsilon) = \begin{array}{c|ccc|ccc} & N_A \downarrow & & & N_B \downarrow & & \\ \hline \varepsilon_1^{(A)} - \varepsilon & & & & H_{11} & \cdots & H_{1N_B} \\ \varepsilon_2^{(A)} - \varepsilon & 0 & 0 & & \cdots & & \cdots \\ N_A \rightarrow & 0 & -\varepsilon & 0 & 0 & 0 & 0 \\ & 0 & 0 & -\varepsilon_2^{(A)} - \varepsilon & & & \\ & & & -\varepsilon_1^{(A)} - \varepsilon & k_i H_{11} & \cdots & k_i H_{1N_B} \\ \hline H_{11} & \cdots & & k_i H_{11} & \varepsilon_1^{(B)} - \varepsilon & & \\ & 0 & & & & 0 & 0 \\ N_B \rightarrow & H_{1N_B} & 0 & k_i H_{1N_B} & 0 & -\varepsilon & 0 \\ & \cdots & 0 & & 0 & 0 & \\ & H_{1N_B} & \cdots & k_i H_{1N_B} & & & \varepsilon_{N_B}^{(B)} - \varepsilon \end{array}, \tag{2.27}$$

where the Coulomb integral term in the Hückel method was set to zero (i.e., $\alpha = 0$) for simplicity. It can be seen that the column and line along N_A are all zero except

for the diagonal element, $-\varepsilon$, while those along N_B have non-zero values in the off-diagonal blocks, which differs from the case of disjoint linkages. This determinant obviously provides one solution with $\varepsilon = 0$. By reducing the rank of the determinant $\Delta_{n-1}(\varepsilon)$ after extracting the isolated $-\varepsilon$, we can extract another $-\varepsilon$ from a series expansion of this part. Then Eq. (2.27) can simply be expressed as

$$\begin{aligned}\Delta_n^{Non-dis}(\varepsilon) = (-\varepsilon)\Bigg\{ & (-\varepsilon)\sum_m \Delta_{n-m}^{Non-dis} - \left(\frac{\varepsilon_{n'_A}^{(A)} + \varepsilon}{k_{n'_A}}\right)\left(\varepsilon_1^{(B)} - \varepsilon\right)\left(\varepsilon_2^{(B)} - \varepsilon\right) \\ & \cdots(-\varepsilon)\cdots\left(\varepsilon_{n_B-1}^{(B)} - \varepsilon\right)\left(\varepsilon_{n_B}^{(B)} - \varepsilon\right)\Bigg\} \\ = {} & (-\varepsilon)^2\Delta_{n-2}^{Non-dis}(\varepsilon).\end{aligned} \tag{2.28}$$

Finally, the determinant for a non-disjoint linkage exhibits the same form as Eq. (2.23), which was derived for a disjoint linkage, and also provides doubly degenerate NBMO levels after the linkage. However, the process for the creation of $(-\varepsilon)^2$ terms in non-disjoint linkage is different from that used for disjoint linkages. Disjoint linkages contain two isolated NBMOs that maintain their levels at the energy of the isolated molecules simply because there are no interactions with other orbitals, while a non-disjoint linkage contains one interacting NBMO in addition to one isolated NBMO. The presence of an interacting NBMO means that the linked carbon atom that has coefficients causes an interaction with the (non-NBMO) orbitals in the other molecule while still maintaining the original NBMO level, even after the interaction, because of the condition that molecule A must fulfill the pairing theorem, that is, it must be an alternant HC.

A simple model of the linkage between two allyl radicals, as shown in Fig. 2.2, is used for specific elucidation of (a) disjoint and (b) non-disjoint linkages. The secular determinants to be solved based on the zeroth-order MOs (isolated two allyl radicals), corresponding to Eqs. (2.18) and (2.27), are also given for disjoint (Eq. (2.29)) and non-disjoint (Eq. (2.30)) linkages, respectively.

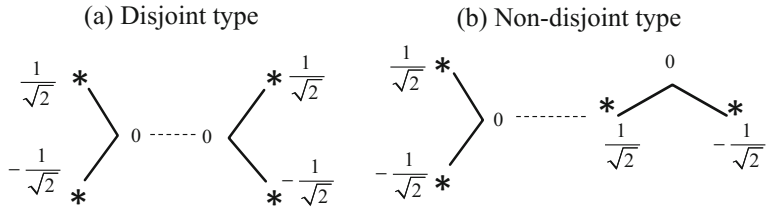

Fig. 2.2 MO coefficients of **a** disjoint and **b** non-disjoint HCs following linkage formation between two allyl radicals

$$\Delta_6^{Dis}(\varepsilon) = \begin{vmatrix} \varepsilon_1-\varepsilon & 0 & 0 & \frac{\beta}{2} & 0 & -\frac{\beta}{2} \\ 0 & \varepsilon_2-\varepsilon & 0 & 0 & 0 & 0 \\ 0 & 0 & \varepsilon_3-\varepsilon & -\frac{\beta}{2} & 0 & \frac{\beta}{2} \\ \frac{\beta}{2} & 0 & -\frac{\beta}{2} & \varepsilon_1-\varepsilon & 0 & 0 \\ 0 & 0 & 0 & 0 & \varepsilon_2-\varepsilon & 0 \\ -\frac{\beta}{2} & 0 & \frac{\beta}{2} & 0 & 0 & \varepsilon_3-\varepsilon \end{vmatrix} = 0 \tag{2.29}$$

$$\Delta_6^{Non-dis}(\varepsilon) = \begin{vmatrix} \varepsilon_1-\varepsilon & 0 & 0 & \frac{\sqrt{2}}{4}\beta & \frac{\beta}{2} & \frac{\sqrt{2}}{4}\beta \\ 0 & \varepsilon_2-\varepsilon & 0 & 0 & 0 & 0 \\ 0 & 0 & \varepsilon_3-\varepsilon & -\frac{\sqrt{2}}{4}\beta & -\frac{\beta}{2} & -\frac{\sqrt{2}}{4}\beta \\ \frac{\sqrt{2}}{4}\beta & 0 & -\frac{\sqrt{2}}{4}\beta & \varepsilon_1-\varepsilon & 0 & 0 \\ \frac{\beta}{2} & 0 & -\frac{\beta}{2} & 0 & \varepsilon_2-\varepsilon & 0 \\ \frac{\sqrt{2}}{4}\beta & 0 & -\frac{\sqrt{2}}{4}\beta & 0 & 0 & \varepsilon_3-\varepsilon \end{vmatrix} = 0 \tag{2.30}$$

The first diagonal block in each matrix represents the secular equation for the left allyl molecule and the second diagonal block indicates that for the right allyl molecule in each of the linkage types shown in the upper figure. It is evident that Eq. (2.29) yields two isolated NBMOs, $(\varepsilon_2 - \varepsilon)^2$, that do not mix with other terms, while Eq. (2.30) gives one isolated NBMO, $(\varepsilon_2 - \varepsilon)$, from the left allyl molecule and another NBMO, $(\varepsilon_2 - \varepsilon)$, from the right allyl molecule that will interact with ε_1 by $\beta/2$ and with ε_3 by $-\beta/2$ in the left allyl molecule; these elements are finally cancelled after the interaction. These matrices in the secular equations can be understood from the orbital interactions before and after the linkage, schematically presented in Fig. 2.3 for disjoint (upper) and non-disjoint (lower) linkages.

The upper interaction model in Fig. 2.3 corresponds to the case in which two original NBMOs are still isolated after the interaction, in what is known as a "disjoint" linkage, and the lower interaction model to the case in which one NBMO interacts while the other remains isolated, in what is known as a "non-disjoint" linkage. In the latter case, it is evident that the NBMO from the allyl molecule on the right maintains its original level, $\varepsilon = \alpha$, even following the interaction between the occupied and unoccupied orbitals in the allyl molecule left by $\beta/2$ and $-\beta/2$, respectively, corresponding to the terms in Eq. (2.30). The NBMO from the right-hand side (where the starred atom is the linkage position) remains unchanged as a result of the interaction with the other orbitals in the allyl molecule on the left. Non-disjoint linkages keep the original NBMOs when the left molecule satisfies the pairing theorem because the stabilization (resulting from a decrease in the energy caused by the interaction between the occupied orbital ε_1 in the left allyl and the NBMO in the right allyl) and destabilization (resulting from an increase in the energy caused by the interaction between the unoccupied orbital ε_3 in the left allyl and the NBMO in the right allyl) completely cancel, resulting in an NBMO level that is unchanged from the original.

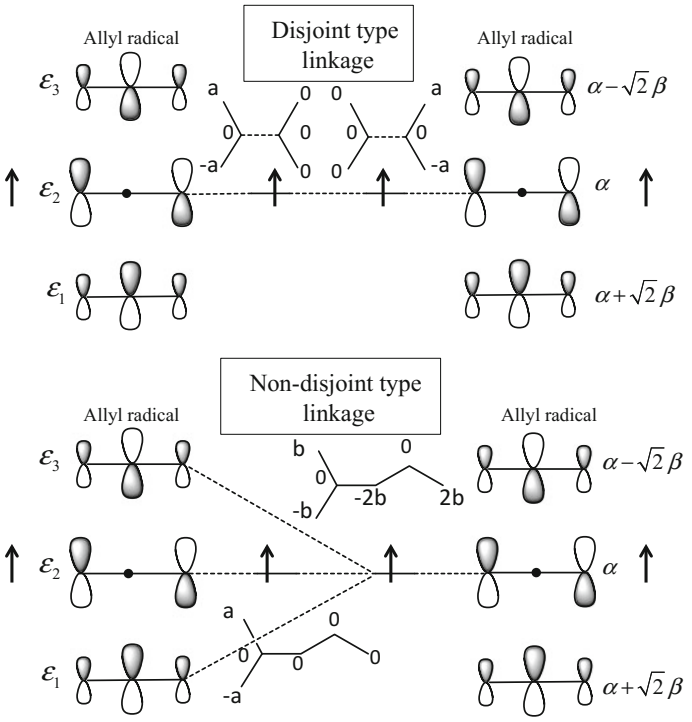

Fig. 2.3 Schematic illustrations of orbital interactions in disjoint and non-disjoint linkages between two allyl radicals

Therefore, as shown in the right-hand side of Fig. 2.1, molecule A, in which the unstarred atom is linked with molecule B, must be restricted to an alternant HC that satisfies the pairing theorem. This feature is the so-called 0–* linked non-disjoint effect caused by the unstarred carbon atom of the alternant HC and a starred carbon atom of an alternant or non-alternant HC. That is, a weak interaction between two radicals through an indirect interaction between the NBMO in molecule B and the non-NBMO orbitals in molecule A might lead to high spin stabilization. The maintenance of degeneracy is related to Hund's rule, which states that the term with the maximum multiplicity has the lowest energy for a given electron configuration. Therefore, the non-disjoint linkages described here would apply to the design of high spin organic polymers that could potentially show magnetic properties.

On the contrary, as described in Sect. 2.3.1, a disjoint linkage is useless from a magnetic design point of view because no interactions between radicals can be expected. Finally, we can conclude that only a non-disjoint linkage between an unstarred carbon atom in an alternant HC and a starred carbon atom in an alternant HC or a non-alternant HC can possibly generate a high-spin state in the resulting super-molecule. This concept can be also applied to the polyradical systems seen in one-dimensional polymers or two-dimensional sheets.

2.4 Atomic-Orbital-Based Proof for Disjoint and Non-disjoint Heteroatom-Included Hydrocarbons

The above mentioned method of predicting NBMO degeneracy in super-molecules supposes pure HC systems, but, for wider application, can be extended to systems that include heteroatoms. Most high-spin organic systems possess heteroatoms, and, therefore, any rule that can be applied only to pure HC systems is of little use for the general design of ferromagnets. It is necessary to determine a rule that can also be employed to design techniques that incorporate heteroatoms into HC compounds while maintaining the original NBMO levels even after two molecules are linked in a disjoint manner. To be widely applicable, the rule should be as flexible as possible about the position of the heteroatoms. That is to say, a simple method of replacing some carbon atoms in an HC with heteroatoms while reserving their NBMO levels is necessary. By systematical searching at the Hückel level, we showed that there are two possible linkage patterns in a super-molecule that can result in two NBMOs (not necessarily $\varepsilon = \alpha$) in the dimer after the linkage is formed. The first suitable linkage can occur when all the starred carbons are replaced by identical heteroatoms (denoted as "Type-I" hereafter) and the other can occur when some or all of the unstarred carbon atoms are replaced by the same or different heteroatoms (denoted as "Type-II" hereafter). Therefore, we can divide the super-molecule into two molecules, each of which has an NBMO and can then construct a mathematical proof to understand why these systems make it possible to maintain the parent NBMOs at the Hückel level. All of the isolated molecules capable of forming degenerate NBMOs are first classified as Type-I or Type-II; an example of this is shown in Fig. 2.4. Type-I provides an NBMO with $\lambda = x\beta$; the remaining levels are distributed symmetrically, satisfying the paring theorem around $\lambda = x\beta/2$. On the other hand, for Type-II molecules, the NBMO level maintains $\lambda = 0$, but the paring theorem is not satisfied because the heteroatoms that replace the inactive carbon atoms destroy the orbital symmetry even though they do not affect the NBMO level. Using these properties in HHC systems, we can discuss super-molecules that maintain their NBMO levels after linkage formation. Some examples of non-disjoint linkages considered for Type-I and Type-II molecules are depicted in the same figure.

Mathematical proofs that Type-I and Type-II systems maintain the NBMOs of their parent molecules are described below for both disjoint and non-disjoint linkages using both AO-and MO-based secular equations.

To understand the electronic states of HHC systems at the Hückel level, we first consider Type-I, in which all of the starred carbons are replaced by a unique heteroatom, X. We suppose that the Coulomb term on the heteroatom is corrected as x through resonance integral β as

$$\alpha_X = \alpha + x\beta, \tag{2.31}$$

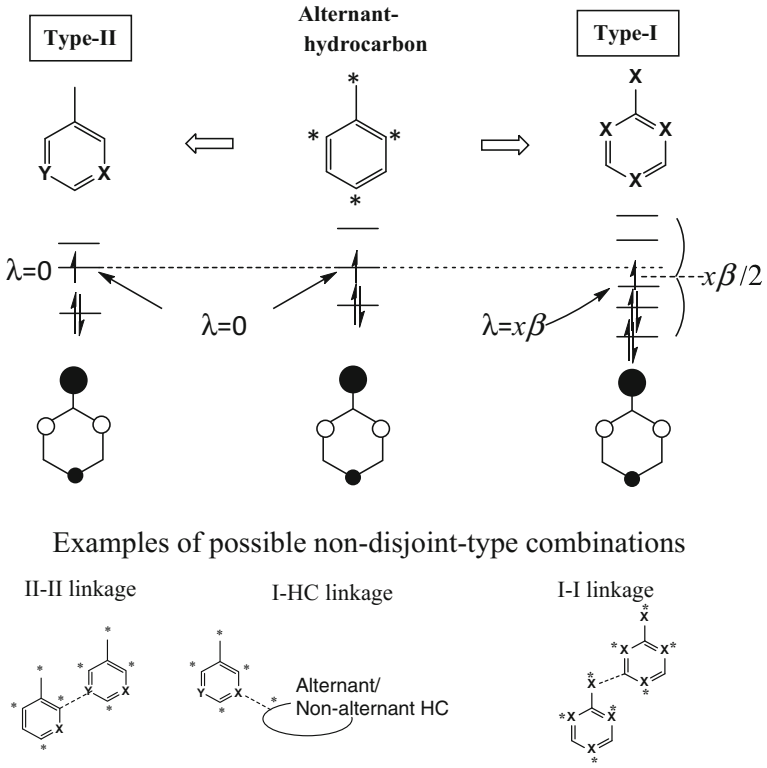

Fig. 2.4 Energy levels of benzyl radical (alternant HC) and related Type-I and Type-II HHCs. Examples of possible non-disjoint combinations are depicted in the lower part of this figure

and that the resonance integral between the carbon (C) and heteroatom (X) is corrected as

$$\beta_{CX} = l\beta. \tag{2.32}$$

The adjusted diagonal term in the secular equation in the AO base is

$$\alpha_X - \varepsilon = -\varepsilon + x\beta \quad (\text{for } \alpha = 0), \tag{2.33}$$

If all of the starred carbon atoms are replaced with the same type of heteroatom with a Coulomb integral of α_X, following the method of Tyutyulkov and Polansky [6], the secular equations show the following forms under the nearest-neighbor approximation in the Hückel method:

$$\begin{cases} (-\varepsilon + x\beta)C_r + \sum_{s=h+1}^{n} \beta_{rs} C_s = 0 & (r = 1, 2, \ldots, h) \\ -\varepsilon C_r + \sum_{s=1}^{h} \beta_{rs} C_s = 0 & (r = h+1, h+2, \ldots, n) \end{cases}, \tag{2.34}$$

where h is the number of starred atoms. The secular determinant is given in each submatrix of starred and unstarred atoms by

$$\Delta(\varepsilon) = \begin{array}{c|c|c} & \text{*-part} & \text{0-part} \\ \hline \text{*-part} & (-\varepsilon + x\beta)I & \beta \\ \hline \text{0-part} & \beta^T & -\varepsilon I \end{array}, \tag{2.35}$$

where I is the unit matrix and β is the resonance integral between the starred and unstarred atoms in neighboring molecules and has the form

$$\beta = \begin{pmatrix} \beta_{1,h+1} & \beta_{1,h+2} & \cdots & \\ \beta_{2,h+1} & \beta_{2,h+2} & & \\ \vdots & & \ddots & \\ & & & \beta_{h,n} \end{pmatrix},$$

and β^{T} represents the transposed matrix of β. By multiplying the first h columns (the columns corresponding to the *-part) of Eq. (2.35) times $1/(-\varepsilon + x\beta)$ and multiplying the last n–h rows (the rows corresponding to the 0-part) times $(-\varepsilon + x\beta)$, one obtains the following identity:

$$\Delta(\varepsilon) = (-\varepsilon + x\beta)^{2h-n} \begin{array}{c|c} I & \beta \\ \hline \beta^T & \varepsilon(\varepsilon - x\beta)I \end{array}. \tag{2.36}$$

In general, $\Delta(\varepsilon) = 0$ has $(2\,h - n)$ degenerate solutions corresponding to the NBMO level $\varepsilon = x\beta$. For simplicity, if $(2\,h - n) = 1$ (i.e., the molecule is an odd-alternant molecule), then molecules of this type have one NBMO with $\varepsilon = x\beta$.

2.4.1 Heteroatom-Included Hydrocarbon Type-I Disjoint (HHC-AO-I-D)

We have defined the substitution in which all of the starred carbon atoms are replaced by the same type of heteroatoms as Type-I. First, we suppose a disjoint linkage, that is, a linkage between the unstarred atom of molecule A (the 0-position of A: A(0)) and the unstarred atom of molecule B (the 0-position of B: B(0)). The secular determinant is expressed as

$$\Delta_n^{Dis}(\varepsilon)[\text{Type-I}] = \begin{array}{c|cccc} & \mathrm{A}(*) & \mathrm{A}(0) & \mathrm{B}(*) & \mathrm{B}(0) \\ \hline \mathrm{A}(*) & (-\varepsilon + x\beta)I & \beta_1 & 0 & 0 \\ \mathrm{A}(0) & \beta_1^T & -\varepsilon I & 0 & P \\ \mathrm{B}(*) & 0 & 0 & (-\varepsilon + x\beta)I & \beta_2 \\ \mathrm{B}(0) & 0 & P^T & \beta_2^T & -\varepsilon I \end{array}, \tag{2.37}$$

where $x\beta$ in the diagonal blocks represents the Coulomb term of the starred heteroatoms, all of which replace the original starred carbons. P has only one non-zero element, because only one new bond is assumed between molecules A and B. β_1 and β_2 are the resonance integrals between starred and unstarred atoms within molecules A and B, respectively. After reducing the rank, Eq. (2.37) can simply be written as

$$\Delta_n^{Dis}(\varepsilon)[\text{Type-I}] = (-\varepsilon + x\beta)^2 \Delta_{n-2}^{Dis}(\varepsilon)[\text{Type-I}], \tag{2.38}$$

where

$$\Delta_{n-2}^{Dis}(\varepsilon)[\text{Type-I}] = \begin{array}{c|cccc} I & \beta_1 & 0 & 0 \\ \hline \beta_1^T & \varepsilon(\varepsilon - x\beta)I & 0 & (-\varepsilon + x\beta)P \\ \hline 0 & 0 & I & \beta_2 \\ \hline 0 & (-\varepsilon + x\beta)P^T & \beta_2^T & \varepsilon(\varepsilon - x\beta)I \end{array}, \tag{2.39}$$

giving two solutions with $\varepsilon = x\ \beta$ when $\Delta_n^{Dis}(\varepsilon)[\text{Type-I}] = 0$.

2.4.2 Heteroatom-Included Hydrocarbon Type-I Non-disjoint (HHC-AO-I-N)

Next, non-disjoint linkages are discussed to show that two NBMOs are preserved in the situation in which a linkage exists between the inactive atom (0) of molecule A (A(0)) and the active atom (*) of molecule B (B(*)). The secular determinant in this case is written as

$$\Delta_n^{Non-dis}(\varepsilon)[\text{Type-I}]= \begin{array}{c|cccc} & \mathrm{A}(*) & \mathrm{A}(0) & \mathrm{B}(*) & \mathrm{B}(0) \\ \hline \mathrm{A}(*) & (-\varepsilon+x\beta)I & \beta_1 & 0 & 0 \\ \hline \mathrm{A}(0) & \beta_1^T & -\varepsilon I & P & 0 \\ \hline \mathrm{B}(*) & 0 & P^T & (-\varepsilon+x\beta)I & \beta_2 \\ \hline \mathrm{B}(0) & 0 & 0 & \beta_2^T & -\varepsilon I \end{array}. \tag{2.40}$$

The multiplications to reduce the rank can be implemented in the same manner as was used for Eq. (2.37) so that Eq. (2.40) becomes

$$\Delta_n^{Non-dis}(\varepsilon)[\text{Type-I}] = (-\varepsilon+x\beta)^2\Delta_{n-2}^{Non-dis}(\varepsilon)[\text{Type-I}], \tag{2.41}$$

where

$$\Delta_{n-2}^{Non-dis}(\varepsilon)[\text{Type-I}]= \begin{array}{cccc} I & \beta_1 & 0 & 0 \\ \hline \beta_1^T & \varepsilon(\varepsilon-x\beta)I & P & 0 \\ \hline 0 & P^T & I & \beta_2 \\ \hline 0 & 0 & \beta_2^T & \varepsilon(\varepsilon-x\beta)I \end{array}. \tag{2.42}$$

Then, $\Delta_n^{Non-dis}(\varepsilon)[\text{Type-I}] = 0$ provides two solutions with $\varepsilon = x\beta$. However, the difference between the physical meanings of Eqs. (2.38) and (2.41) for the disjoint and non-disjoint linkages, respectively, is not apparent, apart from the fact that both of them have the same factor of $(-\varepsilon+x\beta)^2$ in the final form. The magnitude of the interaction between the NBMOs is important for producing a high-spin state, but

this treatment based on AOs cannot provide such information. This problem can be solved by treating the interaction between NBMOs with an MO-based expression of the secular equation, by which the differences between Eqs. (2.38) and (2.41) will be rationalized in Sect. 2.5 using polyene with odd-number carbon atoms as an example.

2.4.3 *Heteroatom-Included Hydrocarbon Type-II Disjoint (HHC-AO-II-D)*

Next, we explore another case that provides degenerate NBMOs after a linkage is formed between HCs that include heteroatoms. This case is defined as Type-II, in which arbitrary inactive atoms (0) of molecules A and B are replaced with arbitrary heteroatoms. We again suppose a disjoint linkage first, that is, between A(0) and B (0). In the same manner as for the case of the Type-I disjoint linkage, i.e., Eq. (2.37), the secular determinant can be expressed as

$$\Delta_n^{Non-dis}(\varepsilon)\,[\text{Type-II}] = \begin{array}{c|cccc} & \mathrm{A}(*) & \mathrm{A}(0) & \mathrm{B}(*) & \mathrm{B}(0) \\ \hline \mathrm{A}(*) & -\varepsilon I & \beta_1 & 0 & 0 \\ \mathrm{A}(0) & \beta_1^T & A_1 & P & 0 \\ \mathrm{B}(*) & 0 & P^T & -\varepsilon I & \beta_2 \\ \mathrm{B}(0) & 0 & 0 & \beta_2^T & B_1 \end{array}, \tag{2.43}$$

where

$$A_1 = \begin{pmatrix} -\varepsilon & & & & & & \\ & \ddots & & & & & \\ & & -\varepsilon + x\beta_i & & 0 & & \\ & & & \ddots & & & \\ & & 0 & & -\varepsilon + x\beta_j & & \\ & & & & & \ddots & \\ & & & & & & -\varepsilon \end{pmatrix} \tag{2.44}$$

for molecule A and

$$B_1 = \begin{pmatrix} -\varepsilon & & & & & & \\ & \ddots & & & & & \\ & & -\varepsilon + x\beta_k & & & & \\ & & & \ddots & & & \\ & & & & -\varepsilon + x\beta_l & & \\ & & & & & \ddots & \\ & & & & & & -\varepsilon \end{pmatrix} \tag{2.45}$$

for molecule B, indicating that some or all of the inactive carbon atoms (0) are replaced with arbitrary heteroatoms. The definitions of β_1 and β_2 are the same as before. P in Eq. (2.43) shows that a connection between an inactive atom (0) of molecule A (A(0)) and an inactive atom of molecule B (B(0)) exists in the off-diagonal blocks. After reducing the matrix, Eq. (2.43) becomes

$$\Delta_n^{Dis}(\varepsilon)[\text{Type-II}] = (-\varepsilon)^2 \Delta_{n-2}^{Dis}(\varepsilon)[\text{Type-II}], \tag{2.46}$$

where

$$\Delta_{n-2}^{Dis}(\varepsilon)[\text{Type}-\text{II}] = \left|\begin{array}{c|c|c|c} -\varepsilon I & \beta_1 & 0 & 0 \\ \hline \beta_1^T & A_1 & 0 & P \\ \hline 0 & 0 & -\varepsilon I & \beta_2 \\ \hline 0 & P^T & \beta_2^T & B_1 \end{array}\right|. \tag{2.47}$$

Therefore, the equation $\Delta_n^{Dis}(\varepsilon)[\text{Type-II}] = 0$ has two solutions with $\varepsilon = 0$. Two degenerate NBMOs remain after the formation of a 0–0 linkage, as observed for the all-HC disjoint molecules.

2.4.4 *Heteroatom-Included Hydrocarbons Type-II Non-disjoint (HHC-AO-II-N)*

Next, the case in which there is a bond formed between an inactive atom (0) of molecule A (A(0)) and an active atom (*) of molecule B (B(*)) is examined. The secular determinant is written as

$$\Delta_n^{Non-dis}(\varepsilon)\,[\text{Type-II}] = \begin{array}{c|cccc} & \mathrm{A}(*) & \mathrm{A}(0) & \mathrm{B}(*) & \mathrm{B}(0) \\ \hline \mathrm{A}(*) & -\varepsilon I & \beta_1 & 0 & 0 \\ \mathrm{A}(0) & \beta_1^T & A_1 & P & 0 \\ \mathrm{B}(*) & 0 & P^T & -\varepsilon I & \beta_2 \\ \mathrm{B}(0) & 0 & 0 & \beta_2^T & B_1 \end{array}, \tag{2.48}$$

where P has only one non-zero element. The same multiplications as before can be performed on Eq. (2.48) to obtain

$$\Delta_n^{Non-dis}(\varepsilon)[\text{Type-II}] = (-\varepsilon)^2 \Delta_{n-2}^{Non-dis}(\varepsilon)[\text{Type-II}], \tag{2.49}$$

where

$$\Delta_{n-2}^{Non-dis}(\varepsilon)[\text{Type-II}] = \begin{array}{cccc} I & \beta_1 & 0 & 0 \\ \beta_1^T & -\varepsilon A_1 & P & 0 \\ 0 & P^T & I & \beta_2 \\ 0 & 0 & \beta_2^T & -\varepsilon B_1 \end{array}. \tag{2.50}$$

Equation (2.50) again results in two solutions with $\varepsilon = 0$ when $\Delta_n^{Non-dis}(\varepsilon)[\text{Type-II}] = 0$. Therefore, A(0)–B(*) bonding has no effect on the two degenerate NBMOs, maintaining two degenerate NBMOs with $\varepsilon = 0$; this feature is similar to the case of pure HC systems.

This proof is based on the assumption that two HHC Type-II molecules are combined, but it can be also generalized to mixed systems composed of a HHC Type-II as molecule A (inactive site) and a pure HC (see Fig. 2.4) or another HHC system as molecule B (active site) if molecule B has an NBMO with $\varepsilon = 0$.

Finally, we can summarize the results for all of the cases (HCs and Type-I and -II HHCs) with disjoint (0–0) and non-disjoint (0–*) linkages, as shown in Table 2.1, in which the ranks of all of the determinants are two less than those of two whole molecules.

It is evident that, for both 0–0 and 0–* linkages between two molecules, there are always two degenerate solutions with $\varepsilon = 0$ for HCs and Type-II HHCs and with $\varepsilon = x\beta$ for Type-I HHCs. In the latter case, $x\beta$ is defined as the Coulomb

Table 2.1 Summary of determinants for HCs and Type-I and Type-II HHCs

Linkage	System		
	HCs	Type-I (Heteroatoms at starred positions)	Type-II (Heteroatoms at unstarred positions)
Disjoint (0–0)	$(-\varepsilon)^2\Delta_{n-2}^{Dis}(\varepsilon)$	$(-\varepsilon+x\beta)^2\Delta_{n-2}^{Dis}(\varepsilon)$	$(-\varepsilon)^2\Delta_{n-2}^{Dis}(\varepsilon)$
Non-disjoint (0–*)	$(-\varepsilon)^2\Delta_{n-2}^{Non-dis}(\varepsilon)$	$(-\varepsilon+x\beta)^2\Delta_{n-2}^{Non-dis}(\varepsilon)$	$(-\varepsilon)^2\Delta_{n-2}^{Non-dis}(\varepsilon)$

parameter and depends on the type of heteroatom placed at the starred positions. In fact, the value of x does not affect $(-\varepsilon)^2$ for Type-II, unlike in Type-I. Therefore, the ability to maintain two NBMO levels with $\varepsilon = 0$ also remains for mixed systems consisting of HCs and Type-II HHCs because the factor $(-\varepsilon)^2$ does not include $x\beta$. We have also confirmed that the equations derived for HHC, if $x\beta$ is set to zero, are equivalent to those of HCs.

2.5 Molecular-Orbital-Based Proof for Disjoint and Non-disjoint Heteroatom-Included Hydrocarbons

A general proof analogous to that for HC systems is not easy for HHC systems. Here we use polyene with odd-number carbon atoms as a parent molecule because the analytical expression of the MOs is known.

2.5.1 Heteroatom-Included Hydrocarbons Type-I Disjoint (HHC-MO-I-D)

First, we examine the NBMOs of Type-I polyene (Fig. 2.5) in an MO base using analytical solutions of

$$C_{ir}^{(0)} = \sqrt{\frac{2}{N+1}}\sin\left(\frac{\pi\cdot i\cdot r}{N+1}\right), \quad r = 1, 2, \ldots, N \tag{2.51}$$

Instead of diagonalizing the Hamiltonian matrix H in an AO base, we can diagonalize H', the matrix transformed in polyene's MO base, as

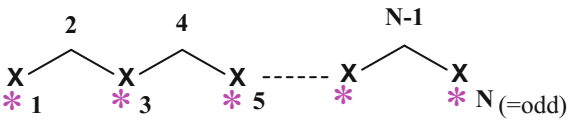

Fig. 2.5 Structure of Type-I polyene

$$C^{\dagger(0)} H C^{(0)} = H'. \tag{2.52}$$

The matrix elements are represented as

$$H'_{i,j} = \frac{2}{N+1} \sum_r \sum_s \sin\left(\frac{\pi \cdot i \cdot r}{N+1}\right) \sin\left(\frac{\pi \cdot j \cdot s}{N+1}\right) \cdot H_{rs}, \tag{2.53}$$

where H_{rs} denotes the Hückel matrix elements in the AO base of Type-I polyene in which all of the starred atoms are replaced by heteroatoms with Coulomb integrals of Eq. (2.31). The secular equation to be solved can be expressed as

$$H' = \begin{vmatrix}
\varepsilon_1 - \varepsilon & 0 & 0 & \cdots & 0 & \cdots & 0 & 0 & \frac{x\beta}{2} \\
0 & \varepsilon_2 - \varepsilon & 0 & \cdots & 0 & \cdots & 0 & \frac{x\beta}{2} & 0 \\
0 & 0 & \ddots & & \vdots & & 0 & 0 & 0 \\
\vdots & \vdots & & & 0 & & \frac{x\beta}{2} & 0 & \vdots \\
0 & 0 & \cdots & 0 & \varepsilon_{NBMO} - \varepsilon & 0 & \cdots & 0 & 0 \\
\vdots & \vdots & & 0 & \frac{x\beta}{2} & 0 & & \vdots & \vdots \\
0 & 0 & & 0 & 0 & & & 0 & 0 \\
0 & \frac{x\beta}{2} & 0 & \cdots & 0 & \cdots & 0 & \varepsilon_{N-1} - \varepsilon & 0 \\
\frac{x\beta}{2} & 0 & 0 & \cdots & 0 & \cdots & 0 & 0 & \varepsilon_N - \varepsilon
\end{vmatrix}, \tag{2.54}$$

where the diagonal terms are the sums of the orbital energies of simple polyene itself and the contributions from heteroatoms replaced on starred (*) positions as

$$\varepsilon_i = \varepsilon_i(HC) + \varepsilon_i(X), \tag{2.55}$$

where

$$\varepsilon_i(HC) = \alpha + 2\beta \cos\left(\frac{\pi \cdot i}{N+1}\right), \tag{2.56}$$

$$\begin{aligned}
\varepsilon_i(X) &= \frac{2}{N+1}\left\{ x\beta \sum_r^X \sin^2\left(\frac{r \cdot \pi \cdot i}{N+1}\right) + 2(l-1)\beta \sum_r^X \sin\left(\frac{r \cdot \pi \cdot i}{N+1}\right) \sin\left(\frac{(r+1) \cdot \pi \cdot i}{N+1}\right) \right\} \\
&= \frac{1}{2} x\beta + (l-1)\beta \cos\left(\frac{\pi \cdot i}{N+1}\right) \qquad \text{if } i \neq (N+1)/2 \\
&= x\beta \qquad \text{if } i = (N+1)/2
\end{aligned} \tag{2.57}$$

Equation (2.57) comes from an intramolecular interaction that occurs by replacing carbon with heteroatom X, which differs from an intermolecular interaction that has no effect on the diagonal elements in each molecule. It must be noted

that the summation on X in Eq. (2.57) runs only over starred heteroatoms of the same type [7]. The NBMO level that corresponds to $i = (N+1)/2$ is given by $\varepsilon_{NBMO} = x\beta$. The terms related to the NBMOs, $H'_{i,NBMO}$ and $H'_{NBMO,j}$, in Eq. (2.53) are

$$\begin{aligned} H'_{i,NBMO} &= \frac{2}{N+1}\sum_{r}\sum_{s}\sin\left(\frac{\pi\cdot i\cdot r}{N+1}\right)\sin\left(\frac{\pi\cdot s}{2}\right)\cdot H_{rs} \\ &= \frac{2l\beta}{N+1}\sum_{r=1}^{N}\sin\left(\frac{\pi\cdot i\cdot r}{N+1}\right)\sum_{s=1}^{(r-B)}\sin\left(\frac{\pi\cdot s}{2}\right) = 0 \end{aligned} \tag{2.58}$$

and

$$\begin{aligned} H'_{NBMO,j} &= \frac{2}{N+1}\sum_{r}\sum_{s}\sin\left(\frac{\pi\cdot r}{2}\right)\sin\left(\frac{\pi\cdot j\cdot s}{N+1}\right)\cdot H_{rs} \\ &= \frac{2l\beta}{N+1}\sum_{r=1}^{N}\sin\left(\frac{\pi\cdot r}{2}\right)\sum_{s=1}^{(r-B)}\sin\left(\frac{\pi\cdot j\cdot s}{N+1}\right) = 0 \end{aligned} \tag{2.59}$$

respectively. Therefore, ε_{NBMO} experiences no mixing with other orbitals, as can be seen from Eq. (2.54). We can therefore solve the two-by-two simultaneous equations and obtain new orbital energies for the HHC system using

$$\varepsilon'_i = \frac{x\beta}{2} - \sqrt{\left(\varepsilon_i - \frac{x\beta}{2}\right)^2 + \frac{(x\beta)^2}{4}} \tag{2.60}$$

and

$$\varepsilon'_{NBMO} = x\beta \tag{2.61}$$

In a Type-I system, the pairing theorem holds around $\frac{x\beta}{2}$ (see Fig. 2.4), and, thus, for orbital energies, has the relation

$$\varepsilon'_i - \frac{x\beta}{2} = -\left(\varepsilon'_{N+1-i} - \frac{x\beta}{2}\right), \tag{2.62}$$

and for coefficients

$$C_{n-1+1,r} = -K_i C_{i,r}, \quad (r:\ \text{starred}) \tag{2.63}$$

and

$$C_{n-1+1,r} = \frac{1}{K_i} C_{i,r}, \quad (r: \text{ unstarred}), \tag{2.64}$$

where

$$K_i = \pm\sqrt{\frac{x\beta - \varepsilon_i}{-\varepsilon_i}} \quad or \quad K_i = \pm\sqrt{\frac{\varepsilon_{N-i+1}}{\varepsilon_{N-i+1} - x\beta.}} \tag{2.65}$$

Using these relations, the existence of NBMOs in combined super-molecules can be examined in the form of MO-based secular equations.

Next, we consider a disjoint combination of two unstarred atoms of a Type-I HHC. We define the zeroth-order MOs to be solved for Type-I HHCs (not for polyene); the MO-based secular equation can be constructed using a method similar to that described in Sect. 2.3 for HCs and can be expressed as

$$\Delta_n^{Dis}(\varepsilon)[\text{Type-I}] = \begin{array}{c|cccccc} & \text{NBMO(A)} & & & & \text{NBMO(B)} & \\ & \varepsilon_1^{(A)} - \varepsilon & 0 & \cdots & \cdots & 0 & \cdots \\ \text{NBMO(A)} & 0 & \varepsilon_{N_A}^{(A)} - \varepsilon & 0 & 0 & 0 & 0 \\ & \cdots & 0 & \varepsilon_{n_A}^{(A)} - \varepsilon & \cdots & 0 & \cdots \\ & \cdots & 0 & \cdots & \varepsilon_1^{(B)} - \varepsilon & 0 & \cdots \\ \text{NBMO(B)} & 0 & 0 & 0 & 0 & \varepsilon_{N_B}^{(B)} - \varepsilon & 0 \\ & \cdots & 0 & \cdots & \cdots & 0 & \varepsilon_{n_B}^{(B)} - \varepsilon \end{array} \tag{2.66}$$

The matrix elements have the same form as Eq. (2.18) because Eqs. (2.19)–(2.22) are satisfied as well. That is, at least one coefficient, either the rth or the sth, is zero because the coefficients under discussion are related to N_A or N_B even though ΔH_{rs} (=ΔH_{pq}) is non-zero at the linkage position. On the other hand, $\Delta H_{rs} = 0$ whenever the NBMO-related coefficients are non-zero on a starred atom, because the linkage occurs only between the pth and qth AOs. Therefore, disjoint HHC Type-I systems exhibit properties identical to those of disjoint HCs because the starred and unstarred positions in the HC systems are constant in HHC systems, even though the values of the NBMO coefficients change. Therefore, a disjoint combination between two Type-I HHC molecules also maintains the original NBMOs, in a similar manner to Eq. (2.23), giving

$$\Delta_n^{Dis}(\varepsilon) = (-\varepsilon + x\beta)^2 \Delta_{n-2}^{Dis}(\varepsilon). \tag{2.67}$$

This is consistent with Table 2.1, and the two NBMOs are isolated without any interaction between the two parent molecules. As described in Sects. 2.2.1 and

2.3.1; however, this kind of NBMO arrangement does not contribute to spin parallelization between the two radicals because no exchange interaction is generated between the non-interacting NBMOs. In the next Sect. 2.5.2, we therefore consider non-disjoint combinations of HHC Type-I molecules.

2.5.2 *Heteroatom-Included Hydrocarbons Type-I Non-disjoint (HHC-MO-I-N)*

The secular equation based on MOs for Type-I can be written as in Sect. 2.3.2 in the form,

$$\Delta_n^{Non-dis}(\varepsilon)[\text{Type-I}] = \begin{array}{c} \\ \text{NBMO(A)} \\ \\ \\ \text{NBMO(B)} \\ \\ \end{array} \begin{array}{c} \begin{array}{cccccc} \text{NBMO(A)} & & & & \text{NBMO(B)} & \end{array} \\ \begin{vmatrix} \varepsilon_1^{(A)}-\varepsilon & 0 & \cdots & \cdots & \cdots & \cdots \\ 0 & \varepsilon_{N_A}^{(A)}-\varepsilon & 0 & 0 & 0 & 0 \\ \vdots & 0 & \varepsilon_{n_A}^{(A)}-\varepsilon & \cdots & \cdots & \cdots \\ \vdots & 0 & \cdots & \varepsilon_1^{(B)}-\varepsilon & 0 & \cdots \\ \vdots & 0 & \cdots & 0 & \varepsilon_{N_B}^{(B)}-\varepsilon & 0 \\ \vdots & 0 & \cdots & 0 & 0 & \varepsilon_{n_B}^{(B)}-\varepsilon \end{vmatrix} \end{array}, \tag{2.68}$$

where the matrix elements have the form

$$H_{i,j}^{(\mathrm{AB})} = \sum_{r=1}^{n_\mathrm{A}} \sum_{s=1}^{n_\mathrm{B}} C_{ir}^{(\mathrm{A})} C_{js}^{(\mathrm{B})} H_{rs}^{(\mathrm{AB})} = C_{ip}^{(\mathrm{A})} C_{jq}^{(\mathrm{B})} H_{pq}^{(\mathrm{AB})}.$$

It is evident that the NBMO in molecule A is isolated, while that in molecule B interacts with other orbitals, as is the case for non-disjoint HCs. However, after the derivation using the relations

$$H_{i,j}^{(AB)} = kH_{n-i+1,j}^{(AB)}, \quad H_{i,j}^{(AB)} = kH_{i,n-j+1}^{(AB)}, \quad k = \pm 1 \tag{2.69}$$

and

$$H_{n_\mathrm{A}-i+1,j}^{(\mathrm{AB})} = C_{n\mathrm{A}-i+1,p}^{(\mathrm{A})} C_{j,q}^{(\mathrm{B})} H_{pq}^{(\mathrm{AB})} = \frac{1}{K_i} C_{i,p}^{(\mathrm{A})} C_{j,q}^{(\mathrm{B})} H_{p,q}^{(\mathrm{AB})} = \frac{1}{K_i} H_{i,j}^{(\mathrm{AB})}, \tag{2.70}$$

we can finally obtain

$$\Delta_n^{Non-dis}(\varepsilon)[\text{Type-I}] = \begin{array}{|ccc|c|ccc|}\hline -2\varepsilon & & 0 & 0 & A_{OV} & 0 & 0 & 0 \\ & \ddots & & & & & & \\ 0 & & -2\varepsilon & & & & & \\ \hline 0 & & & \varepsilon_{N_A}^{(A)} - \varepsilon & 0 & 0 & 0 & 0 \\ \hline & A_{OV} & & 0 & \varepsilon_{n_A}^{(A)} - \varepsilon & \multicolumn{3}{c|}{A_V\text{-}B} \\ \hline 0 & & & 0 & & & & \\ 0 & & & 0 & A_V\text{-}B & \multicolumn{3}{c|}{\text{Molecule B}} \\ 0 & & & 0 & & & & \\ \hline \end{array} \tag{2.71}$$

and

$$= (x\beta - \varepsilon)^2 \times \left[2\{Polynomial\} + |A_{ov}|^2 \bullet \left|Molecule\, B^{(n-1)}\right|\right], \tag{2.72}$$

where

$$\Delta_n(\varepsilon) = (x\beta - \varepsilon)^2 (2 - \frac{x\beta}{\varepsilon_1^A})\Delta_{n-2}^{(1)} + (x\beta - \varepsilon)(-1)^{n_A}\{-K_1(x\beta - \varepsilon_1 - \varepsilon)\}\Delta_{n-2}^{(2)}. \tag{2.73}$$

The rank of the second term on the right-hand side can be further reduced to

$$\Delta_{n-2n'_A}^{(2)}(\varepsilon) = -K_{n'_A}(x\beta - \varepsilon_{n'_A}^A - \varepsilon)(\varepsilon_1^B - \varepsilon)(\varepsilon_2^B - \varepsilon)\cdots(x\beta - \varepsilon)\cdots(\varepsilon_{n_B}^B - \varepsilon) \tag{2.74}$$

until the second term vanishes, where another $(x\beta - \varepsilon)$ can be extracted. Finally, we can also extract $(x\beta - \varepsilon)^2$ from the second term.

Therefore, the original NBMO levels of $x\beta$ are retained even after a non-disjoint combination is formed. This MO-based result is consistent with the AO-based proof in Eq. (2.41).

2.5.3 *Heteroatom-Included Hydrocarbons Type-II Disjoint (HHC-MO-II-D)*

We define the Type-II system for the polyene radical as shown in Fig. 2.6: Heteroatoms (X, Y, etc.) are placed at unstarred atoms, that is, on even-numbered atoms. The positions and types of heteroatoms are more flexible than in Type-I HHCs under the condition that the NBMO in the parent molecule is retained. Any

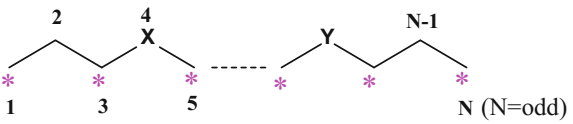

Fig. 2.6 Structure of Type-II polyene

type of heteroatom can be placed at any of the unstarred positions of polyene, while maintaining the NBMO level in the original pure HC polyene radical, as shown in Fig. 2.4. The pairing theorem is not valid for Type-II HHCs, but the disjoint connection can be proven in the same way as described in Sects. 2.3.1 and 2.5.1 by MO basis. In fact, the electronic structure is very similar to that of a non-alternant HC, and, therefore, a disjoint combination between a Type-II HHC and another molecule should follow the rule that was previously described [2]. Consequently, a 0–0 combination between two Type-II HHCs or a Type-II HHC and an HC (HHC) does not affect the original NBMO levels of $\lambda = 0$.

2.5.4 *Heteroatom-Included Hydrocarbons Type-II Non-disjoint (HHC-MO-II-N)*

For a non-disjoint combination of Type-II HHCs, the two NBMOs with $\lambda = 0$ also remain unchanged after the combination according to the 0–* rule in the framework shown in Fig. 2.1. The electronic structure of molecule A must satisfy the pairing theorem so that the stabilizing and destabilizing interactions between molecules A and B, which occur through the NBMO of molecule B with $\lambda = 0$, cancel, leaving the two NBMOs unchanged. One of the two NBMOs is isolated, but the other remains as a result of the interaction with molecule A. Therefore, a Type-II HHC molecule can act as molecule B in Fig. 2.1, and this type of super-molecule can be expected to exhibit a high-spin state rather than a low-spin state. The mathematical proof for the two degenerate NBMOs remaining in this type of combination also follows that described in Sect. 2.5.2.

References

1. Yonezawa, T., Nagata, T., Kato, H., Imamura, A., Morokuma, K.: Ryoshi Kagaku Nyumon. Kagaku Dojin, Tokyo (1983)
2. Aoki, Y., Imamura, A.: A simple treatment to design NBMO degenerate systems in alternant and non-alternant hydrocarbons. Theor. Chim. Acta. **84**, 155–180 (1992)
3. Onitsuka, S., Aoki, Y.: Guidelines proposed for designing organic ferromagnets by using a quantum chemical approach. Theor. Chem. Acc. **130**, 789–806 (2011)
4. Aoki, Y., Imamura, A.: A simple rule to find nondisjoint NBMO degenerate systems for designing high-spin organic molecules. Int. J. Quant. Chem. **74**, 491–502 (1999)
5. Whangbo, M.-H.: Perturbational Molecular Orbital Analysis. In: Computational Theoretical Organic Chemistry, vol. 67, pp. 233–252. Springer, New York (1981)
6. Tyutyulkov, N., Polansky, O.: An extension of the Coulson-Rushbrooke theorem. Chem. Phys. Lett. **139**, 281–284 (1987)
7. Zhu, X., Aoki, Y.: Development of molecular fragment interaction method for designing organic ferromagnets. J. Math. Chem. **54**, 1585–1595 (2016)

Chapter 3
Simple High-Spin Index L_{ij} for Ferromagnetic Organic Molecules

Abstract The assessment of the high-spin stability of a molecule using indices, rules, etc. plays an important role in the design of ferromagnetic materials. In this chapter, we propose a simple high-spin stability index L_{ij}, which is related to the exchange integral K_{ij}, using computational and analytical approaches. The computational approach requires only non-bonding molecular orbital coefficients and subsequent unitary rotations to calculate the index $L_{ij}^{\min}$. On the other hand, the analytical approach can predict the index $L_{ij}^{\min}$ for larger systems without requiring direct quantum chemistry calculations. Using a variety of examples, we examine the reliability of the index by comparing the results with the high-spin stability $\Delta E(L-H)$ obtained from ab initio calculations including electron correlation effects. We also note that L_{ij} provides us with an efficient strategy for designing high-spin systems while considering the correlation effects.

3.1 Introduction

As mentioned in the previous chapter, many types of rules, indices, and values have been proposed for predicting magnetic properties. However, it is worthwhile to pursue a more useful method that exhibits both high efficiency and reliability in the design of promising ferromagnetic materials. In this chapter, we introduce very simple high-spin index L_{ij}; we estimate the index using two different approaches, i.e., computational and analytical approaches. The effectiveness of the index will be discussed based on its application to many example systems.

Y. Aoki et al., *Quantum Chemical Approach for Organic Ferromagnetic Material Design*,
SpringerBriefs in Electrical and Magnetic Properties of Atoms, Molecules, and Clusters,
DOI 10.1007/978-3-319-49829-4_3

3.2 High-Spin Stability Index L_{ij} (Computational Approach)

3.2.1 L_{ij} *for Diradical Systems*

In the previous chapter, we proposed the simple "(0–*) linkage" rule to design high-spin molecules, in which a (0–*) linkage between radical units generated non-disjoint non-bonding molecular orbital (NBMO) degenerate systems [1]. Figure 3.1 shows the allyl radical (AR) dimer with a non-disjoint (0–*) linkage. The model was realized by connecting the 0-site of AR(A) with a *-site of AR(B). The "*" (star) sign represents an active carbon atom with a finite NBMO coefficient, while the "0" (unstarred) sign represents an inactive carbon atom with no NBMO coefficient. The non-disjoint (0–*) linkage generates NBMO mixings (overlaps) between radical units, even when considering a unitary rotation, and the degenerate NBMOs are maintained after causing the interaction. On the other hand, the (0–0) linkage also produces two degenerate NBMOs (see Fig. 3.2), where the 0-site of AR(A) connects with the 0-site of AR(B). However, the NBMO coefficients can be localized onto each unit after the unitary rotation, and NBMO mixings cannot be

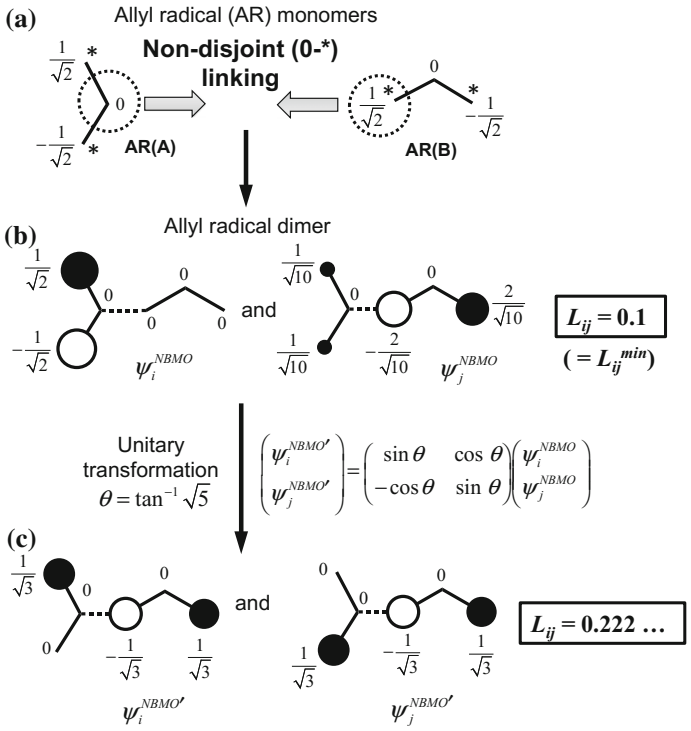

Fig. 3.1 AR dimer model with non-disjoint (0–*) linkage: **a** NBMO coefficients of each AR monomer, **b** NBMOs of AR dimer before unitary rotations, and **c** NBMOs of dimer after rotations ($\theta = \tan^{-1}\sqrt{5}$). Modified with permission from Ref. [1]. Copyright 1999 John Wiley & Sons, Inc.

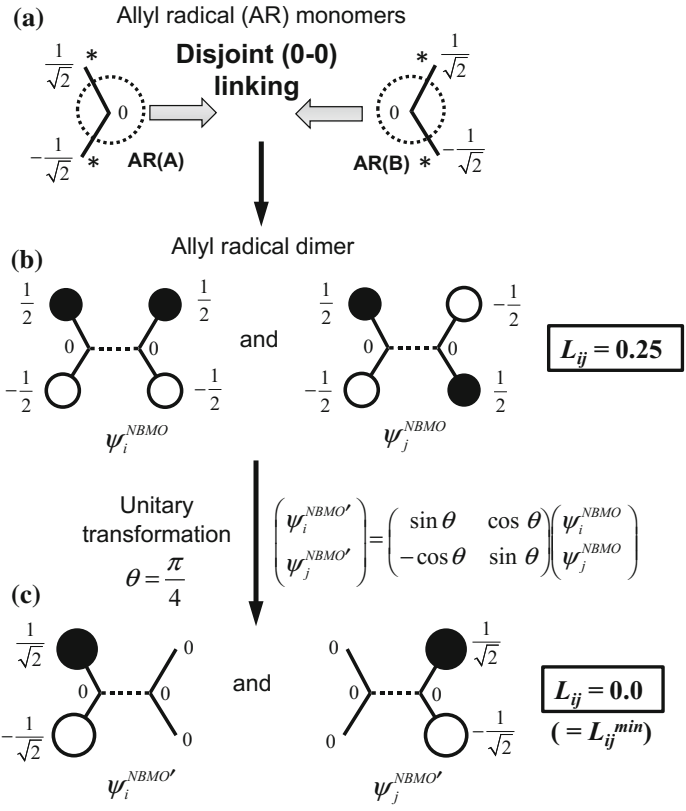

Fig. 3.2 AR dimer model with disjoint (0–0) linkage: **a** NBMO coefficients of each AR monomer, **b** NBMOs of AR dimer before unitary rotations, and **c** NBMOs of AR dimer after rotations $(\theta = \pi / 4)$. Modified with permission from Ref. [1]. Copyright 1999 John Wiley & Sons, Inc.

expected from such a disjoint (0–0) linkage. Based on the comparison with the (0–0) linkage, the former non-disjoint (0–*) linkage has the potential to generate exchange interactions between two radical electrons and holds the promise of realizing a high-spin system.

In this study, we also proposed a simple index L_{ij} for estimating the NBMO mixing (overlaps) and predicting the high-spin stability of hydrocarbon systems [1]; this study was later extended to systems containing heteroatoms [2]. For the diradical molecule, L_{ij} is defined by the coefficients of two degenerate NBMOs, ψ_i^{NBMO} and ψ_j^{NBMO}, as

$$L_{ij} = \sum_r (C_{ri} C_{rj})^2, \tag{3.1}$$

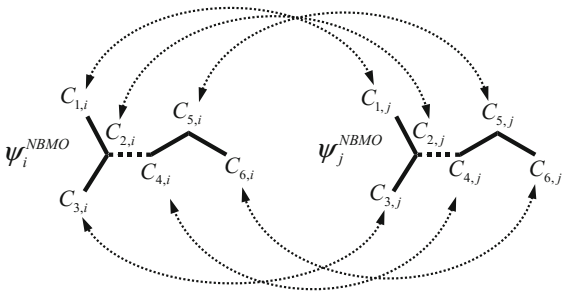

Fig. 3.3 Schematic illustration for calculating L_{ij} from coefficients of two NBMOs, ψ_i^{NBMO} and ψ_j^{NBMO}. Modified with permission from Ref. [1]. Copyright 1999 John Wiley & Sons, Inc.

where C_{ri} represents the coefficient of the r-th atomic orbital (AO) in ψ_i^{NBMO} within the framework of the linear combination of atomic orbitals (LCAO) approximation. Equation (3.1) consists of the product of the molecular orbital (MO) coefficients at the same position (more properly, at the same AO) between ψ_i^{NBMO} and ψ_j^{NBMO}. For example, L_{ij} for the non-disjoint (0–*) AR dimer can be calculated using (see Fig. 3.3)

$$L_{ij} = |C_{1,i}C_{1,j}|^2 + |C_{2,i}C_{2,j}|^2 + |C_{3,i}C_{3,j}|^2 + |C_{4,i}C_{4,j}|^2 + |C_{5,i}C_{5,j}|^2 + |C_{6,i}C_{6,j}|^2. \quad (3.2)$$

The magnitude of L_{ij} depends on whether the coefficients of the two NBMOs exist on the same sets of atoms or not. The freedom of the unitary rotations should be considered when estimating L_{ij}. For example, for a non-disjoint (0–*) linkage, the unitary rotation changes L_{ij} from 0.1 (Fig. 3.1b) to 0.222… (Fig. 3.1c). However, the NBMO coefficients cannot be confined to the different sets of atoms, even by a unitary rotation, and always give $L_{ij} > 0$. In contrast, for disjoint (0–0) linkages, the NBMO coefficients can be confined to the different sets of atoms and give $L_{ij} = 0.0$ after the rotation (Fig. 3.2c); prior to the rotation, $L_{ij} = 0.25$ (Fig. 3.2b).

To avoid the under-specification of L_{ij} in the unitary rotations, the minimum value of L_{ij}, namely, $L_{ij}^{\min}$, can be determined as follows. The two NBMOs in a diradical system, ψ_i^{NBMO} and ψ_j^{NBMO}, can be expanded within the LCAO approximation as

$$\psi_i^{NBMO} = \sum_r C_{ri}\chi_r, \text{ and } \psi_j^{NBMO} = \sum_r C_{rj}\chi_r. \quad (3.3)$$

The common (2 × 2) unitary rotation can be described as

$$\begin{pmatrix} \psi_i^{NBMO'} \\ \psi_j^{NBMO'} \end{pmatrix} = \begin{pmatrix} \sin\theta & \cos\theta \\ -\cos\theta & \sin\theta \end{pmatrix} \begin{pmatrix} \psi_i^{NBMO} \\ \psi_j^{NBMO} \end{pmatrix}, \quad (3.4)$$

where $\psi_i^{NBMO'}$ and $\psi_j^{NBMO'}$ are the NBMOs after the unitary rotation and are expressed as

$$\psi_i^{NBMO'} = \sum_r C_{ri}^{'} \chi_r, \text{ and } \psi_j^{NBMO'} = \sum_r C_{rj}^{'} \chi_r, \tag{3.5}$$

respectively. From these equations, the transformed NBMOs can be given by

$$\begin{aligned} \psi_i^{NBMO'} &= \sin\theta\, \psi_i^{NBMO} + \cos\theta\, \psi_j^{NBMO} \\ &= \sin\theta \sum_r C_{ri}\chi_r + \cos\theta \sum_r C_{rj}\chi_r \\ &= \sum_r (\sin\theta\, C_{ri} + \cos\theta\, C_{rj})\chi_r \\ &= \sum_r C'_{ri}\chi_r \end{aligned} \tag{3.6}$$

and

$$\begin{aligned} \psi_j^{NBMO'} &= -\cos\theta\, \psi_i^{NBMO} + \sin\theta\, \psi_j^{NBMO} \\ &= \sum_r (-\cos\theta\, C_{ri} + \sin\theta\, C_{rj})\chi_r \\ &= \sum_r C'_{rj}\chi_r. \end{aligned} \tag{3.7}$$

Thus, the NBMO coefficients after the rotation are provided as

$$C'_{ri} = \sin\theta C_{ri} + \cos\theta C_{rj}, \text{ and } C'_{rj} = -\cos\theta C_{ri} + \sin\theta C_{rj}. \tag{3.8}$$

After unitary rotations, $L'_{ij}(\theta)$ can be expanded by

$$\begin{aligned} L'_{ij}(\theta) &= \sum_r (C'_{ri}C'_{rj})^2 = \sum_r \left\{(\sin\theta C_{ri} + \cos\theta C_{rj})(-\cos\theta C_{ri} + \sin\theta C_{rj})\right\}^2 \\ &= \sin^2\theta\cos^2\theta \sum_r \left(C_{rj}^2 - C_{ri}^2\right)^2 \\ &\quad - 2\sin\theta\cos\theta\cos 2\theta \sum_r \left(C_{rj}^2 - C_{ri}^2\right) C_{ri}C_{rj} + \cos^2 2\theta \sum_r C_{ri}^2 C_{rj}^2 \\ &= \sin^2\theta\cos^2\theta\alpha_{ij} - 2\sin\theta\cos\theta\cos 2\theta\gamma_{ij} + \cos^2 2\theta\beta_{ij} \\ &= \frac{1}{4}\alpha_{ij} + \cos^2 2\theta\left(-\frac{1}{4}\alpha_{ij} + \beta_{ij}\right) - \sin 2\theta\cos 2\theta\gamma_{ij} \\ &= \frac{1}{8}(\alpha_{ij} + 4\beta_{ij}) - \left\{\frac{1}{2}\gamma_{ij}\sin 4\theta + \frac{1}{8}(\alpha_{ij} - 4\beta_{ij})\cos 4\theta\right\}, \end{aligned} \tag{3.9}$$

where $L'_{ij}(\theta)$ is a function of the rotation angle θ. In Eq. (3.9), α_{ij}, β_{ij}, and γ_{ij} are respectively defined as

$$\alpha_{ij} = \sum_r \left(C_{rj}^2 - C_{ri}^2\right)^2, \quad \beta_{ij} = \sum_r C_{ri}^2 C_{rj}^2, \quad \text{and } \gamma_{ij} = \sum_r \left(C_{rj}^2 - C_{ri}^2\right) C_{ri} C_{rj}. \tag{3.10}$$

Equation (3.9) can then be rewritten using constants, A and φ, as

$$\begin{aligned} L'_{ij}(\theta) &= \frac{1}{8}(\alpha_{ij} + 4\beta_{ij}) - \{A \sin 4\theta \cos\varphi + A \cos 4\theta \sin\varphi\} \\ &= \frac{1}{8}(\alpha_{ij} + 4\beta_{ij}) - A \sin(4\theta + \varphi), \end{aligned} \tag{3.11}$$

where

$$A \cos\varphi = \frac{1}{2}\gamma_{ij}, \text{ and } A \sin\varphi = \frac{1}{8}(\alpha_{ij} - 4\beta_{ij}). \tag{3.12}$$

From the sum of the squares of Eq. (3.12), A can be derived as

$$\begin{aligned} (A\cos\varphi)^2 + (A\sin\varphi)^2 &= A^2\left(\cos^2\varphi + \sin^2\varphi\right) \\ &= A^2 = \left(\frac{1}{2}\gamma_{ij}\right)^2 + \left\{\frac{1}{8}(\alpha_{ij} - 4\beta_{ij})\right\}^2 \\ &= \frac{1}{4}\left\{\gamma_{ij}^2 + \frac{1}{16}(\alpha_{ij} - 4\beta_{ij})^2\right\}, \\ A &= \pm\frac{1}{2}\sqrt{\gamma_{ij}^2 + \frac{1}{16}(\alpha_{ij} - 4\beta_{ij})^2}. \end{aligned} \tag{3.13}$$

On the other hand, from the ratio of Eq. (3.12), we can obtain φ as

$$\begin{aligned} \frac{A\sin\varphi}{A\cos\varphi} &= \tan\varphi = \left\{\frac{1}{8}(\alpha_{ij} - 4\beta_{ij})\right\} \Big/ \left(\frac{1}{2}\gamma_{ij}\right) = \frac{\alpha_{ij} - 4\beta_{ij}}{4\gamma_{ij}}, \\ \varphi &= \tan^{-1}\left(\frac{\alpha_{ij} - 4\beta_{ij}}{4\gamma_{ij}}\right). \end{aligned} \tag{3.14}$$

The first term of Eq. (3.11), $(1/8)(\alpha_{ij} + 4\beta_{ij})$, is positive. Thus, $L'_{ij}(\theta)$ gives the minimum value when the second term, $-A\sin(4\theta + \varphi)$, is at its smallest value. The possible conditions for the minimum $L'_{ij}(\theta)$ are given by

$$\begin{aligned} 4\theta + \varphi &= \frac{\pi}{2}, \quad \theta = \frac{1}{4}\left(\frac{\pi}{2} - \varphi\right) \quad (if,\ A > 0) \\ 4\theta + \varphi &= \frac{3}{2}\pi, \quad \theta = \frac{1}{4}\left(\frac{3}{2}\pi - \varphi\right) \quad (if,\ A < 0). \end{aligned} \tag{3.15}$$

Finally, the minimum $L'_{ij}(\theta)(= L_{ij}^{\prime(\min)})$ can be obtained as

$$L_{ij}^{\prime(\min)} = \frac{1}{8}(\alpha_{ij} + 4\beta_{ij}) - \frac{1}{2}\sqrt{\gamma_{ij}^2 + \frac{1}{16}(\alpha_{ij} - 4\beta_{ij})^2}. \tag{3.16}$$

Here, $L_{ij}^{\prime(\min)}$ corresponds to the smallest NBMO mixing within the unitary rotations. For our convenience $L_{ij}^{\prime(\min)}$ is rewritten as simply $L_{ij}^{\min}$.

According to the above procedures, we obtained $L_{ij}^{\min} = 0.1$ for the non-disjoint (0–*) model (see Fig. 3.1b); here, the NBMOs before the unitary rotations accidentally gave the minimum L_{ij} for this model. In contrast, $L_{ij}^{\min} = 0.0$ for the disjoint (0–0) model (see Fig. 3.2c) can be obtained by unitary rotations. By comparing the values of $L_{ij}^{\min}$ between the models, we can uniquely judge that the (0–*) model has NBMO mixings larger than those of the (0–0) model, leading to the higher spin stability of the former model. It should be noted that the comparison of L_{ij} before unitary rotations $(L_{ij}^{(0-*)} = 0.1 < L_{ij}^{(0-0)} = 0.25)$ provided us with the different conclusion from the $L_{ij}^{\min}$ result.

3.2.2 $\mathbf{L_{ij}}$ *for Polyradical System*

Although it is a simplified method, L_{ij} can be generalized for polyradical systems with more than two NBMOs by summing all of the combinations of NBMO mixings in the system as

$$L_{ij} = \sum_{i,j(>i)} L_{ij}^{\circ} = \sum_{i,j(>i)} \sum_{r} (C_{ri}C_{rj})^2, \tag{3.17}$$

where L_{ij}° is the "*component* NBMO mixing" between the *i*th and *j*th NBMOs. Figure 3.4 shows the procedures for determining $L_{ij}^{\min}$ for a polyradical system. The (2×2) unitary rotation can be applied to determine the minimum value of each L_{ij}°, that is, $L_{ij}^{\min\circ}$ (Fig. 3.4a). The NBMO coefficients can be changed by each rotation. Thus, a series of unitary rotations for all of the NBMO combinations is self-consistently repeated until all of the coefficients become invariant under rotations (Fig. 3.4b). For example, $L_{ij}^{\min}$ for a triradical system can be determined self-consistently as

Cycle 1

$$\text{Step1}: L_{12}^{\circ} = \sum\nolimits_r (C_{r1}C_{r2})^2 \xrightarrow{\theta_1} L_{12}^{\min\circ} = \sum\nolimits_r (C_{r1}^{\prime(\theta_1)}C_{r2}^{\prime(\theta_1)})^2$$

$$\text{Step2}: L_{13}^{\circ} = \sum\nolimits_r (C_{r1}^{\prime(\theta_1)}C_{r3})^2 \xrightarrow{\theta_2} L_{13}^{\min\circ} = \sum\nolimits_r (C_{r1}^{\prime(\theta_2)}C_{r3}^{\prime(\theta_2)})^2$$

$$\text{Step3}: L_{23}^{\circ} = \sum\nolimits_r (C_{r2}^{\prime(\theta_1)}C_{r3}^{\prime(\theta_2)})^2 \xrightarrow{\theta_3} L_{23}^{\min\circ} = \sum\nolimits_r (C_{r2}^{\prime(\theta_3)}C_{r3}^{\prime(\theta_3)})^2$$

Cycle 2

$$\text{Step1}: L_{12}^{\circ} = \sum\nolimits_r (C_{r1}^{\prime(\theta_2)}C_{r2}^{\prime(\theta_3)})^2 \xrightarrow{\theta_4} L_{12}^{\min\circ} = \sum\nolimits_r (C_{r1}^{\prime(\theta_4)}C_{r2}^{\prime(\theta_4)})^2 \tag{3.18}$$

$$\text{Step2}: L_{13}^{\circ} = \sum\nolimits_r (C_{r1}^{\prime(\theta_4)}C_{r3}^{\prime(\theta_3)})^2 \xrightarrow{\theta_5} L_{13}^{\min\circ} = \sum\nolimits_r (C_{r1}^{\prime(\theta_5)}C_{r3}^{\prime(\theta_5)})^2$$

$$\text{Step3}: L_{23}^{\circ} = \sum\nolimits_r (C_{r2}^{\prime(\theta_4)}C_{r3}^{\prime(\theta_5)})^2 \xrightarrow{\theta_6} L_{23}^{\min\circ} = \sum\nolimits_r (C_{r2}^{\prime(\theta_6)}C_{r3}^{\prime(\theta_6)})^2$$

Cycle 3

$$\text{Step1}: L_{12}^{\circ} = \sum\nolimits_r (C_{r1}^{\prime(\theta_5)}C_{r2}^{\prime(\theta_6)})^2 \xrightarrow{\theta_7} L_{12}^{\min\circ} = \sum\nolimits_r (C_{r1}^{\prime(\theta_7)}C_{r2}^{\prime(\theta_7)})^2$$

…,

where $C_{r1}^{\prime(\theta_1)}$ is the NBMO coefficient after a unitary rotation with angle θ_1. The numbers corresponding to "cycle" and "step" in Eq. (3.18) are represented by the large (solid line) and small (broken line) loops in Fig. 3.4, respectively. For a polyradical system, $L_{ij}^{\min}$ is given by the NBMO coefficients after self-consistency as (Fig. 3.4c)

$$L_{ij}^{\min} = \sum_{i,j(>i)} L_{ij}^{\min\circ} = \sum_{i,j(>i)} \sum_r (C_{ri}^{\prime(\min)}C_{rj}^{\prime(\min)})^2. \tag{3.19}$$

3.2.3 *Alternate Explanation of* $\mathbf{L_{ij}}$

At the Hartree–Fock (HF) MO level, the total energies of the open-shell singlet (S) (Fig. 3.5a) and triplet (T) (Fig. 3.5b) states of a biradical system with two degenerate NBMOs, ψ_i^{NBMO} and ψ_j^{NBMO}, can be expressed as

$$\begin{aligned} E_{total}^{(S)} = {} & E^0 + H_j^{core} + \sum_{k=1}^{n} \left(2J_{kj} - K_{kj}\right) - H_i^{core} \\ & - \sum_{k=1}^{n} (2J_{ik} - K_{ik}) - \left(J_{ij} - K_{ij}\right) + K_{ij} + \Omega, \end{aligned} \tag{3.20}$$

and

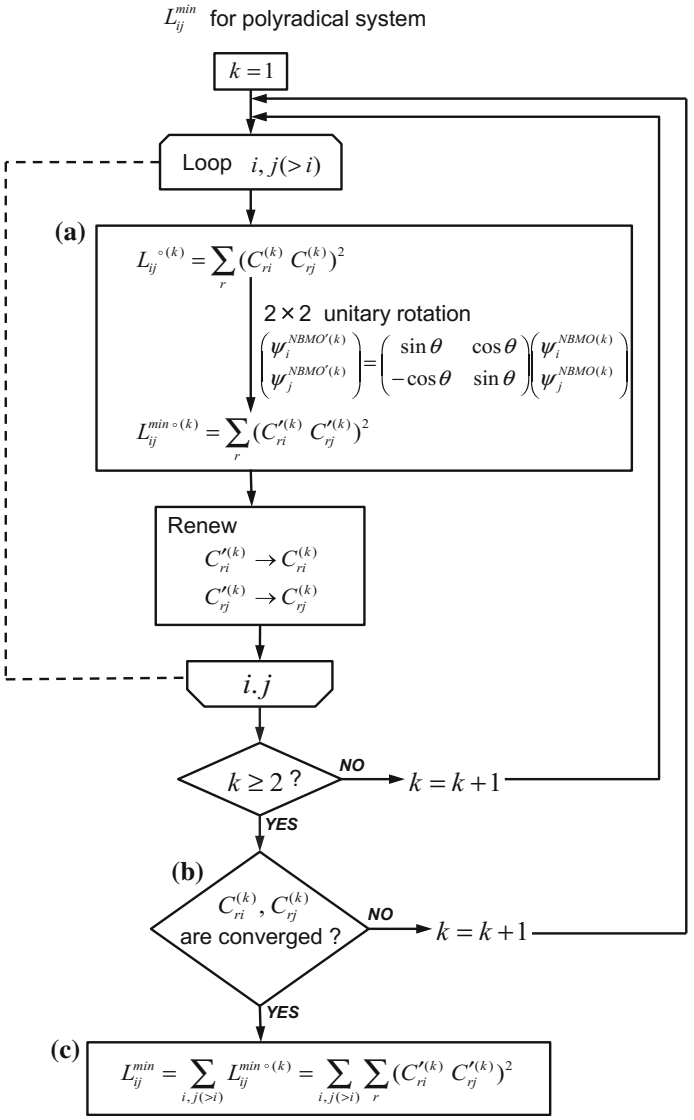

Fig. 3.4 Procedure for minimizing L_{ij} for polyradical systems based on (2 × 2) unitary rotation and self-consistent loops

$$E_{total}^{(T)} = E^0 + H_j^{core} + \sum_{k=1}^{n} \left(2J_{kj} - K_{kj}\right) - H_i^{core} - \sum_{k=1}^{n} (2J_{ik} - K_{ik}) - \left(J_{ij} - K_{ij}\right) - K_{ij} + \Omega, \tag{3.21}$$

respectively. In these equations, E^0 and Ω represent the total electronic energy of the closed-shell singlet state (Fig. 3.5c) and the total nucleus–nucleus repulsion energy, respectively. H_i^{core}, J_{ij}, and K_{ij} represent the MO-based molecular core, Coulomb, and exchange integrals, respectively, which are given by

$$H_i^{core} = \int \psi_i(1)\left\{-\frac{\hbar^2}{2m}\Delta_1 + V(1)\right\}\psi_i(1)d\tau_1, \tag{3.22}$$

$$J_{ij} = \iint \psi_i(1)\psi_i(1)\frac{e^2}{r_{12}}\psi_j(2)\psi_j(2)d\tau_1 d\tau_2, \tag{3.23}$$

and

$$K_{ij} = \iint \psi_i(1)\psi_j(1)\frac{e^2}{r_{12}}\psi_i(2)\psi_j(2)d\tau_1 d\tau_2. \tag{3.24}$$

From Eqs. (3.20) and (3.21), the total energy difference between the open-shell singlet and triplet states is given by

$$E_{total}^{(S)} - E_{total}^{(T)} = 2K_{ij}. \tag{3.25}$$

That is, the triplet state is more stable than the open-singlet state by $2K_{ij}$, where $K_{ij} > 0$. By focusing on its one-center and higher-order terms, K_{ij} can be rewritten using an AO-based description as

$$\begin{aligned} K_{ij} &= \sum_r \sum_s \sum_t \sum_u C_{ri}C_{sj}C_{ti}C_{uj}\,(rs\,|\,tu) \\ &= \sum_r (C_{ri}C_{rj})^2 (rr\,|\,rr) + \sum_r \sum_{s\neq r} \sum_{t\neq r} \sum_{u\neq r} C_{ri}C_{sj}C_{ti}C_{uj}\,(rs\,|\,tu). \end{aligned} \tag{3.26}$$

where the indices r, s, t, and u are the numbers of the AOs, and $(rs|tu)$ is the AO-based 2e-integral. If we assume that the one-center 2e-integral term in

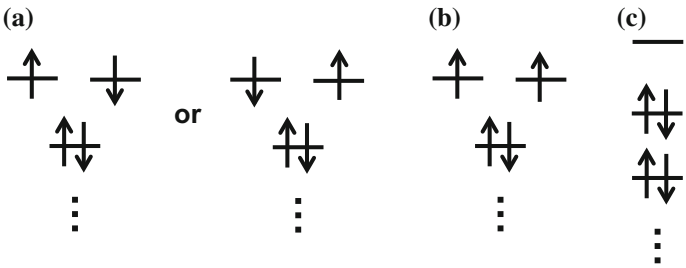

Fig. 3.5 Electron configurations: **a** open-singlet, **b** triplet, and **c** closed-singlet states for a diradical molecule

Eq. (3.26) mainly contributes to K_{ij} and that all of the one-center 2e-integrals have the same value, that is, (11|11) = (22|22) = (33|33) = ⋯ = *const*., Eq. (3.26) can be rewritten by neglecting higher-order terms as

$$E_{total}^{(S)} - E_{total}^{(T)} = 2K_{ij} \approx 2\sum_{r} (C_{ri}C_{rj})^2 (rr \mid rr) \propto \sum_{r} (C_{ri}C_{rj})^2 = L_{ij}. \qquad (3.27)$$

Equation (3.27) shows that L_{ij} is directly related to the high-spin stability, $E_{total}^{(S)} - E_{total}^{(T)}$, through K_{ij}. Therefore, the tendency of a system to exhibit high-spin stability can be predicted by L_{ij} without performing heavy fourfold loop $2K_{ij}$ or direct $E_{total}^{(S)} - E_{total}^{(T)}$ calculations. In particular, the latter method often faces serious self-consistent field (SCF) convergence problems for the low-spin state calculations. L_{ij} can be obtained from only the NBMO coefficients, and the NBMO coefficients can be obtained using a wide range of quantum-chemistry (QC)-based calculations, for example, the Hückel method, semi-empirical MO methods, ab initio MO methods, and so on.

Within the framework of the HF method, the total energy of the singlet state is variable and depends on the unitary rotation angle θ, whereas the triplet state energy does not depend on θ, as shown in Fig. 3.6 (one can simply prove it using 2×2 unitary transformation). Consequently, the singlet–triplet energy difference and the corresponding value of L_{ij} vary with θ, and θ^{min}, which gives the lowest singlet state energy, is expected to give the minimum $L_{ij}^{\min}$. $L_{ij}^{\min}$ provides us with the minimum possible NBMO mixings leading to high-spin stability.

3.2.4 *Effects of Electron Correlation on High-Spin Stability*

Consideration of electron correlation effects is essential when discussing high-spin stability because such effects are the dominant factors that stabilize the low-spin state compared with the high-spin state; they therefore contribute to the reduction of the high-spin stability.

Figure 3.6 shows the singlet and triplet energies at both the HF and second-order Møller–Plesset (MP2) levels for three different situations: (a) a disjoint model with $E^T(HF) \approx E^S(HF)$ at θ^{min}, (b) a non-disjoint model with $E^T(HF) < E^S(HF)$ at θ^{min}, and (c) a non-disjoint model with $E^T(HF) \ll E^S(HF)$ at θ^{min}. As shown by the change from the HF level to the MP2 level, the singlet state is more stabilized by correlation effects compared with the triplet state. In Fig. 3.6a (disjoint model), the singlet and triplet states have the same HF energy at θ^{min} due to zero $L_{ij}^{\min}$ value as well as zero exchange integral between NBMOs. The correlation effects largely stabilize the singlet state, and a singlet ground state is expected as the result. In Fig. 3.6b (non-disjoint model), high-spin stability occurs at the HF level due to a finite $L_{ij}^{\min}$ value as well as an existing exchange integral between NBMOs. However, singlet–triplet energy inversion occurs as the result of correlation effects.

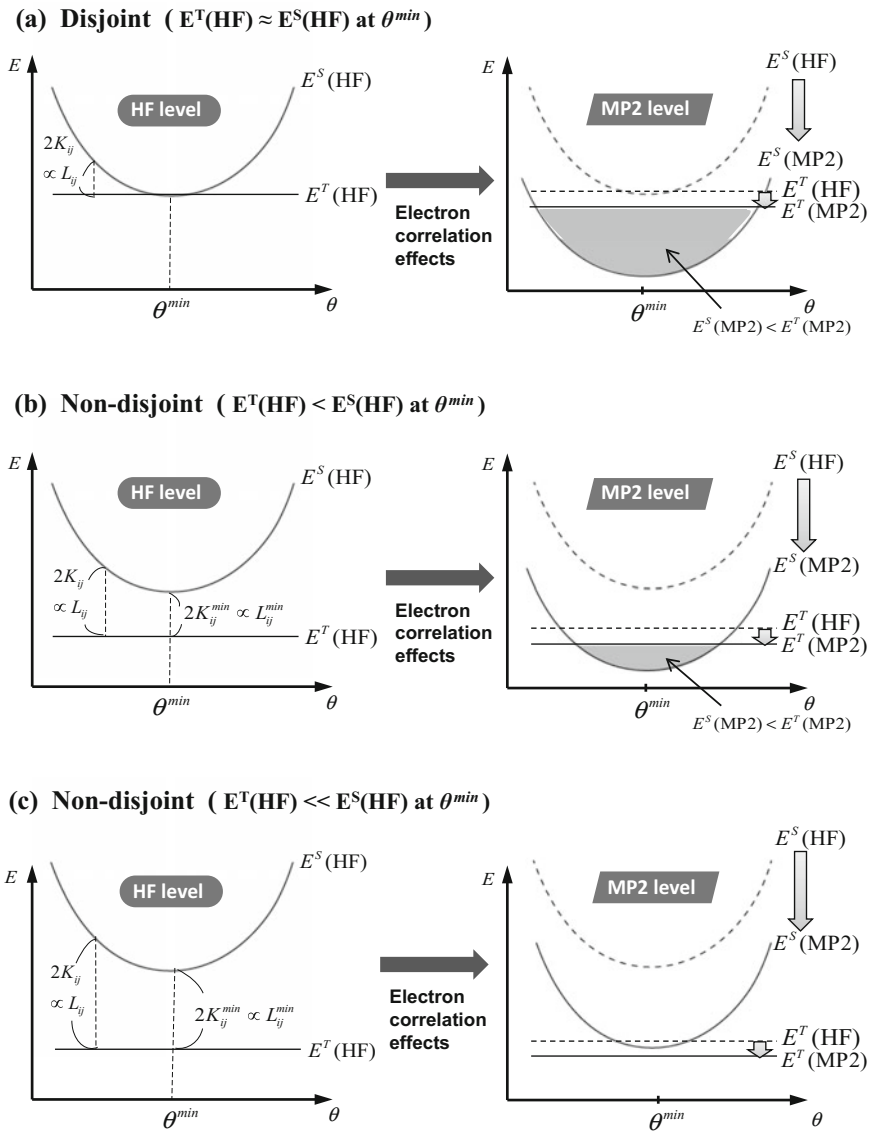

Fig. 3.6 Schematic illustration of θ dependences of singlet and triplet energies for **a** disjoint linkage, **b** non-disjoint linkage with $E^T(HF) < E^S(HF)$, and **c** non-disjoint linkage with $E^T(HF) \ll E^S(HF)$. Modified with permission from Ref. [1]. Copyright 1999 John Wiley & Sons, Inc.

In Fig. 3.6c (non-disjoint model), larger high-spin stability occurs at the HF level compared with the case shown in Fig. 3.6b. A large preference for high-spin stability at the HF level can prevent singlet–triplet inversion, even after the inclusion

of correlation effects. Our purpose is to find systems such as those shown in Fig. 3.6c that show high-spin stability even when electron correlation effects are considered.

Of course, it is possible to confirm the occurrence of the inversion by performing post-HF calculations; however, post-HF calculations have much higher computational costs than HF-level calculations, and it is not realistic to use such calculations to identify high-spin systems from a large number of candidates.

3.2.5 *Comparison Between* L_{ij}^{min} *and Ab Initio MP2 Calculations*

To confirm the reliability of $L_{ij}^{\min}$, the index $L_{ij}^{\min}$ was compared with the direct ab initio calculations at the MP2 level using eight models, as shown in Fig. 3.7. Figure 3.7a–c show diradical models; the upper and bottom models correspond to disjoint (0–0) and non-disjoint (0–*) linkage models, respectively. Figure 3.7d illustrates triradical models; the upper and bottom models, respectively, correspond to disjoint (0–0) and non-disjoint (0–*) linkages between part-A, which consists of a non-disjoint (0–*) linkage dimer, and monomeric part-B. Each panel includes the $L_{ij}^{\min}$ value obtained using the Hückel method. ΔE^{S-T}(HF) and ΔE^{S-T}(MP2) are the singlet–triplet energy differences ($E^{singlet} - E^{triplet}$) at the HF and MP2 levels, respectively. Similarly, ΔE^{D-Q}(HF) and ΔE^{D-Q}(MP2) are the doublet–quartet energy differences ($E^{doublet} - E^{quartet}$) at the HF and MP2 levels, respectively.

In all of the models, ΔE^{S-T}(HF) and ΔE^{D-Q}(HF) are positive, which means these models show high-spin stability at the HF level. The point here is the extent to which the electron correlation effects reduce the high-spin stability. In the AR dimer models (Fig. 3.7a), the absolute value of ΔE^{S-T} decreases with the change from HF to MP2 for both the disjoint and non-disjoint linkages. Although ΔE^{S-T} for both linkages remains positive, even at the MP2 level, the non-disjoint linkage is more positive than the disjoint linkage, which suggests larger high-spin stability in the former case. In the models consisting of benzyl and AR units (Fig. 3.7b), ΔE^{S-T} decreases with the change from HF to MP2 for both the disjoint and non-disjoint linkages. ΔE^{S-T} for the non-disjoint type remains positive, even at the MP2 level, while ΔE^{S-T} for the disjoint type becomes negative at the MP2 level. Consequently, only the non-disjoint type is expected to have a high-spin stability. In the model consisting of two benzyl radical (BR) units (Fig. 3.7c), ΔE^{S-T} increases and becomes negative for both the disjoint and non-disjoint linkages upon changing from HF to MP2. However, ΔE^{S-T}(MP2) of the non-disjoint type is larger than that of the disjoint type. In triradical models with a linkage between parts A and B (Fig. 3.7d), ΔE^{D-Q}(MP2) for the non-disjoint type is more positive than that of the disjoint type. Therefore, the non-disjoint type has a larger high-spin stability than the disjoint type.

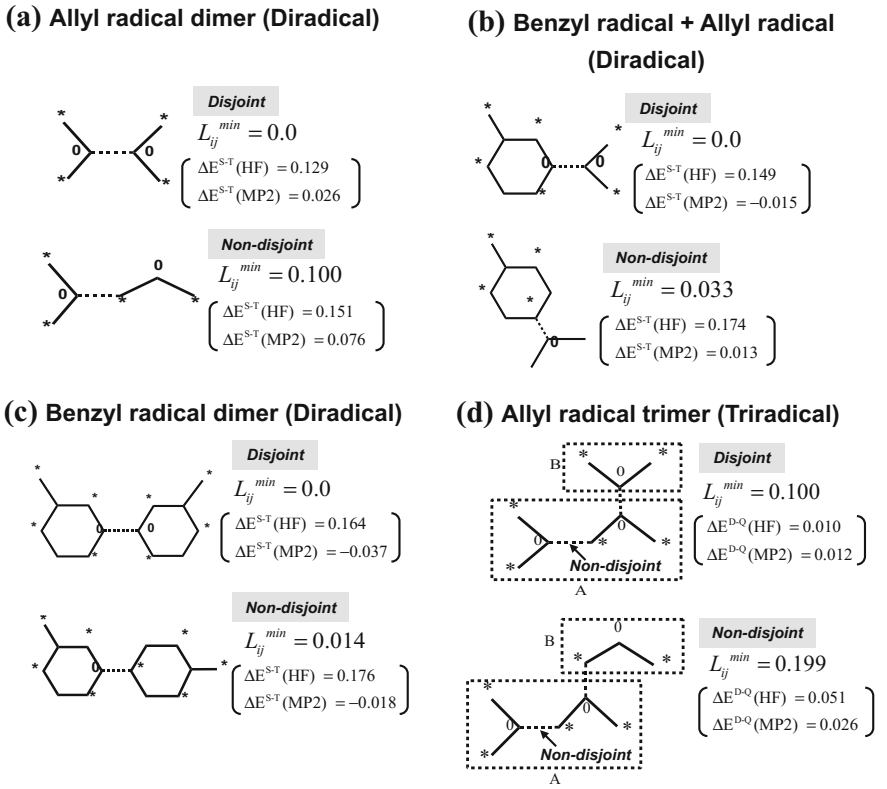

Fig. 3.7 **a–c** Diradical models with disjoint (*upper*) and non-disjoint (*bottom*) linkages between radical monomers. **d** Triradical models with disjoint (*upper*) and non-disjoint (*bottom*) linkages between AR (0–*) dimer (part A) and monomer (part B). Each panel includes L_{ij}^{min}, calculated using Hückel method, and singlet–triplet(or doublet–quartet) energy difference, ΔE^{S-T} (or ΔE^{D-Q}) estimated from ab initio MO calculations. Modified with permission from Ref. [1]. Copyright 1999 John Wiley & Sons, Inc.

It was found that, for all of the cases shown in Fig. 3.7, L_{ij}^{min} for the non-disjoint type was larger than that of the disjoint type. We can conclude that L_{ij}^{min} can accurately predict the tendency for high-spin stability when considering electron correlation effects; therefore, L_{ij}^{min} can be useful for the efficient design of organic ferromagnetic materials.

We propose here a practical strategy using L_{ij}^{min} to find high-spin systems efficiently (see Fig. 3.8). First, systems with large values of L_{ij}^{min} at the HF level are identified from a large number of possible molecules as the first selection (Fig. 3.8a). Next, post-HF calculations such as MP2 are applied to the selected

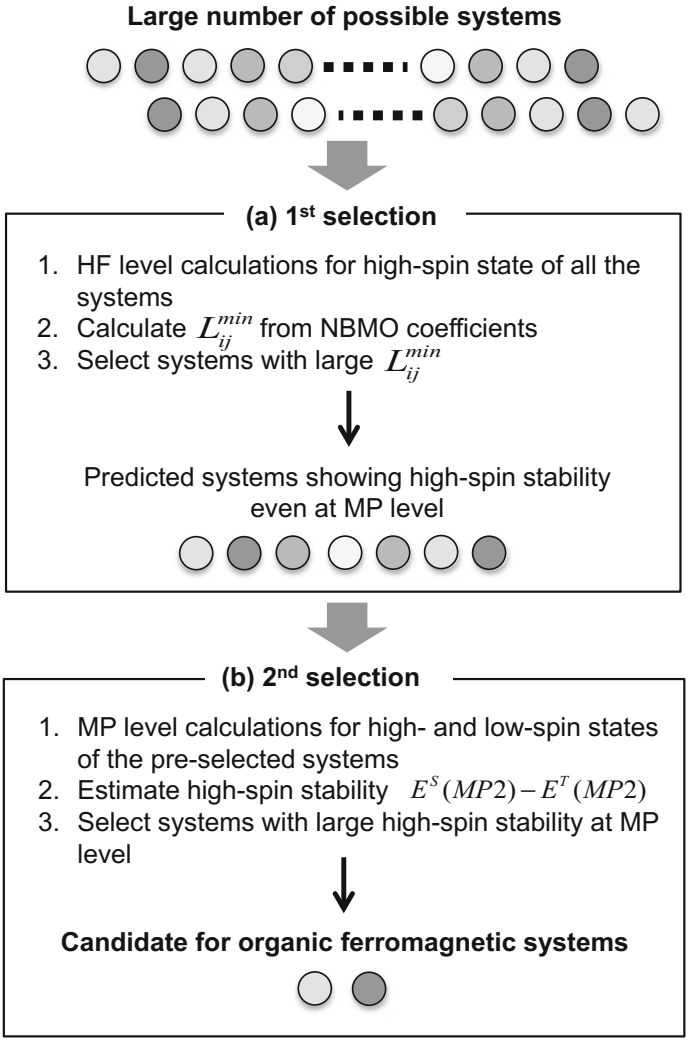

Fig. 3.8 Proposed strategy for selecting organic ferromagnetic candidates using $L_{ij}^{\min}$; **a** 1st selection in which systems with large $L_{ij}^{\min}$ are selected at the HF level, and **b** 2nd selection in which the selected candidates are calculated at a post-HF level to confirm the high-spin stability while considering electron correlation effects

candidates to confirm the high-spin stability while considering electron correlation effects as the second selection (Fig. 3.8b). This two-step selection process can make it possible to identify ferromagnetic candidate materials efficiently from a large number of possible systems.

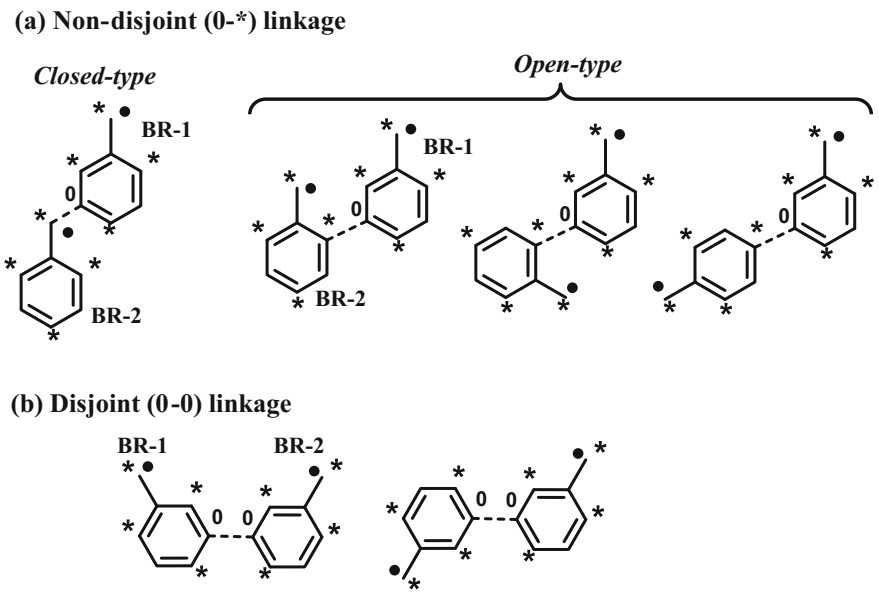

Fig. 3.9 Three different types of linkages between BR units: **a** (*left*) closed non-disjoint (0–*), (*right*) open non-disjoint (0–*), and **b** disjoint (0–0) linkage models. Modified with permission from Ref. [3]. Copyright 2006 American Chemical Society

3.3 Analytical Approach to L_{ij}

$L_{ij}^{\min}$ is useful for predicting whether or not a system will exhibit ferromagnetism because its calculation only requires the NBMO coefficients for the high-spin state. For huge systems, however, it is often hard to obtain MO coefficients. Here, we introduce an analytical prediction (AP) method that allows the efficient calculation of $L_{ij}^{\min}$ for a large system [3]. This analytical approach can be realized without performing direct QC calculations by predicting the NBMO shapes corresponding to $L_{ij}^{\min}$ using only the "zero-sum rule" of the NBMO method.

3.3.1 Closed and Open Non-disjoint (0–) Linkages*

We now focus on the system based on a BR unit, which is often used in typical organic ferromagnetic materials. For the BR dimer consisting of *BR-1* and *BR-2* (Fig. 3.9), two types of linkage models, that is, non-disjoint (0–*) (Fig. 3.9a) and disjoint (0–0) (Fig. 3.9b) linkage models, can be defined. The (0–*) linkage can be further divided into *closed* and *open* (0–*) models depending on their linkage position, as shown in Fig. 3.9a. In the closed model, the radical center of BR-2, denoted as "•", links to the inactive carbon atom ("0") at the *meta* position of BR-1.

Here, the radical center corresponds to the active carbon ("*") with the largest NBMO coefficient in the radical unit. On the other hand, in the open model, the active carbon at the *ortho* or *para* positions of BR-2 links to the inactive carbon at the *meta* position of BR-1. In the following subsection, we explain the AP method for calculating $L_{ij}^{\min}$ for both the closed and open (0–*) models.

3.3.2 Closed (0–*) Linkage: Benzyl Radical Dimer (Diradical Model)

Figure 3.10 illustrates the AP procedures for predicting the NBMO shapes of a BR dimer model with a closed (0–*) linkage. The procedure can be summarized as follows:

(i) First, the whole system is divided into separate BR units. According to the conventional NBMO zero-sum rule, the NBMO coefficients are assigned separately for each BR unit using different letters *a, b*, *c*, etc. within the area of each unique unit.

(ii) Next, the assignment is continued to the area outside of the BR unit of interest. When we are focused on BR-1, for example, the zero-sum assignment is expanded to the BR-2 region. According to the rule, however, the NBMO on BR-1 (NBMO1, assigned by *a*) cannot be expanded to the BR-2 region. In contrast, the rule allows for the expansion of the NBMO on BR-2 (NBMO2, assigned by *b*) to the region of BR-1. Consequently, NBMO1 is localized only on the BR-1 unit, while NBMO2 can be delocalized onto both the BR-1 and BR-2 units. For the sake of convenience, NBMO1, which is delocalized onto one benzene ring, is defined as a *single ring* (SR)-type NBMO, whereas NBMO2, which is delocalized onto two benzene rings, is defined as a *double ring* (DR)-type NBMO.

(iii) The NBMO coefficients, *a* and *b*, can be obtained by normalization as

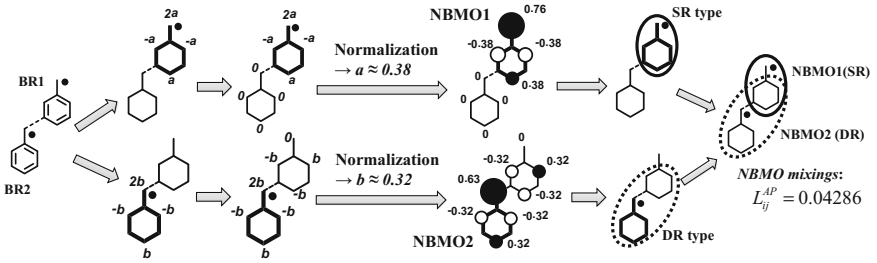

Fig. 3.10 AP of NBMO shapes and L_{ij} for closed (0–*) BR dimer. Modified with permission from Ref. [3]. Copyright 2006 American Chemical Society

$$\begin{aligned}
\textbf{NBMO1 (SR type)}: \sum_r C_{NBMO1,r}^2 &= (2a)^2 + 2(-a)^2 + a^2 = 7a^2 = 1 \\
\textbf{NBMO2 (DR type)}: \sum_r C_{NBMO2,r}^2 &= (2b)^2 + 4(-b)^2 + 2b^2 = 10b^2 = 1 \\
a = \frac{1}{\sqrt{7}} \approx 0.37796, &\quad b = \frac{1}{\sqrt{10}} \approx 0.31623.
\end{aligned} \tag{3.28}$$

(iv) Finally, L_{ij} can be calculated from the NBMO coefficients as

$$\begin{aligned}
L_{ij} &= \sum_r (C_{ri}C_{rj})^2 = (ab)^2 + (ab)^2 + (ab)^2 = 3(\mathrm{ab})^2 = 3\left(\frac{1}{\sqrt{7}} \times \frac{1}{\sqrt{10}}\right)^2 \\
&= \frac{3}{70} \approx 0.04286 = L_{ij}^{AP(1,SR\leftrightarrow 2,DR)},
\end{aligned} \tag{3.29}$$

where L_{ij} is denoted as $L_{ij}^{AP(1,SR\leftrightarrow 2,DR)}$, which means the analytically predicted L_{ij} for the mixing between NBMO1 (SR-type) and NBMO2 (DR-type).

It should be stressed that these procedures only include calculations that may be undertaken mentally [(i) and (ii)] and through simple number work [(iii) and (iv)].

Figure 3.11 shows $L_{ij}^{\min}$ and the corresponding NBMO shapes for the BR dimer calculated using the simple Hückel MO (HMO) method and subsequent unitary rotations. It was found that our AP results in Fig. 3.10 accurately predicted both $L_{ij}^{\min}$ and the NBMO shapes calculated using the HMO method. $L_{ij}^{\min}$(HMO) was slightly larger than $L_{ij}^{AP(1,SR\leftrightarrow 2,DR)}$. This difference can be explained by the fact that the AP approach is capable of predicting more ideal minimum NBMO mixings, though the HMO treatment reaches the vicinity of the minimum point after the unitary rotation. The AP approach is therefore a promising method of finding the ideal minimum of L_{ij}.

3.3.3 *Closed (0–*) Linkage: Benzyl Radical Trimer (Triradical Model)*

Figure 3.12 shows three possible models of the closed (0–*) BR trimer, that is, trimer-A, trimer-B, and trimer-C. Each model consists of three BR units, BR-1, BR-2, and BR-3, and involves three NBMOs.

In the same manner as for the dimer model, we can predict $L_{ij}^{\min}$ for the trimer models without QC calculations. First, we focus on trimer-A, which exhibits a linear form. After assigning the NBMO coefficients within each BR unit based on

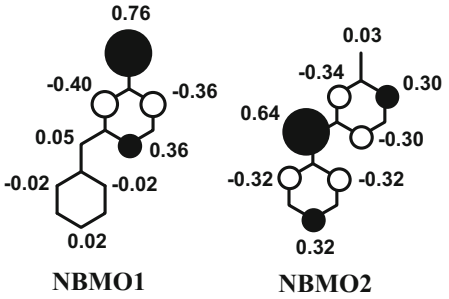

Fig. 3.11 NBMO coefficients corresponding to $L_{ij}^{\min}$ for closed (0–*) BR dimer calculated using simple HMO method followed by unitary rotation. Modified with permission from Ref. [3]. Copyright 2006 American Chemical Society

***NBMO mixings*:** $L_{ij}^{min\,(HMO)} = 0.04302$

the zero-sum rule, the assignment is extended to the whole molecule by the same rule. We use the letters, a, b, and c for NBMO1, NBMO2, and NBMO3, respectively. As a result, we can obtain the SR-type orbital NBMO1 and the DR-type orbitals NBMO2 and NBMO3. By normalizing the coefficients, we can obtain

$$\text{Trimer-A} : a = \frac{1}{\sqrt{7}} (\text{for SR type}), \quad b = c = \frac{1}{\sqrt{10}} (\text{for DR type}). \tag{3.30}$$

Thus, L_{ij}^{AP} can be estimated as

$$\begin{aligned} \text{Trimer-A} : L_{ij}^{AP} &= \sum_{i,j(>i)} L_{ij}^{AP\circ} = L_{ij}^{AP\circ(1,\text{SR}\leftrightarrow 2,DR)} \\ &\quad + L_{ij}^{AP\circ(1,SR\leftrightarrow 3,DR)} + L_{ij}^{AP\circ(1,SR\leftrightarrow 3,DR)} \\ &= 3 \times (ab)^2 + 0 + 3 \times (bc)^2 \\ &= 3\left(\frac{1}{\sqrt{7}} \times \frac{1}{\sqrt{10}}\right)^2 + 3\left(\frac{1}{\sqrt{10}} \times \frac{1}{\sqrt{10}}\right)^2 \\ &= \frac{3}{70} + \frac{3}{100} \approx 0.07286. \end{aligned} \tag{3.31}$$

Similarly, for trimer-B, NBMO1, NBMO2, and NBMO3 correspond to SR-, DR-, and DR-type, respectively. We can obtain the normalized coefficients and L_{ij}^{AP} as

$$\begin{aligned} &\text{Trimer-B} : a = \frac{1}{\sqrt{7}} \ (\text{for SR type}), \quad b = c = \frac{1}{\sqrt{10}} \ (\text{for DR type}) \\ &L_{ij}^{AP} = \sum_{i,j(>i)} L_{ij}^{AP\circ} = L_{ij}^{AP\circ(1,SR\leftrightarrow 2,DR)} + L_{ij}^{AP\circ(1,SR\leftrightarrow 3,DR)} + L_{ij}^{AP\circ(2,DR\leftrightarrow 3,DR)} \\ &\quad = 3 \times (ab)^2 + 3 \times (ac)^2 + 3 \times (bc)^2 = \frac{3}{70} + \frac{3}{70} + \frac{3}{100} \approx 0.11571. \end{aligned} \tag{3.32}$$

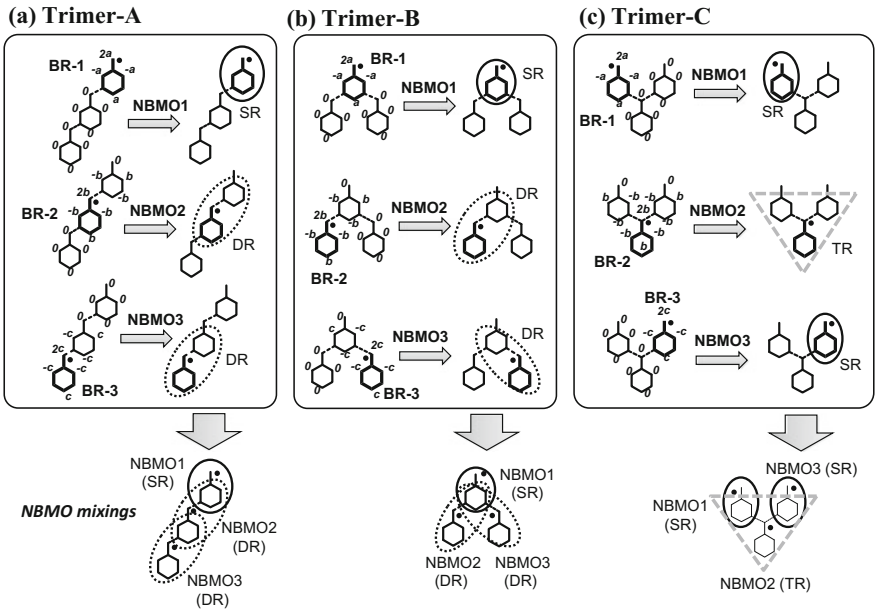

Fig. 3.12 AP of NBMO shapes and L_{ij} for closed (0–*) BR trimers, **a** trimer-A, **b** trimer-B, and **c** trimer-C. Modified with permission from Ref. [3]. Copyright 2006 American Chemical Society

For trimer-C, both NBMO1 and NBMO3 are SR-type. In contrast, NBMO2 is delocalized onto three benzene rings; therefore, we call this orbital a *triple ring* (TR)-type NBMO. The normalized coefficients and L_{ij}^{AP} value can be obtained as

$$\begin{aligned}
&\text{Trimer-C}: a = c = \frac{1}{\sqrt{7}} \text{ (for SR type)};\\
&\sum_r C_{NBMO2,r}^2 = (2b)^2 + 6(-b)^2 + 3b^2 = 13b^2 = 1;\\
&\qquad b = \frac{1}{\sqrt{13}} \approx 0.27735 \text{ (TR type)}\\
&L_{ij}^{AP} = \sum_{i,j(>i)} L_{ij}^{AP\circ} = L_{ij}^{AP\circ(1,SR\leftrightarrow 2,TR)} + L_{ij}^{AP\circ(1,SR\leftrightarrow 3,SR)} + L_{ij}^{AP\circ(2,TR\leftrightarrow 3,SR)}\\
&\qquad = 3\times(ab)^2 + 0 + 3\times(bc)^2 = 3\left(\frac{1}{\sqrt{7}}\times\frac{1}{\sqrt{13}}\right)^2\\
&\qquad + 3\left(\frac{1}{\sqrt{13}}\times\frac{1}{\sqrt{7}}\right)^2 = \frac{3}{91} + \frac{3}{91} \approx 0.06593. \qquad (3.33)
\end{aligned}$$

3.3.4 Closed (0–*) Linkage: Benzyl Radical Pentamer (Pentaradical Model)

As an example of a more complicated case, we investigated a BR pentamer model consisting of five BR units (BR-1 to BR-5) with five NBMOs. We selected one of the pentamer isomers, as shown in Fig. 3.13 (pentamer-A), to show the L_{ij}^{AP} estimation. For pentamer-A, the letters *a*–*e* were used for NBMO1–NBMO5. NBMO1 and NBMO2 were assigned as SR-type, whereas NBMO3 was DR-type. NBMO4 and NBMO5 were found to be TR-type. Therefore, the normalized NBMO coefficients are

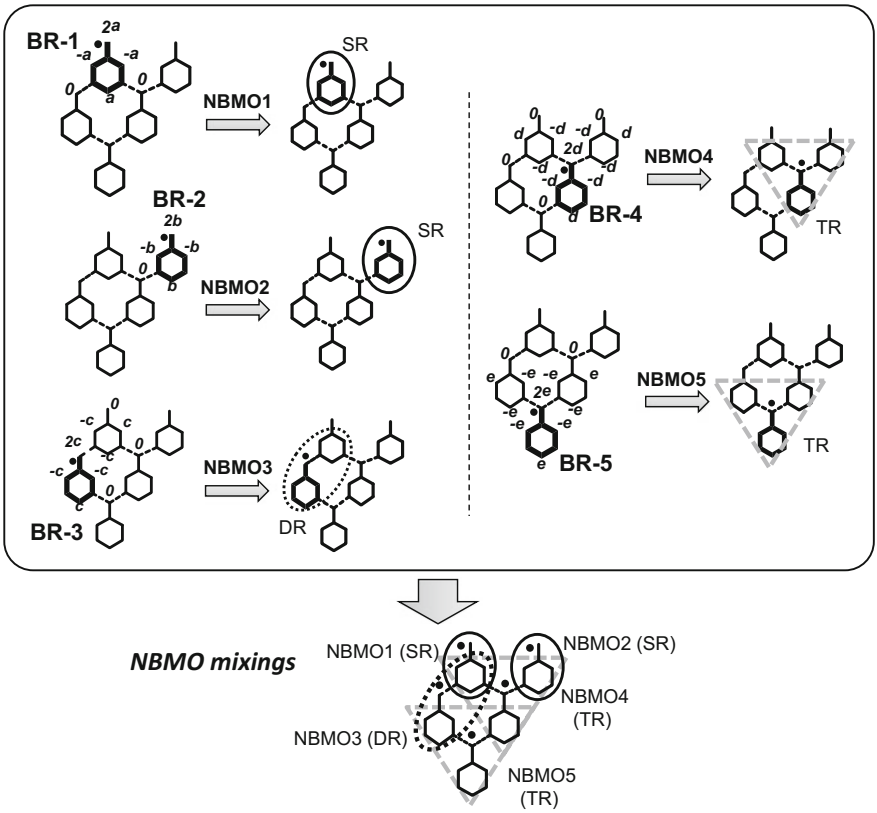

Fig. 3.13 AP of NBMO shapes with smallest overlaps for closed (0–*) BR pentamer (pentamer-A). Modified with permission from Ref. [3]. Copyright 2006 American Chemical Society

$$\begin{aligned}&\text{Pentamer-A}: a = b = \frac{1}{\sqrt{7}}\ (\text{for SR type}), \quad c = \frac{1}{\sqrt{10}}\ (\text{for DR type}),\\ &d = e = \frac{1}{\sqrt{13}}(\text{for TR type}).\end{aligned} \tag{3.34}$$

L_{ij}^{AP} for pentamer-A can be calculated as

$$\begin{aligned}\text{Pentamer-A}: L_{ij}^{AP} &= \sum_{i,j(>i)} L_{ij}^{AP\circ} = L_{ij}^{AP\circ(1,SR\leftrightarrow 3,DR)} + L_{ij}^{AP\circ(1,SR\leftrightarrow 4,TR)} + L_{ij}^{AP\circ(2,SR\leftrightarrow 4,TR)}\\ &\quad + L_{ij}^{AP\circ(3,DR\leftrightarrow 4,TR)} + L_{ij}^{AP\circ(3,DR\leftrightarrow 5,TR)} + L_{ij}^{AP\circ(4,TR\leftrightarrow 5,TR)}\\ &= 3\times(ac)^2 + 3\times(ad)^2 + 3\times(bd)^2 + 3\times(cd)^2 + 3\times(ce)^2 + 3\times(de)^2\\ &= \frac{3}{70} + \frac{3}{91} + \frac{3}{91} + \frac{3}{130} + \frac{3}{130} + \frac{3}{169} \approx 0.17270.\end{aligned} \tag{3.35}$$

In a closed (0–*) system, the NBMOs may be classified into only three types, i.e., SR, DR, and TR, even when considering systems with more than three benzene rings. In other words, there is no NBMO that is delocalized across more than three benzene rings within the framework of a closed (0–*) system.

3.3.5 *Closed (0–*) Linkage: Tetraradical Model Including Methylene and Methylidyne Radical Units*

Figure 3.14 shows a tetraradical model with a non-disjoint (0–*) linkage. The model includes both the methylene (:CH_2) and methylidyne (:CH·) radical units, MR-1 and MR-2, respectively, in addition to two BR units, BR-1 and BR-2.

Basically, the NBMO shapes can be predicted in a similar manner to that described in the previous subsections. First, the NBMO coefficients are assigned within each radical unit. The letters a, b, c, and d were used for MR-1, BR-1, MR-2, and BR-2 units, respectively. Although the conventional zero-sum rule was applied for assigning the BR units, "2a" and "2c" were assigned exceptionally for MR-1 and MR-2, respectively. After that, the assignment of NBMO coefficients was extended to the area of the other radical units according to the zero-sum rule. As a result, NBMO1–NBMO4 were obtained; NBMO1, NBMO2, and NBMO4 were assigned as SR-type, while NBMO3 was DR-type. Thus, we can obtain the normalized NBMO coefficients and L_{ij}^{AP} as

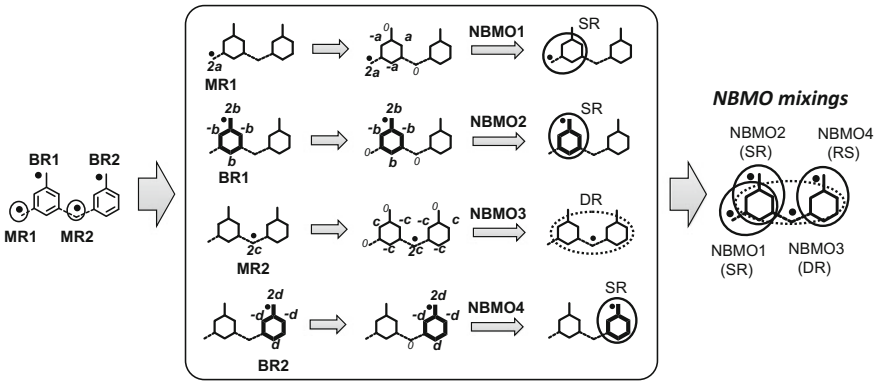

Fig. 3.14 AP of NBMO shapes with smallest overlaps for closed (0–*) tetraradical model that includes methylene (:CH_2) and methylidyne (:CH·) radical units (MR units). Modified with permission from Ref. [3]. Copyright 2006 American Chemical Society

$$
\begin{aligned}
a = b = d &= \frac{1}{\sqrt{7}}(\text{for SR type}), \quad c = \frac{1}{\sqrt{10}}\ (\text{for DR type}) \\
L_{ij}^{AP} &= \sum_{i,j(>i)} L_{ij}^{AP\circ} = L_{ij}^{AP\circ(1,SR\leftrightarrow 2,SR)} + L_{ij}^{AP\circ(1,SR\leftrightarrow 3,DR)} + L_{ij}^{AP\circ(1,SR\leftrightarrow 4,SR)} \\
&\quad + L_{ij}^{AP\circ(2,SR\leftrightarrow 3,DR)} + L_{ij}^{AP\circ(2,SR\leftrightarrow 4,SR)} + + L_{ij}^{AP\circ(3,DR\leftrightarrow 4,SR)} \\
&= 3\times(ab)^2 + 3\times(ac)^2 + 0 + 3\times(bc)^2 + 0 + 3\times(cd)^2 \\
&= \frac{3}{49} + \frac{3}{70} + \frac{3}{70} + \frac{3}{70} \approx 0.18980.
\end{aligned}
\tag{3.36}
$$

As shown here, by adding the initial assignments of "2*a*" and "2*c*" for the MR units to the AP procedures, L_{ij}^{AP} can also be estimated for the system that includes MR units.

3.3.6 *General Procedures for the Analytical Prediction of* L_{ij} *for Closed (0–*) Linkage Models*

It has been noted that there are three types of NBMO shapes for closed (0–*) linkage models; that is, SR-, DR-, and TR-type NBMOs, which are delocalized onto one, two, and three benzene rings, respectively. Based on the results discussed in the previous subsections, these three types of NBMOs are sufficient to assign NBMOs, even in very large closed (0–*) systems. From their combinations, six

possible types of NBMO mixings, and their corresponding L_{ij}^{AP} values, can be obtained as follows:

$$\begin{aligned}
&\text{SR} \leftrightarrow \text{SR: } L_{ij}^{AP\circ(SR\leftrightarrow SR)} = 3 \times (\alpha_i^{SR}\alpha_j^{SR})^2 = 3 \times \left(\frac{1}{\sqrt{7}} \times \frac{1}{\sqrt{7}}\right)^2 = \frac{3}{49} \approx 0.06122,\\
&\text{SR} \leftrightarrow \text{DR: } L_{ij}^{AP\circ(SR\leftrightarrow DR)} = 3 \times (\alpha_i^{SR}\alpha_j^{DR})^2 = 3 \times \left(\frac{1}{\sqrt{7}} \times \frac{1}{\sqrt{10}}\right)^2 = \frac{3}{70} \approx 0.04286,\\
&\text{SR} \leftrightarrow \text{TR: } L_{ij}^{AP\circ(SR\leftrightarrow TR)} = 3 \times (\alpha_i^{SR}\alpha_j^{TR})^2 = 3 \times \left(\frac{1}{\sqrt{7}} \times \frac{1}{\sqrt{13}}\right)^2 = \frac{3}{91} \approx 0.03297,\\
&\text{DR} \leftrightarrow \text{DR: } L_{ij}^{AP\circ(DR\leftrightarrow DR)} = 3 \times (\alpha_i^{DR}\alpha_j^{DR})^2 = 3 \times \left(\frac{1}{\sqrt{10}} \times \frac{1}{\sqrt{10}}\right)^2 = \frac{3}{100} = 0.03,\\
&\text{DR} \leftrightarrow \text{TR: } L_{ij}^{AP\circ(DR\leftrightarrow TR)} = 3 \times (\alpha_i^{DR}\alpha_j^{TR})^2 = 3 \times \left(\frac{1}{\sqrt{10}} \times \frac{1}{\sqrt{13}}\right)^2 = \frac{3}{130} \approx 0.02308,\\
&\text{and}\\
&\text{TR} \leftrightarrow \text{TR: } L_{ij}^{AP\circ(TR\leftrightarrow TR)} = 3 \times (\alpha_i^{TR}\alpha_j^{TR})^2 = 3 \times \left(\frac{1}{\sqrt{13}} \times \frac{1}{\sqrt{13}}\right)^2 = \frac{3}{169} \approx 0.01775.
\end{aligned} \tag{3.37}$$

Here, α_i^x (x = SR, DR, or TR) is the normalized coefficient of the i-th NBMO having an x-type shape, that is, SR, DR, or TR. α_i^x depends only on the NBMO shape and was already determined in the previous subsections as

$$\alpha_i^{SR} = \alpha_j^{SR} = \frac{1}{\sqrt{7}}, \quad \alpha_i^{DR} = \alpha_j^{DR} = \frac{1}{\sqrt{10}}, \quad \text{and} \quad \alpha_i^{TR} = \alpha_j^{TR} = \frac{1}{\sqrt{13}}. \tag{3.38}$$

We define the number of possible mixings of NBMO components $L_{ij}^{AP\circ(x_i\leftrightarrow x_j)}$ in the system as $N^{AP\circ(x_i\leftrightarrow x_j)}$, where x_i (= SR, DR, or TR) and x_j (= SR, DR, or TR) are the shapes of the i-th and j-th NBMOs, respectively. L_{ij}^{AP} for the whole system can be generally defined by

$$\begin{aligned}
L_{ij}^{AP} = {} & N^{AP\circ(SR\leftrightarrow SR)}L_{ij}^{AP\circ(SR\leftrightarrow SR)} + N^{AP\circ(SR\leftrightarrow DR)}L_{ij}^{AP\circ(SR\leftrightarrow DR)}\\
& + N^{AP\circ(SR\leftrightarrow TR)}L_{ij}^{AP\circ(SR\leftrightarrow TR)} + N^{AP\circ(DR\leftrightarrow DR)}L_{ij}^{AP\circ(DR\leftrightarrow DR)}\\
& + N^{AP\circ(DR\leftrightarrow TR)}L_{ij}^{AP\circ(DR\leftrightarrow TR)} + N^{AP\circ(TR\leftrightarrow TR)}L_{ij}^{AP\circ(TR\leftrightarrow TR)}.
\end{aligned} \tag{3.39}$$

Equation (3.39) is the general formulation for L_{ij}^{AP} for closed (0–*) BR systems with or without MR units. $N^{AP\circ(x_i\leftrightarrow x_j)}$ for each term can be counted by hand. Thus, L_{ij}^{AP} can be estimated from Eq. (3.39) using the $L_{ij}^{AP\circ}$ values listed in Eq. (3.37).

For example, the BR pentamer model in Fig. 3.13 has one SR ↔ DR, two SR ↔ TR, two DR ↔ TR, and one TR ↔ TR mixings. Thus, L_{ij}^{AP} can immediately be calculated as

$$\begin{aligned} L_{ij}^{AP} &= 0 \times L_{ij}^{AP\circ(SR\leftrightarrow SR)} + 1 \times L_{ij}^{AP\circ(SR-DR)} + 2 \times L_{ij}^{AP\circ(SR-TR)} + 0 \times L_{ij}^{AP\circ(DR-DR)} \\ &\quad + 2 \times L_{ij}^{AP\circ(DR-TR)} + 1 \times L_{ij}^{AP\circ(TR-TR)} \\ &= 1 \times \left(\frac{3}{70}\right) + 2 \times \left(\frac{3}{91}\right) + 2 \times \left(\frac{3}{130}\right) + 1 \times \left(\frac{3}{169}\right) \approx 0.17270. \end{aligned} \tag{3.40}$$

As another example, the tetraradical model containing MR units shown in Fig. 3.14 has one SR ↔ SR and three SR ↔ DR mixings. L_{ij}^{AP} is

$$\begin{aligned} L_{ij}^{AP} &= 1 \times L_{ij}^{AP\circ(SR\leftrightarrow SR)} + 3 \times L_{ij}^{AP\circ(SR-DR)} + 0 \times L_{ij}^{AP\circ(SR-TR)} + 0 \times L_{ij}^{AP\circ(DR-DR)} \\ &\quad + 0 \times L_{ij}^{AP\circ(DR-TR)} + 0 \times L_{ij}^{AP\circ(TR-TR)} \\ &= 1 \times \left(\frac{3}{49}\right) + 3 \times \left(\frac{3}{70}\right) \approx 0.18980. \end{aligned} \tag{3.41}$$

3.3.7 *Analytical Prediction of* L_{ij} *for Quasi-One-Dimensional Closed (0–*) Benzyl Radical Systems*

In this subsection, discuss the formulation of L_{ij}^{AP} as a function of N^{NBMO} for various quasi-one-dimensional closed (0–*) BR systems, which are shown in Figs. 3.15 and 3.17, where N^{NBMO} defines the number of NBMOs in a model. In two-line (2L) models, that is **2L-1**, **2L-2**, and **2L-3** in Fig. 3.15, the BR (or MR) units align in two lines, whereas in three-line (3L) models, that is **3L-1**, **3L-2**, and **3L-3** in Fig. 3.17, the units align in three lines.

Formulation of L_{ij}^{AP} for Two-Line Models

First, we formulate L_{ij}^{AP} for 2L models, i.e., **2L-1**, **2L-2**, and **2L-3**, which are shown in Fig. 3.15. The right-hand side of the figure shows the process of assigning the NBMO shapes using SR, DR, or TR for each NBMO. According to the assigned shape, we can systematically count the number of component NBMO mixings in the system. Figure 3.16 shows an example component count for the NBMO mixings in **2L-1**. We can count the number corresponding to each overlap-type (i.e., SR ↔ DR, DR ↔ DR, etc.) in the system at each N^{NBMO}. By using simple sequence treatments, the number of components with each type of NBMO mixing can be obtained for an arbitrary system size ($N^{NBMO} = n$).

Table 3.1 summarizes the number of components with each type of NBMO mixing as a function of N^{NBMO} for models **2L-x** (**x** = 1, 2, and 3). Here, L_{ij}^{AP} of **2L-1** for $N^{NBMO} = n$ can be formulated by Eq. (3.39) as

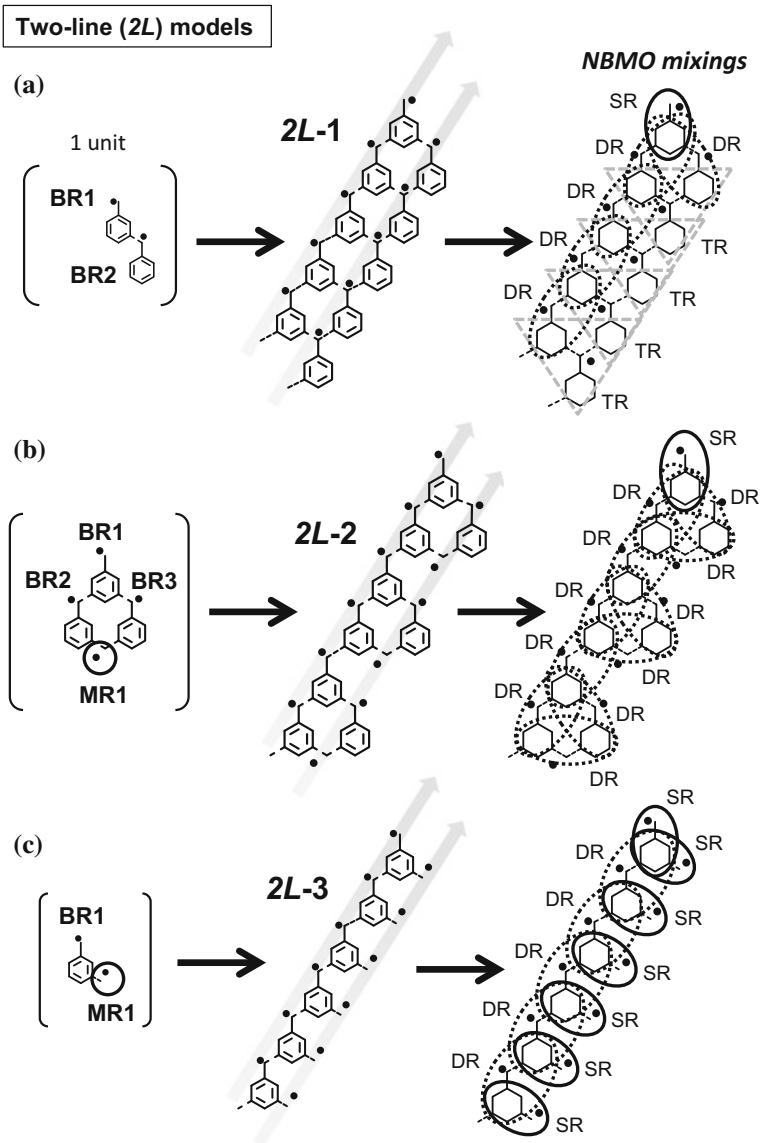

Fig. 3.15 AP of NBMO shapes with smallest overlaps for 2L models of quasi-one dimensional closed (0–*) BR systems. Each unit structure is shown in parentheses. Modified with permission from Ref. [3]. Copyright 2006 American Chemical Society

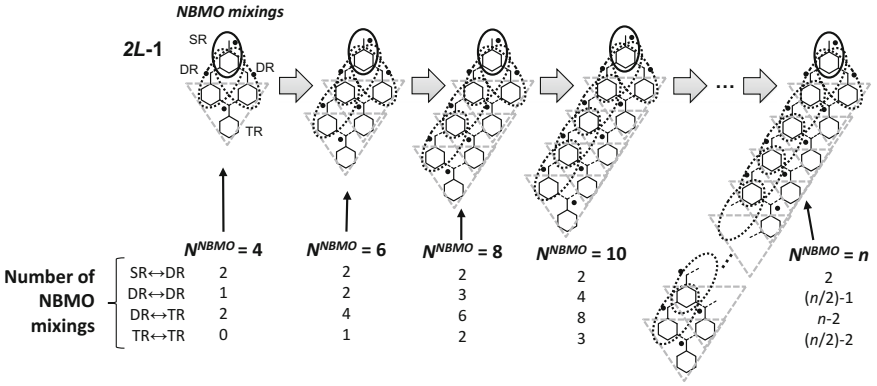

Fig. 3.16 Formulation of the number of components with each type of NBMO mixing for model **2L-1** used for predicting L_{ij}^{AP}. Modified with permission from Ref. [3]. Copyright 2006 American Chemical Society

Table 3.1 Number of components with each type of NBMO mixing at $N^{NBMO} = n$ for 2L and 3L models

Model	Number of components (NBMO mixing), $L_{ij}^{AP\circ}$						Condition of n
	SR ↔ SR	SR ↔ DR	SR ↔ TR	DR ↔ DR	DR ↔ TR	TR ↔ TR	
2L-1	0	2	0	$(n/2) - 1$	$n - 2$	$(n/2) - 2$	n = 4, 6, 8, 10, …
2L-2	0	2	0	$(7/4)n - 4$	0	0	n = 4, 8, 12, 16, …
2L-3	1	$n - 1$	0	$(n/2) - 2$	0	0	n = 2, 4, 6, 8, …
3L-1	0	2	0	$n/3$	$(2/3)n$	$(4/3)n - 7$	n = 6, 9, 12, 15, …
3L-2	0	3	$2(n/3 - 1)$	$(n/3) - 1$	$2(n/3 - 1)$	$(n/3) - 2$	n = 6, 9, 12, 15, …
3L-3	0	2	0	$n/2$	$(5/4)n - 3$	$(3/8)n - 2$	n = 8, 16, 24, 32, …

Modified with permission from Ref. [3]. Copyright 2006 American Chemical Society

Model 2L-1:

$$\begin{aligned} L_{ij}^{AP} &= 2L_{ij}^{AP\circ(SR\leftrightarrow DR)} + \left(\frac{n}{2} - 1\right) L_{ij}^{AP\circ(DR\leftrightarrow DR)} + (n-2) L_{ij}^{AP\circ(DR\leftrightarrow TR)} \\ &\quad + \left(\frac{n}{2} - 2\right) L_{ij}^{AP\circ(TR\leftrightarrow TR)} \\ &= \frac{6}{70} + \left(\frac{n}{2} - 1\right)\frac{3}{100} + (n-2)\frac{3}{130} + \left(\frac{n}{2} - 2\right)\frac{3}{169}. \end{aligned} \tag{3.42}$$

Basically, for all of the models discussed here, L_{ij}^{AP} increases with increasing system size. Thus, when comparing L_{ij}^{AP} among the different models, it is convenient to use the average value of L_{ij}^{AP} at the n limit ($n \to \infty$), i.e., $\lim_{n\to\infty}(L_{ij}^{AP}/n)$. The average value for **2L-1** is

$$\frac{L_{ij}^{AP}}{n} = \left\{\frac{6}{70n} + \left(\frac{1}{2} - \frac{1}{n}\right)\frac{3}{100} + \left(1 - \frac{2}{n}\right)\frac{3}{130} + \left(\frac{1}{2} - \frac{2}{n}\right)\frac{3}{169}\right\}, \tag{3.43}$$

and its n limit can be obtained as a unique value:

$$\lim_{n\to\infty}\frac{L_{ij}^{AP}}{n} = 0 + \left(\frac{1}{2} - 0\right)\frac{3}{100} + (1-0)\frac{3}{130} + \left(\frac{1}{2} - 0\right)\frac{3}{169} \approx 0.04695. \tag{3.44}$$

Similarly, L_{ij}^{AP} and $\lim_{n\to\infty}(L_{ij}^{AP}/n)$ can be obtained for **2L-2** and **2L-3** as

Model 2L-2:

$$\begin{aligned} L_{ij}^{AP} &= 2L_{ij}^{AP\circ(SR\leftrightarrow DR)} + \left(\frac{7}{4}n - 4\right)L_{ij}^{AP\circ(DR\leftrightarrow DR)} = \frac{6}{70} + \left(\frac{7}{4}n - 4\right)\frac{3}{100} \\ \lim_{n\to\infty}\frac{L_{ij}^{AP}}{n} &= \lim_{n\to\infty}\left\{\frac{6}{70n} + \left(\frac{7}{4} - \frac{4}{n}\right)\frac{3}{100}\right\} = 0 + \left(\frac{7}{4} - 0\right)\frac{3}{100} = 0.0525, \end{aligned} \tag{3.45}$$

and

Model 2L-3:

$$\begin{aligned} L_{ij}^{AP} &= L_{ij}^{AP\circ(SR\leftrightarrow SR)} + (n-1)L_{ij}^{AP\circ(SR\leftrightarrow DR)} + \left(\frac{n}{2} - 2\right)L_{ij}^{AP\circ(DR\leftrightarrow DR)} \\ &= \frac{3}{49} + (n-1)\frac{3}{70} + \left(\frac{n}{2} - 2\right)\frac{3}{100} \\ \lim_{n\to\infty}\frac{L_{ij}^{AP}}{n} &= \lim_{n\to\infty}\left\{\frac{3}{49n} + \left(1 - \frac{1}{n}\right)\frac{3}{70} + \left(\frac{1}{2} - \frac{2}{n}\right)\frac{3}{100}\right\} \\ &= 0 + (1-0)\frac{3}{70} + \left(\frac{1}{2} - 0\right)\frac{3}{100} \approx 0.05786, \end{aligned} \tag{3.46}$$

respectively. Therefore, $\lim_{n\to\infty}(L_{ij}^{AP}/n)$ predicts the order of high-spin stability as **2L-3**(≈ 0.05786) > **2L-2** (= 0.0525) > **2L-1** (≈ 0.04695).

Formulation of L_{ij}^{AP} for Three-Line Models

We can formulate L_{ij}^{AP} for 3L models, i.e., **3L-1**, **3L-2**, and **3L-3**, which are shown in Fig. 3.17, in the same way as for the 2L models. Table 3.1 also lists the number of components with each type of NBMO mixing as a function of N^{NBMO} for

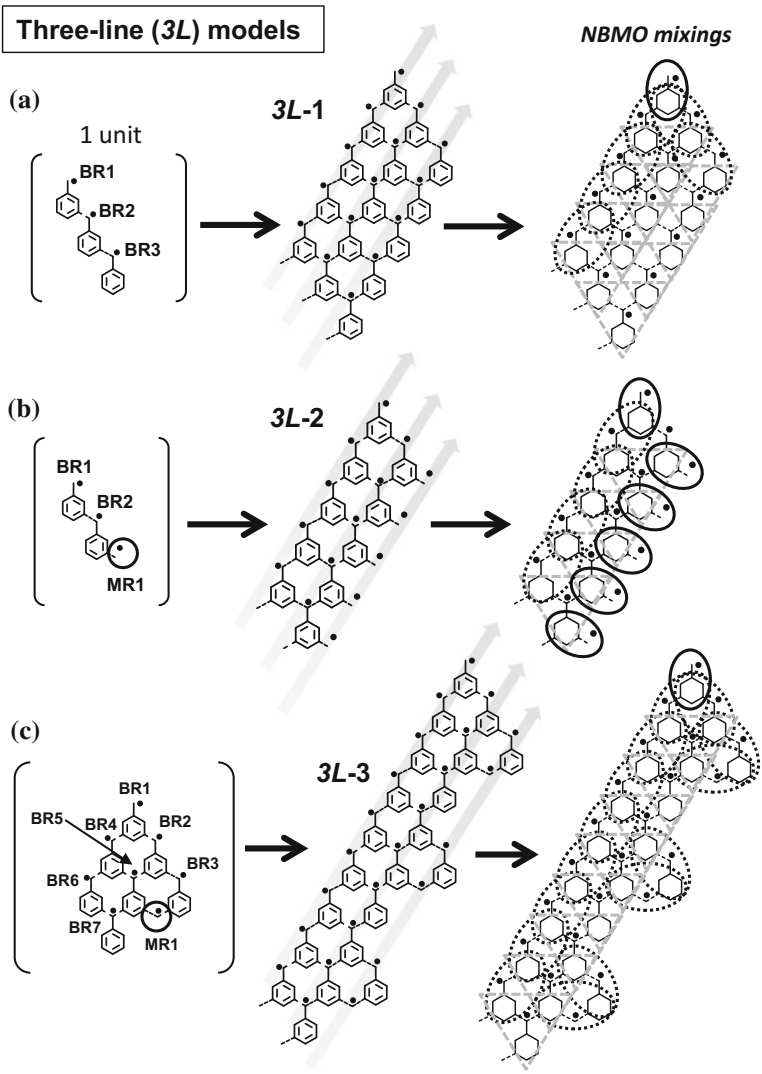

Fig. 3.17 AP of NBMO shapes with smallest overlaps for 3L models of quasi-one-dimensional BR closed (0–*) systems. Modified with permission from Ref. [3]. Copyright 2006 American Chemical Society

models **3L-x** (**x** = 1, 2, and 3). L_{ij}^{AP} and $\lim_{n\to\infty}(L_{ij}^{AP}/n)$ can be estimated for **3L-1** to **3L-3** by

Model 3L-1:

$$\begin{aligned} L_{ij}^{AP} &= 2L_{ij}^{AP\circ(SR\leftrightarrow DR)} + \left(\frac{n}{3}\right)L_{ij}^{AP\circ(DR\leftrightarrow DR)} + \left(\frac{2}{3}n\right)L_{ij}^{AP\circ(DR\leftrightarrow TR)} \\ &\quad + \left(\frac{4}{3}n - 7\right)L_{ij}^{AP\circ(TR\leftrightarrow TR)} \\ &= \frac{6}{70} + \frac{n}{100} + \frac{2n}{130} + \left(\frac{4n}{3} - 7\right)\frac{3}{169} \\ \lim_{n\to\infty}\frac{L_{ij}^{AP}}{n} &= \lim_{n\to\infty}\left\{\frac{6}{70n} + \frac{1}{100} + \frac{2}{130} + \left(\frac{4}{3} - \frac{7}{n}\right)\frac{3}{169}\right\} \\ &= 0 + \frac{1}{100} + \frac{2}{130} + \left(\frac{4}{3} - 0\right)\frac{3}{169} \approx 0.04905, \end{aligned} \tag{3.47}$$

Model 3L-2:

$$\begin{aligned} L_{ij}^{AP} &= 3L_{ij}^{AP\circ(SR\leftrightarrow DR)} + \left(\frac{n}{3} - 1\right)\left(2L_{ij}^{AP\circ(SR\leftrightarrow TR)} + L_{ij}^{AP\circ(DR\leftrightarrow DR)} + 2L_{ij}^{AP\circ(DR\leftrightarrow TR)}\right) \\ &\quad + \left(\frac{n}{3} - 2\right)L_{ij}^{AP\circ(TR\leftrightarrow TR)} \\ &= \frac{9}{70} + \left(\frac{n}{3} - 1\right)\left(\frac{6}{91} + \frac{3}{100} + \frac{6}{130}\right) + \left(\frac{n}{3} - 2\right)\frac{3}{169} \\ \lim_{n\to\infty}\frac{L_{ij}^{AP}}{N} &= \lim_{n\to\infty}\left\{\frac{9}{70n} + \left(\frac{1}{3} - \frac{1}{n}\right)\left(\frac{6}{91} + \frac{3}{100} + \frac{6}{130}\right) + \left(\frac{1}{3} - \frac{2}{n}\right)\frac{3}{169}\right\} \\ &= 0 + \left(\frac{1}{3} - 0\right)\left(\frac{6}{91} + \frac{3}{100} + \frac{6}{130}\right) + \left(\frac{1}{3} - 0\right)\frac{3}{169} \approx 0.05328, \end{aligned} \tag{3.48}$$

and

Model 3L-3:

$$\begin{aligned} L_{ij}^{AP} &= 2L_{ij}^{AP\circ(SR\leftrightarrow DR)} + \left(\frac{n}{2}\right)L_{ij}^{AP\circ(DR\leftrightarrow DR)} + \left(\frac{5}{4}n-3\right)L_{ij}^{AP\circ(DR\leftrightarrow TR)} \\ &\quad + \left(\frac{3}{8}n-2\right)L_{ij}^{AP\circ(TR\leftrightarrow TR)} \\ &= \frac{6}{70} + \left(\frac{n}{2}\right)\frac{3}{100} + \left(\frac{5}{4}n-3\right)\frac{3}{130} + \left(\frac{3}{8}n-2\right)\frac{3}{169} \qquad (3.49) \\ \lim_{n\to\infty}\frac{L_{ij}^{AP}}{n} &= \lim_{n\to\infty}\left\{\frac{6}{70n} + \left(\frac{1}{2}\right)\frac{3}{100} + \left(\frac{5}{4}-\frac{3}{n}\right)\frac{3}{130} + \left(\frac{3}{8}-\frac{2}{n}\right)\frac{3}{169}\right\} \\ &= 0 + \left(\frac{1}{2}\right)\frac{3}{100} + \left(\frac{5}{4}-0\right)\frac{3}{130} + \left(\frac{3}{8}-0\right)\frac{3}{169} \approx 0.05050. \end{aligned}$$

3.3.8 *Comparison Between* L_{ij}^{AP} *and Direct Quantum Chemistry Calculations for Quasi-One-Dimensional Closed (0–*) Benzyl Radical Systems*

To confirm the validity of our AP, L_{ij}^{AP} for quasi-one-dimensional closed (0–*) models was compared with the high-spin stability obtained using direct QC calculations. Figure 3.18a shows the relationship between L_{ij}^{AP} and the number of

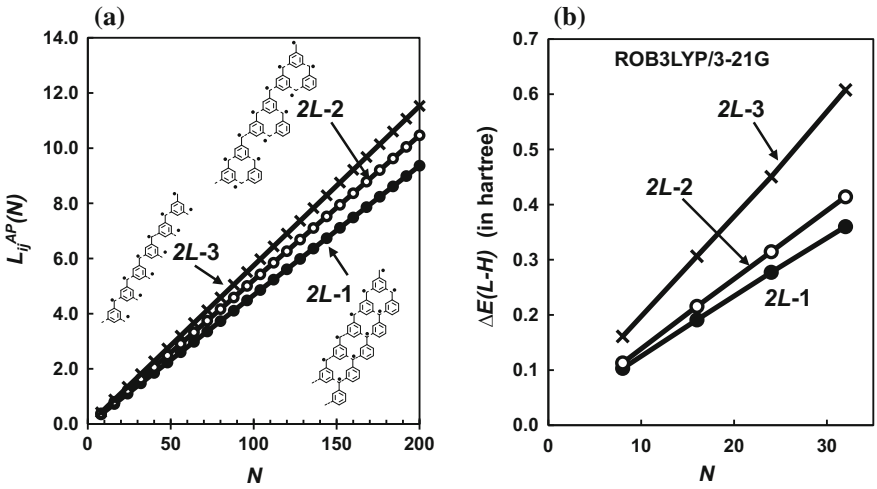

Fig. 3.18 Relationship between N and **a** $L_{ij}^{AP}(N)$, **b** $\Delta E(L–H)$ for 2L models. Modified with permission from Ref. [3]. Copyright 2006 American Chemical Society

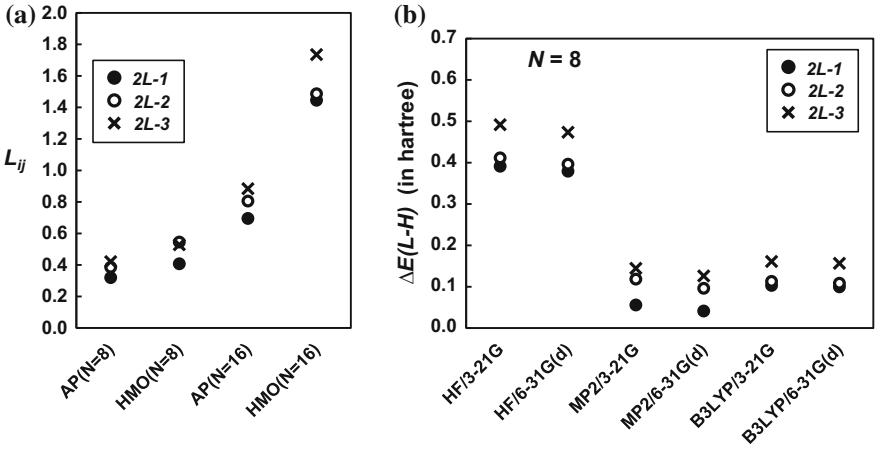

Fig. 3.19 **a** Comparison of L_{ij} for AP and HMO + unitary rotation methods for 2L models (N = 8 and 16). **b** Comparison of $\Delta E(L–H)$ calculated at various levels of theory for 2L models (N = 8). Modified with permission from Ref. [3]. Copyright 2006 American Chemical Society

radical centers N (= N^{NBMO}) for models **2L-1** to **2L-3**. The AP approach predicted the order of high-spin stability to be **2L-3** > **2L-2** > **2L-1** regardless of N. Reasonably, the order is consistent with the results from $\lim_{n\to\infty}(L_{ij}^{AP}/n)$. For the first step, L_{ij}^{AP} was compared with that obtained using the HMO method ($L_{ij}^{\min}$(HMO)) (see Fig. 3.19a). For comparison, N = 8 and 16 were selected as the numbers of radical centers. Although L_{ij}^{AP} is smaller than $L_{ij}^{\min}$(HMO), the order of L_{ij}^{AP} is similar to that of $L_{ij}^{\min}$(HMO) at both N = 8 and 16, except for the inversion of **2L-2** and **2L-3** at N = 8. This difference can be explained by the fact that unitary rotations of $L_{ij}^{\min}$(HMO) did not result in the identification of the ideal minimum L_{ij}, whereas L_{ij}^{AP} corresponds to the minimum.

Next, the AP results were compared with the high-spin stability, $\Delta E_{Total}^{LS-HS}\left(=E_{Total}^{LS}-E_{Total}^{HS}\right)$, estimated using ab initio calculations, where E_{Total}^{LS} and E_{Total}^{HS} are the total energies of the lowest and highest spin states, respectively. Figure 3.19b shows ΔE_{Total}^{LS-HS} for **2L-1** to **2L-3** for N = 8 at various levels of theory, calculated using the Gaussian 03 program [4]. Here, ΔE_{Total}^{LS-HS} was obtained from single-point calculations based on standard geometrical parameters: C–C = 1.395 Å, C–H = 1.100 Å for a benzene ring; C–C = 1.54 Å, C–H = 1.070 Å for CH or CH_2 groups; 120° was adopted for all the bond angles; dihedral angles were selected to maintain a planar structure. The split-valence basis sets 3-21G, 6-31G, and 6-31G(d) were used. We selected the HF, second-order Møller-Plesset perturbation theory (MP2) with frozen core (FC) approximation, and DFT (B3LYP functional) levels of theory. The restricted open-shell HF (ROHF) scheme was selected for calculating the open-shell systems. From Fig. 3.19b, it can

be seen that the order of ΔE_{Total}^{LS-HS} was **2L-3 > 2L-2 > 2L-1** for all the computational conditions. Thus, we can conclude that L_{ij}^{AP} accurately reproduced the order of ΔE_{Total}^{LS-HS} estimated using ab initio calculations. In Fig. 3.19b, the MP2 and DFT results show smaller values of ΔE_{Total}^{LS-HS} than the HF results as a result of correlation effects that mainly stabilize the low-spin state compared with the high-spin state.

To confirm the suitability of L_{ij}^{AP} for predicting high-spin stability for larger values of N, we examined the relationship between ΔE_{Total}^{LS-HS} and N (= 8, 16, 24, and 32) for **2L-1** to **2L-3** at the ROB3LYP/3-21G level (see Fig. 3.18b). The order of ΔE_{Total}^{LS-HS} was found to be **2L-3 > 2L-2 > 2L-1** for any N; the order was the same predicted order as L_{ij}^{AP}. Thus it was confirmed that L_{ij}^{AP} reproduced the trends calculated using ΔE_{Total}^{LS-HS}, even for large N.

Next, 3L systems are discussed. Both L_{ij}^{AP} and N are compared for **3L-1** to **3L-3** (see Fig. 3.20a). The order of high-spin stability predicted by L_{ij}^{AP} was **3L-2 > 3L-3 > 3L-1** for all of the N regions investigated. To confirm the validity of L_{ij}^{AP} for these models, ab initio calculations were performed to obtain ΔE_{Total}^{LS-HS} at $N = 24$ using the ROHF/3-21G and ROB3LYP/3-21G levels of theory (see Fig. 3.20c). At both levels, the order of ΔE_{Total}^{LS-HS} was found to be **3L-2 > 3L-3 > 3L-1**. ΔE_{Total}^{LS-HS} at the HF level was smaller than that at the DFT level because of correlation effects. For comparison, L_{ij}^{AP} at $N = 24$ is plotted in Fig. 3.20b. For the 3L systems, it can therefore be concluded that L_{ij}^{AP} also reproduced the trend observed in ΔE_{Total}^{LS-HS} obtained using ab initio calculations.

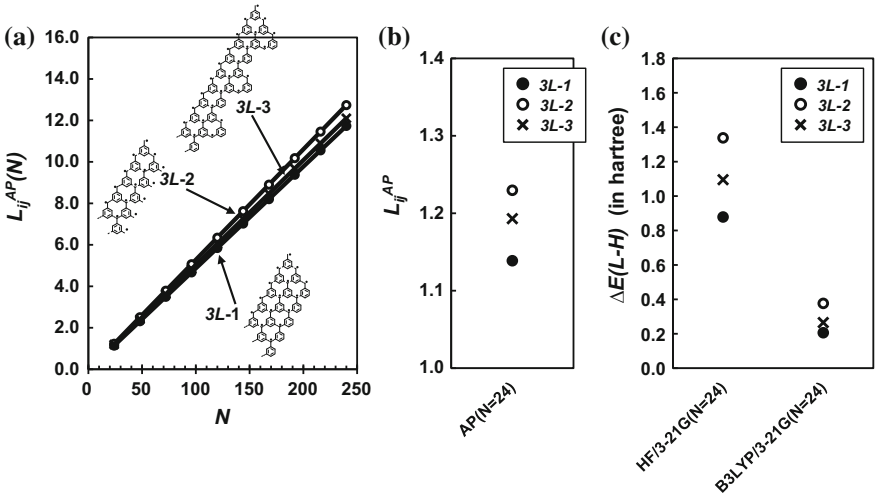

Fig. 3.20 **a** Relationship between N and $L_{ij}^{AP}(N)$ for 3L models. **b** L_{ij}^{AP} and **c** $\Delta E(L–H)$ for 3L models ($N = 24$). Modified with permission from Ref. [3]. Copyright 2006 American Chemical Society

The magnitude and degree of NBMO mixings is directly related to the order of L_{ij}^{AP}; therefore, candidate systems with large L_{ij}^{AP} can be designed using the following strategies:

(1) The order of the magnitude of NBMO mixings is $L_{ij}^{AP\circ(SR\leftrightarrow SR)} > L_{ij}^{AP\circ(SR\leftrightarrow DR)} > L_{ij}^{AP\circ(SR\leftrightarrow TR)} > L_{ij}^{AP\circ(DR\leftrightarrow DR)} > L_{ij}^{AP\circ(DR\leftrightarrow TR)} > L_{ij}^{AP\circ(TR\leftrightarrow TR)}$, as shown in Eq. (3.37). Thus, a large ferromagnetic property can be expected by including large-component NBMO mixings such as $L_{ij}^{AP\circ(SR\leftrightarrow SR)}$, $L_{ij}^{AP\circ(SR\leftrightarrow DR)}$, and $L_{ij}^{AP\circ(SR\leftrightarrow TR)}$.

(2) Large NBMO mixings can be expected when each NBMO mixes with as many adjacent NBMOs as possible. For example, we consider the trimer models in Fig. 3.12. In trimer-A, NBMO1 mixes only with NBMO2. On the other hand, in trimer-B, NBMO1 mixes with both NBMO2 and NBMO3. Here, trimer-B has an advantage compared with trimer-A.

Strategy (1), in particular, was found to be important for achieving large L_{ij}^{AP} when we compared systems with similar sizes. For instance, model **2L-3** has the largest L_{ij}^{AP} of the 2L models because it contains many $L_{ij}^{AP\circ(SR\leftrightarrow DR)}$ components. Similarly, in the 3L models, **3L-2** has the largest L_{ij}^{AP} because this model has many $L_{ij}^{AP\circ(SR\leftrightarrow TR)}$ components. In addition to these approaches, we were able to develop more detailed strategies as follows:

(3) To enlarge L_{ij}^{AP}, each phenyl ring should be linked with many radical centers (denoted by a dot sign). In such cases, large NBMO mixings are expected over the phenyl ring.

(4) To enlarge L_{ij}^{AP}, each radical center should be connected with a small number of phenyl rings. When a radical center connects with phenyl rings, the corresponding NBMO is delocalized over these rings. The delocalization of the NBMO over many phenyl rings makes each NBMO coefficient small after the normalization, and results in smaller values for L_{ij}^{AP}. In contrast, the delocalization over fewer rings keeps each NBMO coefficient large, and results in a larger L_{ij}^{AP}.

Points (1)–(4) can be useful guidelines when designing radical units and their linkages to realize large-L_{ij}^{AP} systems.

Here, every system is assumed to have a planar structure for simplicity. However, this treatment does not prevent functional design because it is obvious that a deviation from the planar structure weakens the ferromagnetism; the magnitude of this weakening can be approximated by considering the orbital overlap between two adjacent p-orbitals used to construct the π-conjugation. In addition, the system is assumed to be isolated in a vacuum. However, for π-conjugated systems, through-bond intramolecular exchange interactions should play a dominant role in ferromagnetic interactions and through-space exchange interactions from the surroundings could result in second-order effects in general.

In the previous subsections, we presented the formulation of a relationship between high-spin stability of a periodic system and N using an analytical approach. On the other hand, for aperiodic random systems, L_{ij}^{AP} can be estimated by counting the number of NBMO mixings one by one instead of formulations.

3.3.9 *Analytical Prediction of* $\mathbf{L_{ij}}$ *for Open Non-disjoint (0–*) Benzyl Radical Systems*

Our analytical method can also be applied to open non-disjoint (0–*) models, as shown in Fig. 3.9a [5]. Figure 3.21 shows the AP procedures for the open (0–*) BR dimer (Fig. 3.21a) and trimer (Fig. 3.21b) models. The prediction method is similar to that used for the closed (0–*) model except for the NBMO shape.

(i) The system is divided into each radical unit (BR1, BR2,…, etc.). NBMO coefficients are assigned within each BR unit by the NBMO zero-sum rule. Different letters, *a*, *b*, *c*, etc., are used for different BR units.

(ii) The NBMO coefficients for each unit are expanded to the region of the other BR units by the zero-sum rule. As can be seen in Fig. 3.21, the NBMOs for the open model are delocalized asymmetrically over more than one BR unit (except for the SR-type NBMOs) and are elongated to the terminal. The NBMOs delocalized asymmetrically over two, three, four,…, *n* benzene

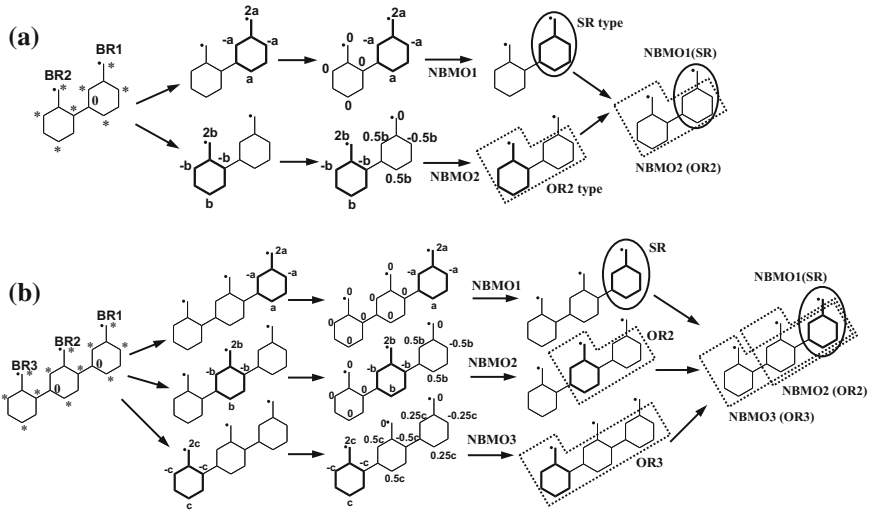

Fig. 3.21 AP of NBMO shapes with smallest overlaps for open (0–*) BR **a** dimer and **b** trimer models

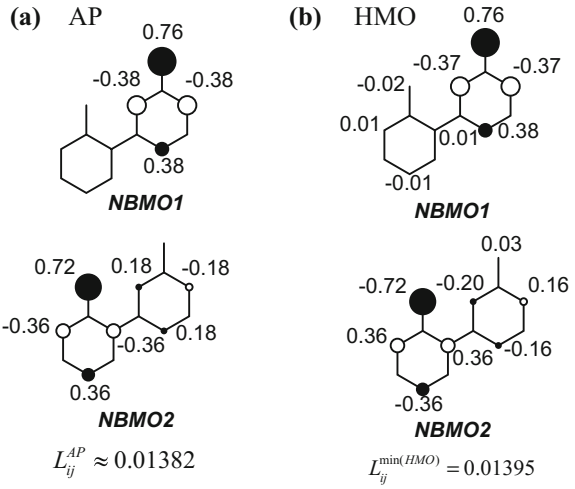

Fig. 3.22 NBMO shapes of open (0–*) BR dimer obtained using **a** AP and **b** HMO + unitary rotation methods

rings are named *open-ring 2*-(OR2-), OR3-, OR4-,…, OR*n*-type NBMOs, respectively.

(iii) The NBMO coefficients for open systems are normalized as

$$\begin{aligned}
&\textbf{NBMO1 (SR type):} \sum_r C_{NBMO1,r}^2 = (2a)^2 + 2(-a)^2 + a^2 = 7a^2 = 1\\
&\textbf{NBMO2 (OR1 type):} \sum_r C_{NBMO2,r}^2 = (2b)^2 + 2(-b)^2 + b^2 + 2(0.5b)^2 + (-0.5b)^2 = 7.75b^2 = 1\\
&\textbf{NBMO3 (OR2 type):} \sum_r C_{NBMO3,r}^2 = (2c)^2 + 2(-c)^2 + c^2 + 2(0.5c)^2 + (-0.5c)^2\\
&\qquad + 2(0.25c)^2 + (-0.25c)^2 = 7.9375c^2 = 1\\
&a = \frac{1}{\sqrt{7}} \approx 0.37796; \quad b = \frac{1}{\sqrt{7.75}} \approx 0.35921; \quad c = \frac{1}{\sqrt{7.9375}} \approx 0.35494
\end{aligned} \tag{3.50}$$

(iv) L_{ij}^{AP} can be calculated for open non-disjoint (0–*) BR dimer and trimer models as

$$\begin{aligned}
\textbf{Dimer model: } L_{ij}^{AP} &= L_{ij}^{AP(1,SR\leftrightarrow 2,OR2)} = \sum_r (C_{ri}C_{rj})^2\\
&= (-0.5ab)^2 + (0.5ab)^2 + (0.5ab)^2\\
&= 3\left(0.5 \times \frac{1}{\sqrt{7}} \times \frac{1}{\sqrt{7.75}}\right)^2 \approx 0.01382,
\end{aligned} \tag{3.51}$$

and

$$\begin{aligned}\textbf{Trimer model}: L_{ij}^{AP} &= \sum_{i,j(>i)} L_{ij}^{AP\circ} = L_{ij}^{AP(1,SR\leftrightarrow 2,OR2)} \\ &\quad + L_{ij}^{AP(1,SR\leftrightarrow 3,OR3)} + L_{ij}^{AP(2,OR2\leftrightarrow 3,OR3)} \\ &= 3(0.5ab)^2 + 3(0.25ac)^2 + 3(0.5bc)^2 + 3(0.125bc)^2 \\ &= 3\left(0.5 \times \frac{1}{\sqrt{7}} \times \frac{1}{\sqrt{7.75}}\right)^2 + 3\left(0.25 \times \frac{1}{\sqrt{7}} \times \frac{1}{\sqrt{7.9375}}\right)^2 \\ &\quad + 3\left(0.5 \times \frac{1}{\sqrt{7.75}} \times \frac{1}{\sqrt{7.9375}}\right)^2 \\ &\quad + 3\left(0.125 \times \frac{1}{\sqrt{7.75}} \times \frac{1}{\sqrt{7.9375}}\right)^2 = \ldots, \end{aligned} \tag{3.52}$$

respectively.

For the dimer model, the NBMO shapes in the AP and HMO methods are compared in Fig. 3.22. The AP approach accurately reproduces the NBMO shapes obtained using the HMO + unitary rotation treatment. As a result, $L_{ij}^{AP} \approx 0.01382$ agrees well with $L_{ij}^{\min(\mathrm{HMO})} = 0.01395$.

We formulated L_{ij}^{AP} for the open (0–*) model **1** (depicted in Fig. 3.23) as a function of N. For reference, the formulation was also conducted for closed model **2** (depicted in Fig. 3.23). The formulation was achieved using the same procedure as for the closed system, although its formulation is more complicated. $L_{ij}^{AP}(N)$ for these models is given by

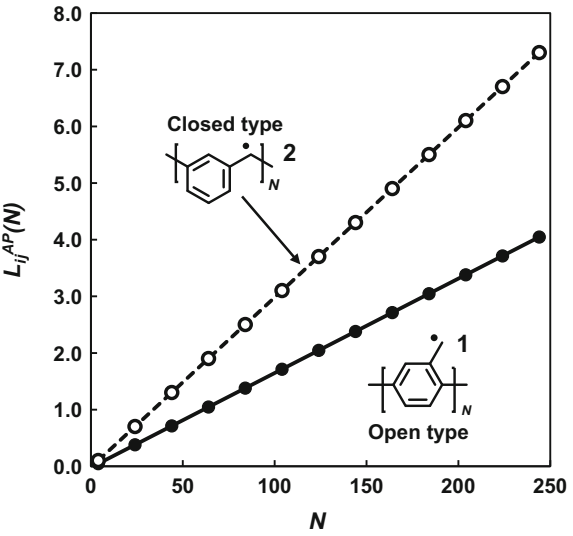

Fig. 3.23 Relationship between $L_{ij}^{AP}(N)$ and N for open **1** and closed **2** (0–*) BR oligomers

$$\textbf{Model 1}: L_{ij}^{AP}(N) = 3\sum_{l=1}^{N}\sum_{m(>l)}^{N}\left(\sum_{i=0}^{l-1}16^k\right)\Bigg/\left\{\left(3\sum_{k=0}^{l-1}4^k+4^l\right)\left(3\sum_{k=0}^{m-1}4^k+4^m\right)\right\}, \tag{3.53}$$

and

$$\textbf{Model 2}: L_{ij}^{AP}(N) = \frac{3}{100}N - \frac{3}{175}. \tag{3.54}$$

The values of $L_{ij}^{AP}(N)$ for these models are plotted in Fig. 3.23. L_{ij}^{AP} for the open model **1** is about half of that for the closed model **2**. These results indicate that the closed (0–*) linkage is more effective for constructing BR-based high-spin systems than the corresponding open linkage.

3.4 (2 × 2) Unitary Rotation for Minimizing L_{ij} and Its Comparison with the Edmiston–Rüdenberg Method

In Sect. 3.2.1, we introduced the (2 × 2)-based unitary rotation for minimizing L_{ij} by localizing NBMOs [see Eq. (3.4)]. In this subsection, we compare the (2 × 2) localization method with the Edmiston–Rüdenberg (ER) localization method [6] for minimizing L_{ij}. In the ER method, the unitary rotations shown in Eq. (3.55) are performed by maximizing the self-repulsion energy (SRE), J_{SRE}, in Eq. (3.56).

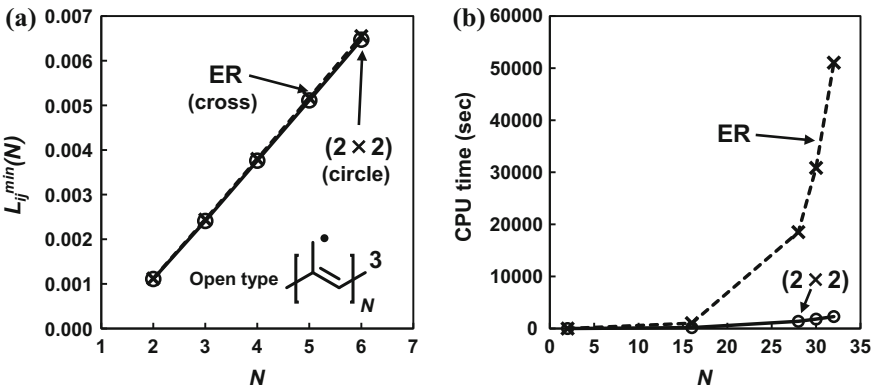

Fig. 3.24 **a** Comparison of $L_{ij}^{\min}(N)$ values calculated using (2 × 2) and ER localization methods for open model **3** at ROHF/STO-3G level. **b** Comparison of CPU times required for each method

$$\varphi'_j = \sum_{i=1}^{n} \varphi_i U_{ij} \quad (j = 1, 2, \ldots, n) \tag{3.55}$$

$$J_{SRE}(\varphi') = \sum_{j=1}^{n} \int |\varphi'(1)|_j^2 \left(\frac{1}{r_{12}}\right) |\varphi'(2)|_j^2 d\mathbf{r}_1 d\mathbf{r}_2 \tag{3.56}$$

For comparison, $L_{ij}^{\min}$ for the open model **3** (depicted in Fig. 3.24a) was calculated at the ROHF/STO-3G level using both localization methods. Figure 3.24a shows the relationship between $L_{ij}^{\min}$ and N, where the highest spin-multiplicity was selected for each N. The (2 × 2) method provided essentially the same $L_{ij}^{\min}$ value as the ER method. Furthermore, the methods gave quite similar NBMO shapes corresponding to $L_{ij}^{\min}$. Figure 3.24b shows the CPU time required to obtain $L_{ij}^{\min}$ for both methods. For larger N, in particular, the (2 × 2) method required much less CPU time than the ER method. Thus, the (2 × 2) method is useful for obtaining $L_{ij}^{\min}$ because of its small computational cost and excellent reliability.

References

1. Aoki, Y., Imamura, A.: A simple rule to find nondisjoint NBMO degenerate systems for designing high-spin organic molecules. Int. J. Quant. Chem. **74**, 491–502 (1999)
2. Onitsuka, S., Aoki, Y.: Guidelines proposed for designing organic ferromagnets by using a quantum chemical approach. Theor. Chem. Acc. **130**, 789–806 (2011)
3. Orimoto, Y., Aoki, Y.: Analytical method for predicting ferromagnetic properties of benzyl-radical polymers based on NBMO theory. J. Chem. Theory Comput. **2**, 786–796 (2006)
4. Frisch, M.J., Trucks, G.W., Schlegel, H.B., Scuseria, G.E., Robb, M.A., Cheeseman, J.R., Montgomery, J.A., Jr., Vreven, T., Kudin, K.N., Burant, J.C., Millam, J.M., Iyengar, S.S., Tomasi, J., Barone, V., Mennucci, B., Cossi, M., Scalmani, G., Rega, N., Petersson, G.A., Nakatsuji, H., Hada, M., Ehara, M., Toyota, K., Fukuda, R., Hasegawa, J., Ishida, M., Nakajima, T., Honda, Y., Kitao, O., Nakai, H., Klene, M., Li, X., Knox, J.E., Hratchian, H.P., Cross, J.B., Adamo, C., Jaramillo, J., Gomperts, R., Stratmann, R.E., Yazyev, O., Austin, A.J., Cammi, R., Pomelli, C., Ochterski, J.W., Ayala, P.Y., Morokuma, K., Voth, G.A., Salvador, P., Dannenberg, J.J., Zakrzewski, V.G., Dapprich, S., Daniels, A.D., Strain, M.C., Farkas, O., Malick, D.K., Rabuck, A.D., Raghavachari, K., Foresman, J.B., Ortiz, J.V., Cui, Q., Baboul, A.G., Clifford, S., Cioslowski, J., Stefanov, B.B., Liu, G., Liashenko, A., Piskorz, P., Komaromi, I., Martin, R.L., Fox, D.J., Keith, T., Al-Laham, M.A., Peng, C.Y., Nanayakkara, A., Challacombe, M., Gill, P.M.W., Johnson, B., Chen, W., Wong, M.W., Gonzalez, C., Pople, J.A.: Gaussian 03, revision C. 02. Gaussian, Inc., Wallingford, CT (2004)
5. Zhu, X., Aoki, Y.: An analytical approach to predict high-spin stability of conjugated hydrocarbon radical polymers using minimized mixing nonbonding molecular orbitals. Curr. Phys. Chem. **3**, 99–112 (2013)
6. Edmiston, C., Ruedenberg, K.: Localized atomic and molecular orbitals. Rev. Mod. Phys. **35**, 457–465 (1963)

Chapter 4
Through-Space/Bond Interaction Analysis of Ferromagnetic Interactions

Abstract In general, through-space (TS) and through-bond (TB) exchange interactions play dominant roles in radical crystals and polymers, respectively. In spite of their importance, the quantitative relationship between these interactions and magnetic properties has not been thoroughly investigated. In this chapter, we introduce one of the candidate methods for this purpose, called the TS/TB interaction analysis method. The TS/TB method makes it possible to investigate specific intra- and/or inter-molecular orbital interaction(s) at the ab initio quantum chemistry level of theory. An analysis using model benzyl radical molecules quantitatively revealed that TB interactions between radicals are the dominant contributors to the high-spin stability of the system. In addition, a detailed analysis showed that electron correlation effects control the high-spin stability.

4.1 Introduction

In the previous chapter, we noted that the exchange interaction controls the ferromagnetic properties of a system and can be of either of two types: through space (TS) or through bonds (TB) . Ferromagnetic systems should be realized by tightly controlling the features of these exchange interactions between spin radicals by adjusting their pathways, strengths, and so on. Two types of strategies, viz., TS and TB approaches, are utilized for designing ferromagnetic systems. The TS and TB approaches were developed to produce *radical crystals* and *radical polymers*, respectively. In general, radical polymers that utilize intramolecular exchange interactions through π-conjugation are expected to have much higher Curie temperatures than radical crystals.

We also noted that quantum chemistry (QC) calculations may facilitate quantitative examination of the exchange interactions and enable greater understanding of inter-radical interactions and ferromagnetic system design. However, conventional QC calculations (except for natural bond orbital (NBO) analysis [1]) basically

Y. Aoki et al., *Quantum Chemical Approach for Organic Ferromagnetic Material Design*, SpringerBriefs in Electrical and Magnetic Properties of Atoms, Molecules, and Clusters,
DOI 10.1007/978-3-319-49829-4_4

provide information for the whole system and do not give specific information about each individual orbital interaction in the system. To better understand the relationship between inter-radical interactions and ferromagnetic properties, it is necessary to analyze the specific orbital interaction(s) in the system beyond the conventional methods.

In this chapter, we introduce a QC-based treatment, called the ab initio TS/TB interaction analysis method [2], to understand the exchange interactions quantitatively from the viewpoint of intramolecular orbital interactions. Here, in particular, we focus on radical polymers given by the TB approach for the design of new high-performance materials.

4.2 Ab Initio Through-Space/Bond Interaction Analysis Method

The ab initio TS/TB interaction analysis method was developed to analyze quantitatively specific orbital interactions in a molecule at the ab initio molecular orbital (MO) level [2]. The effectiveness of the method has been confirmed by applying the TS/TB method to the elucidation of various phenomena in organic systems, including stereoelectronic effects [3, 4], exchange interactions [5], rotational barriers [6, 7], π/σ-conjugation effects [8, 9], and so on [10–12]. This chapter discusses the application of the TS/TB method to elucidate the orbital interaction paths that provide high-spin stability.

4.2.1 How to Analyze Orbital Interactions Using the Through-Space/Bond Method

In the TS/TB method, we can eliminate the contribution of a specific orbital interaction(s) to the system by using extremely large exponents in the basis functions related to the interactions. By comparing the total energies before and after elimination, we can estimate the contribution of the interaction in question to the total energy.

As an example, we consider the elimination of the TS orbital interaction in ethane that occurs between the 1*s*-type atomic orbital (AO) χ_r, belonging to hydrogen atom H_A, and the 1*s*-type AO χ_s, belonging to H_B (see Fig. 4.1a). To achieve the elimination, we artificially enlarge the absolute magnitude of the exponent α of the Gaussian function $(\exp(-\alpha r^2))$ in the basis functions related to the interactions until the orbital overlap between χ_r and χ_s completely disappears; that is, $S_{rs} = \int \chi_r(1)\chi_s(1)d\tau_1 \overset{\text{Enlarge } \alpha}{\longrightarrow} 0$. This enlargement contracts the corresponding AOs, and the AOs are localized on each atomic nucleus as a result. When using such an extremely large α, all of the off-diagonal integral elements related to

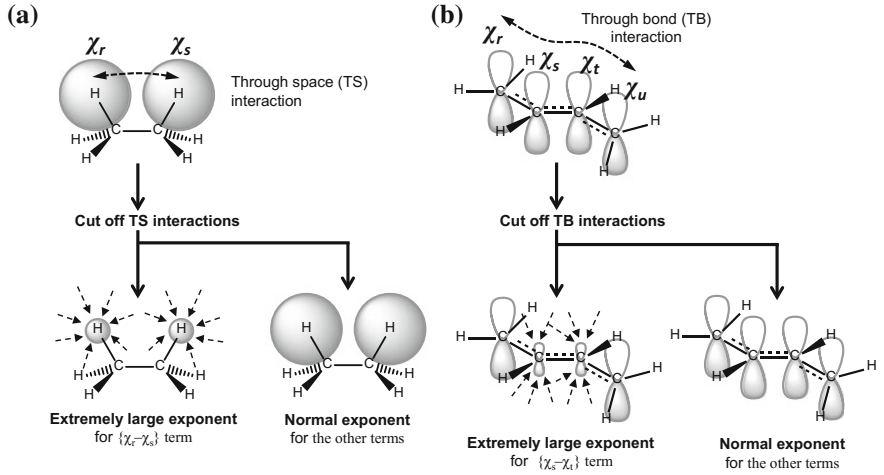

Fig. 4.1 Elimination of orbital interactions using TS/TB analysis for **a** TS interaction between 1*s*-type AOs χ_r and χ_s in ethane, and **b** TB interaction arising from π-conjugation effects in 1, 3-butadiene (Modified with permission from Ref. [3]. Copyright 2005 Wiley Periodicals, Inc.)

the interaction between χ_r and χ_s become zero because there is no overlap between the AOs. That is, the *r*–*s* elements of the kinetic energy integral T_{rs}, the nuclear–electron attractive energy integral $V_{rs}^{A}\{A = \mathrm{H_A}, \mathrm{H_B}, \mathrm{H_C}, \ldots\}$, and the two-electron integrals, (rs|rs), (rs|rr), etc., should be zero under such conditions. The completely localized AOs into the atomic center make a point charge e^- on each atomic nucleus, and the negative charge automatically shields a related amount of nuclear charge, +*Z*e. If we delete all the possible orbital interactions between atoms A and B, the nuclear charges of these atoms are completely shielded by the negative charges caused by the contracted AOs. Both the spatial interactions resulting from AO overlaps and the electrostatic interactions between atoms A and B can be deleted unintentionally. Strictly speaking, this situation can be realized by cancelling the nucleus–nucleus repulsion energy between atoms A and B by the $V_{rr}^{H_B}$, $V_{ss}^{H_A}$, and (rr|ss) terms with the classical electrostatic energies caused by classical point charges generated by the contracted AOs.

Next, we show an example for deleting TB conjugation effects in 1, 3-butadiene, which is depicted in Fig. 4.1b. In this model, a series of *p*-type AOs perpendicular to the molecular plane ($\chi_r \sim \chi_u$) are relevant to the conjugation effects. The simplest way to eliminate the conjugation effects is to delete one of the orbital interactions between two adjacent *p*-type AOs, for example, the interaction between χ_s and χ_t.

The advantage of this treatment is the fact that we can discuss the contributions of the specific interactions using total energies. This method can be applied to examine a variety of phenomena related to various types of intra- and/or intermolecular orbital interactions, such as stereoelectronic effects, electron conjugation, rotational barriers, steric repulsion, and so on.

4.2.2 *Procedures for the Through-Space/Bond Interaction Analysis Method*

The procedure for the ab initio AO-based TS/TB interaction analysis method can be summarized as follows (see also Fig. 4.2):

1. The molecular structure and the information for deleting the orbital interactions are prepared.
2. All of the AO integrals are calculated using two different basis sets, that is, a normal basis set with a normal exponent (α) and an artificial basis set with an extremely large exponent (α'). The normal and artificial AO integrals are separately saved to a disk as *file-1* and *file-2*, respectively.

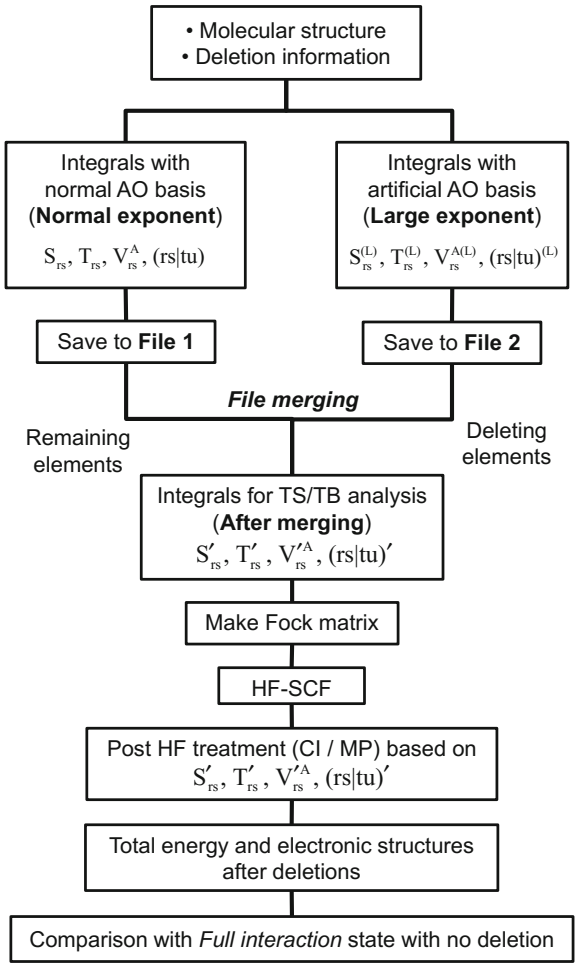

Fig. 4.2 Procedures for AO-based ab initio TS/TB interaction analysis method (Modified with permission from Ref. [3]. Copyright 2005 Wiley Periodicals, Inc.)

3. The integrals for the TS/TB method are obtained by merging *file-1* and *file-2*. In other words, the integral elements corresponding to the remaining interactions are extracted from *file-1* (normal exponent), and the elements corresponding to the deleted interactions are extracted from *file-2* (large exponent). We can thereby obtain the integral sets for eliminating the specific orbital interactions.
4. The Fock matrix after deletion is constructed using the merged integrals. Conventional Hartree–Fock self-consistent field (HF-SCF) calculations are adopted to solve an eigenvalue problem, $|F_{rs} - \varepsilon S_{rs}| = 0$, based on the merged integral sets. After reaching SCF convergence, we can obtain the total energy after deleting the specific orbital interaction(s).
5. Electron correlation effects can be introduced by connecting the TS/TB method to conventional configuration interaction (CI) or Møller–Plesset (MP) perturbation treatments; because the deletion in the TS/TB method is performed at the level of the AO integral element (not at the level of the Fock matrix element), the deletion is automatically reflected in the post-HF calculations, which utilize AO integrals.
6. The total energy (or electronic structure) obtained after deleting the specific orbital interactions is compared with that before the deletion (called the full interaction state). The comparison gives us quantitative information about the contribution of the specific orbital interaction(s) to the total energy/electronic structure.

These procedures are incorporated into the program GAMESS [13]. The ab initio calculations described in this chapter, other than those related to the TS/TB method, were performed using the Gaussian03 program package [14].

A basis other than AOs can be adopted for the TS/TB method. For example, we introduced the NBO-based TS/TB method [3, 4], which is illustrated in Fig. 4.3. In this method, a basis conversion from AO to NBO is required for the integrals. The transformation matrix U is obtained using the conventional NBO procedures [1]. The conversion is conducted using

$$S_{rs}^{\{NBO\}} = \sum_{\mu,v} U_{r\mu}^{\dagger} S_{\mu v} U_{vs}, \tag{4.1}$$

$$T_{rs}^{\{NBO\}} = \sum_{\mu,v} U_{r\mu}^{\dagger} T_{\mu v} U_{vs}, \tag{4.2}$$

$$V_{rs}^{A\{NBO\}} = \sum_{\mu,v} U_{r\mu}^{\dagger} V_{\mu v}^{A} U_{vs}, \text{ and} \tag{4.3}$$

$$(rs \,|\, tu)^{\{NBO\}} = \sum_{\mu,v,\lambda,\sigma} U_{r\mu}^{\dagger} U_{sv}^{\dagger} U_{t\lambda} U_{u\sigma} (\mu v \,|\, \lambda\sigma). \tag{4.4}$$

The conversion is applied to both the normal and artificial AO integrals. In the NBO-based TS/TB method, a specific orbital interaction can be deleted based on

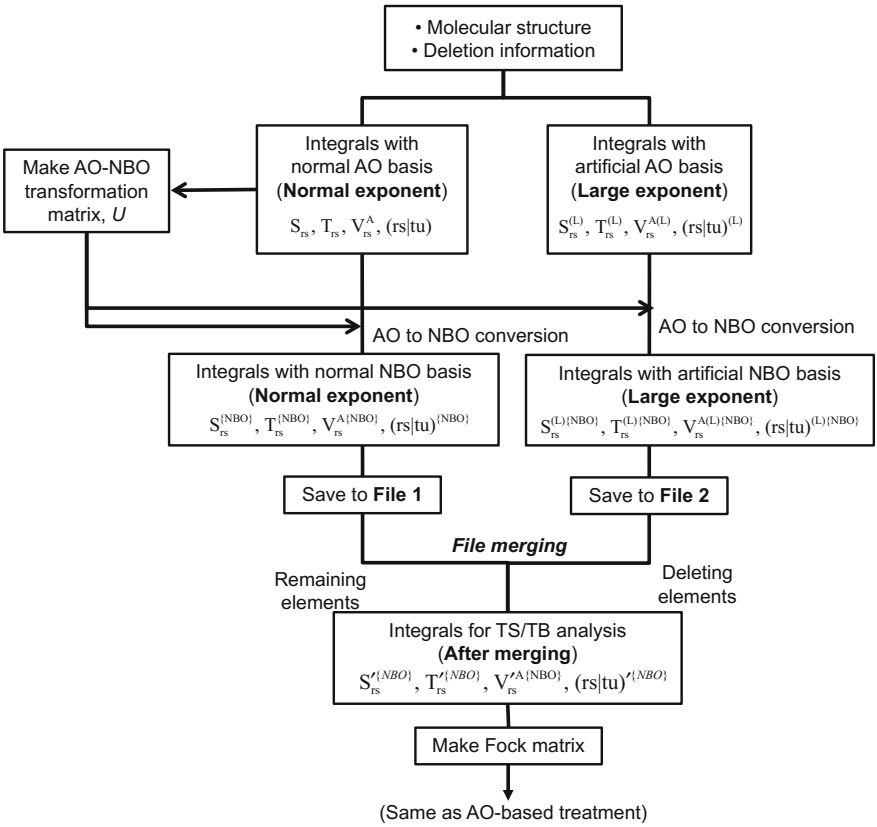

Fig. 4.3 Procedures for NBO-based ab initio TS/TB interaction analysis method (Modified with permission from Ref. [3]. Copyright 2005 Wiley Periodicals, Inc.)

chemically understandable NBO shapes. Following this step, the total energy and electronic structures after deletion can be obtained using procedures similar to the AO-based TS/TB method.

4.2.3 Features of the Through-Space/Bond Interaction Analysis Method

Table 4.1 summarizes the features of the TS/TB interaction analysis method. Table 4.1a–d concern features available in the TS/TB analysis method. In the TS/TB method, the deletion of the orbital interactions is conducted at the level of AO integrals prior to forming the Fock matrix. Thus, the interaction deletion is naturally reflected in any post-HF treatment; for example, in the CI-level TS/TB

Table 4.1 Features of ab initio TS/TB analysis method (Modified with permission from Ref. [3]. Copyright 2005 Wiley Periodicals, Inc.)

	TS/TB analysis method
(a) Cutoff	Integral element level
(b) Available methods	HF, CI, MP, etc. (any post-HF treatment)
(c) Available electron configurations	• Ground state • Excited state
(d) Connection to other methods	• Finite field method • PCM method, etc.
(e) Deletion of two electron integrals	$(rs\|12)_{\text{Coulomb}} \rightarrow 0$ (cutoff) $(r^*\|12)_{\text{Exchange}} \rightarrow 0$ (cutoff), etc.
(f) Basis type for deletion	AO, NHO, NBO bases, etc. (any basis type)
(g) Wavefunction	• SCF • Desired number of SCF cycles
(h) Nucleus–nucleus repulsion	Automatically shielded by electron point charges (deletion of electrostatic interactions)
(i) Types of analyses	• Orbital interactions • Electron transfer • Conjugation • Stereoelectronic effects • Steric repulsion • Rotational barriers, etc.

method, the deletion of the interactions is automatically introduced not only in the ground state electron configuration, but also in various excited electron configurations. Therefore, the TS/TB method is capable of analyzing orbital interactions while considering electron correlation effects in both the ground and excited states. For the same reason (i.e., orbital deletions at the integral level), the TS/TB method can be connected with the finite field (FF) method (TS/TB + FF method), polarizable continuum model (PCM) calculations (TS/TB + PCM method), and so on.

Table 4.1e–h list the details of the interaction deletions. Table 4.1e concerns the treatment of the two-electron integrals during the deletions. The element of the Fock matrix can be described by AO-based integrals as

$$F_{rs} = H_{rs}^{core} + \sum_{t,u} P_{tu}\left[(rs\,|\,tu)_{Coulomb} - \frac{1}{2}(ru\,|\,ts)_{Exchange}\right]. \tag{4.5}$$

Then, the orbital interaction between AOs χ_1 and χ_2 is deleted. In the TS/TB analysis method, all the 2e-integral elements corresponding to the interaction are deleted by using the large exponent. That is, the 2e-integral elements in the element F_{12} are deleted; at the same time, the 2e-integral elements corresponding to the deletion of $\chi_1 \leftrightarrow \chi_2$ in the other Fock matrix elements $(F_{r\neq 1,s\neq 2})$, for example, $(rs\,|\,12)_{Coulomb}$ in $F_{r\neq 1,s\neq 2}$ and $(ru\,|\,12)_{Exchange}$ in $F_{r(\neq 1),2}$, are also automatically deleted as a result of the zero value caused by the large exponent.

Any basis, such as AO, natural hybrid orbital (NHO), natural bond orbital (NBO), etc., can be used for the TS/TB method (Table 4.1f). Generally speaking, the AO-based TS/TB method has the advantage of deleting a pinpoint site, such as the deletion of an orbital interaction between p_Z (atom A) and p_Z (atom B), for instance. On the other hand, the NBO-based TS/TB method has an advantage in that it allows the deletions based on chemically understandable NBO descriptions such as π and σ^* orbitals, and so on. In addition, even if we use a larger basis set, the NBO-based TS/TB method can retain the simple definition of the interaction deletion.

Table 4.1g shows the treatment of the wavefunction. The TS/TB method gives an SCF wavefunction that satisfies the SCF under the deletion of the specific interactions. Of course, we can obtain the results after a desired number of SCF cycles according to our purpose.

Table 4.1h shows the treatment of the nucleus–nucleus repulsion energy. In the TS/TB method, an appropriate amount of electron point charges is generated on the corresponding atomic nucleus by using a large exponent. The electron point charges automatically shield the nuclear point charges. As the result, electrostatic interactions are deleted in addition to the electron delocalization effects. We can select another deletion mode in which the only electron delocalization effects are deleted. Such a high degree of freedom in the TS/TB method promises wide potential applications to electrostatic-interaction-related phenomena such as steric repulsion, rotational barriers, etc., in addition to the analysis of electron delocalization (Table 4.1i).

4.3 Analysis of Inter-radical Interactions Using the Through-Space/Bond Method

4.3.1 Through-Space/Bond Analysis of a Non-disjoint (0−) Benzyl Radical Dimer*

To examine the relationship between high-spin stability and the inter-radical interaction path, the TS/TB method was used to analyze the benzyl radical (BR) dimer **1**, as shown in Fig. 4.4a [5]. The BR dimer **1** has a non-disjoint (0−*)-type linkage between two BR units, BR-1 and BR-2, and is expected to have NBMO mixings leading to exchange interaction between the radicals. We can assume two types of interaction pathways between the radicals: interactions through space (Fig. 4.4b) and through bond (Fig. 4.4c). A key question is *which interaction pathway mainly contributes to the exchange interactions and causes high-spin stability?* Here, the high-spin stability, ΔE_{total}^{LS-HS}, is defined as the total energy difference between the lowest spin state and the highest spin state; that is, $\Delta E_{total}^{LS-HS} = E_{total}^{LS} - E_{total}^{HS}$. Positive or negative values of ΔE_{total}^{LS-HS} mean that the high-spin or low-spin state is more stable, respectively. For model **1**, we explicitly

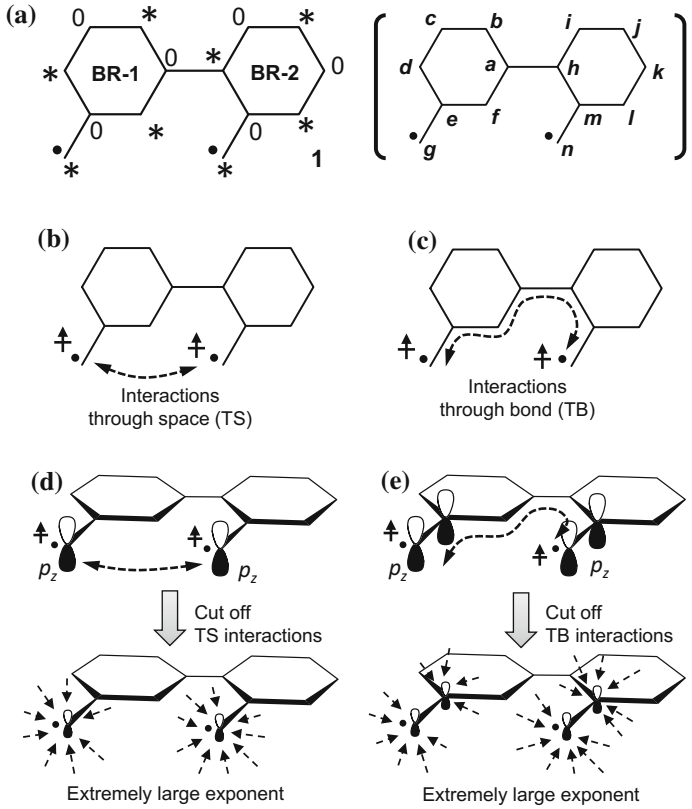

Fig. 4.4 **a** BR dimer model **1** with a non-disjoint (0−*) linkage. Atoms are assigned letters *a*−*n*, as shown in parentheses. Illustrations of **b** TS and **c** TB interaction paths between radicals in **1**. Schematic illustrations for deletion of inter-radical interactions **d** through space and **e** through bond by TS/TB analysis method (Modified with permission from Ref. [5]. Copyright 2006 American Chemical Society)

define the high-spin stability by the energy difference between the singlet (E^S_{total}) and triplet (E^T_{total}) states; that is, $\Delta E^{S-T}_{total} = E^S_{total} - E^T_{total}$.

First, the electronic structure of **1** was calculated by including all of the intramolecular orbital interactions without any interaction deletions. We call this condition the "*full interaction* (FULL)" state. The restricted open-shell second-order MP (ROMP2) method was used to calculate the triplet state. The singlet state was treated as closed shell and calculated using the restricted MP2 (RMP2) method for the first step. Here, a frozen core (FC) approximation was adopted for the MP2 treatments. The full interaction calculation (MP2(FC)/6-311G) was performed based on the ROHF/6-311G optimized geometries; the split-valence triple-zeta basis set 6-311G was used to describe the π-conjugation adequately. The

geometrical optimizations for singlet and triplet states were conducted separately while maintaining the planar structures.

For our convenience, we have rewritten E_{total} as E_{MP2}. We can divide the R(O) MP2 total energy $E_{MP2}(=E_{total})$ into the HF energy (E_{HF}) and the MP2 perturbation energy $(E_{corr(MP2)})$ terms. Thus, the high-spin stability $(\Delta E_{MP2}^{S-T}(=\Delta E_{total}^{S-T}))$ can be rewritten as

$$\begin{aligned}\Delta E_{MP2}^{S-T} &= \left(E_{HF}^{S} + E_{corr(MP2)}^{S}\right) - \left(E_{HF}^{T} + E_{corr(MP2)}^{T}\right) \\ &= \left(E_{HF}^{S} - E_{HF}^{T}\right) + \left(E_{corr(MP2)}^{S} - E_{corr(MP2)}^{T}\right) = \Delta E_{HF}^{S-T} + \Delta E_{corr(MP2)}^{S-T},\end{aligned} \tag{4.6}$$

where ΔE_{HF}^{S-T} is the contribution of the HF energy to the high-spin stability, while $\Delta E_{corr(MP2)}^{S-T}$ shows the contribution of the second-order perturbation energy, corresponding to the electron correlation effects, to the high-spin stability.

The energy diagram for the FULL state of **1** is shown in Fig. 4.5a. The triplet state is more stable than the singlet state by 0.022 a.u. (hartree); that is, $\Delta E_{MP2}^{S-T} = 0.022$ a.u. Although the triplet state is more stable than the singlet state by 0.099 a.u. at the HF level, the relative energy of the triplet state is reduced after considering electron correlation effects using the MP2 treatment; that is, the singlet–triplet gap is reduced from $\Delta E_{HF}^{S-T} = 0.099$ a.u. to $\Delta E_{MP2}^{S-T} = 0.022$ a.u. $(\Delta E_{corr(MP2)}^{S-T} = -0.077$ a.u.). The reduction in the relative stability of the high-spin state is attributable to preferential stabilization of the singlet state $(E_{corr(MP2)}^{Singlet} = -1.335$ a.u.) over the triplet state $(E_{corr(MP2)}^{Triplet} = -1.258$ a.u.) by the correlation effects. Consequently, the high-spin state of **1** is still preferred, even when the correlation effects are considered $(\Delta E_{MP2}^{S-T} = 0.022$ a.u.).

Next, we discuss the deletion of the TS interaction pathway between the radical centers at sites *g* (BR-1) and *n* (BR-2) using the TS/TB method (see Fig. 4.4b). We eliminated all possible combinations of the orbital interactions $p_Z\,(p'_Z, p''_Z, p'''_Z)$ [at site-*g*] $- p_Z(p'_Z, p''_Z, p'''_Z)$ [at site-*n*], where the *z*-axis is perpendicular to the molecular plane of **1**, (see Fig. 4.4d) and p_Z consists of three orbitals, p'_Z, p''_Z, and p'''_Z, with different exponents when treated with triple-zeta basis functions. The results obtained after deleting the TS interaction (i.e., the delete-TS state) are shown in Fig. 4.5b. The deletion changed the diagram very slightly from the FULL state, and we obtained a small change in the stability of the high-spin state from ΔE_{MP2}^{S-T}(FULL) = 0.022 a.u. to ΔE_{MP2}^{S-T}(delete-TS) = 0.024 a.u. The small change means that the TS interaction between the radicals does not substantially contribute to the high-spin stability. For the triplet state of **1**, the distance between the radical centers in the optimized structure was found to be 4.98 Å, which is expected to be too far to allow for effective orbital overlap using p_Z orbitals.

Finally, we consider the TB interaction pathway between radical centers (see Fig. 4.4c). We deleted the interaction by cutting off a part of the TB interaction

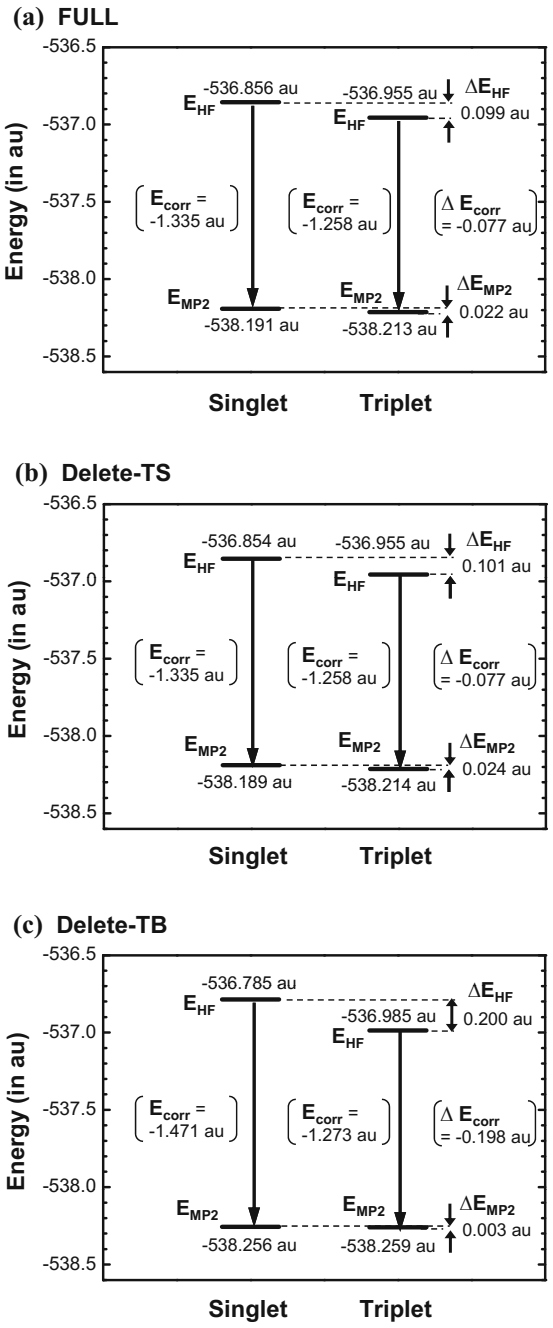

Fig. 4.5 Energy diagram of TS/TB analysis for **a** full interaction state, **b** TS-deleted interaction state, and **c** TB-deleted interaction state in model **1** (ROMP2 (FC)/6-311G//ROHF/6-311G) (Modified with permission from Ref. [5]. Copyright 2006 American Chemical Society)

path, that is, the p_Z(site-e) − p_Z(site-g) and p_Z(site-m) − p_Z(site-n) orbital interactions (see Fig. 4.4e). The deletion was expected to suppress the inter-radical π conjugation that occurs through C–C bonds. The results obtained after deleting the TB interaction (i.e., the delete-TB state) are shown in Fig. 4.5c. Eliminating the TB pathway strongly decreased the stability of the high-spin state from ΔE_{MP2}^{S-T}(FULL) = 0.022 a.u. to ΔE_{MP2}^{S-T}(delete-TB) = 0.003 a.u. It should be noted that the small value of ΔE_{MP2}^{S-T}(delete-TB) resulted from the cancelation of the increase in ΔE_{HF}^{S-T} (0.099 a.u. (FULL) → 0.200 a.u. (delete-TB)) and the decrease in $\Delta E_{corr(MP2)}^{S-T}$(-0.077 a.u. (FULL) → -0.198 a.u. (delete-TB)).

The contribution of the TB interaction to the FULL state (= FULL-delete-TB) is summarized in Table 4.2a. The contributions are ∼0.020 a.u. and ∼88% of the high-spin stability. Furthermore, this contribution resulted from the cancelation of the unfavorable high-spin $\Delta E_{HF}^{S-T}(TB)$ (= −0.101 a.u.) and preferred high-spin $\Delta E_{HF}^{S-T}(TB)$ (= 0.120 a.u.) energy differences. The HF term $\Delta E_{HF}^{S-T}(TB)$ mainly comes from the large stabilization of the singlet state $E_{HF}^{S}(TB)$ (= −0.071 a.u.). On the other hand, the second-order energy term $\Delta E_{corr(MP2)}^{S-T}(TB)$ predominantly arises from the large destabilization of the singlet state $E_{corr(MP2)}^{S}(TB)$ by 0.135 a.u. Therefore, it can be concluded that the most important term in the TB contribution to the high-spin stability is the destabilization of the second-order energy term for the singlet state $E_{corr(MP2)}^{S}(TB)$.

The destabilization of $E_{corr(MP2)}^{S}(TB)$ is the main reason for the positive value of ΔE_{MP2}^{S-T}(FULL). To obtain further details, we examined the MP2 energy term $E_{corr(MP2)}^{S}(FULL)$ for the singlet state of **1**. In particular, we focused on the most important component between the highest occupied (HOMO) and lowest unoccupied molecular orbitals (LUMO) (HOMO–LUMO component), written as

$$E_{corr(MP2)}^{S,HOMO-LUMO}(FULL) = -\frac{|[ia\,|\,ia]|^2}{2(\varepsilon_a - \varepsilon_i)}, \tag{4.7}$$

where ε_i and ε_a are the orbital energies of HOMO (ϕ_i) and LUMO(ϕ_a), respectively. $[ia\,|\,ia]$ is the MO-based two-electron integral, which can be expressed as

$$[ia\,|\,ia] = \int \phi_i^*(1)\phi_a(1)\frac{1}{r_{12}}\phi_i^*(2)\phi_a(2)d\tau_1 d\tau_2. \tag{4.8}$$

Table 4.2b lists the values of $E_{corr(MP2)}^{S,HOMO-LUMO}$, its numerator, and denominator for the "FULL" and "delete-TB" states. The "TB contribution" (=FULL − delete-TB) shows the difference between the FULL and delete-TB states. Deletion of the TB interaction considerably reduced $E_{corr(MP2)}^{S,HOMO-LUMO}$ from −0.015 a.u. (FULL) to −0.098 a.u. (delete-TB). From a different standpoint, the TB interaction increases $E_{corr(MP2)}^{S,HOMO-LUMO}$ by 0.083 a.u. In addition, 61% of the singlet state destabilization

Table 4.2 **a** Contribution of TB interaction to high-spin stability of model **1** (ROMP2(FC)/6-311G//ROHF/6-311G). **b** HOMO–LUMO component of MP2 perturbation energy in singlet state of **1**

(a) Contribution of TB interaction (=FULL − delete-TB)			
	Singlet (in a.u.)	Triplet (in a.u.)	Δ(S − T) (in a.u.)
E_{MP2}(TB)	0.06463	0.04504	0.01958
E_{HF}(TB)	−0.07066	0.03023	−0.10090
$E_{corr(MP2)}$(TB)	0.13529	0.01481	0.12048
(b) HOMO–LUMO component of the MP2 energy (singlet state)			
	$E_{corr(MP2)}^{S,HOMO-LUMO}\left\{=-\lvert[ia\rvert ia]\rvert^2/2(\varepsilon_a-\varepsilon_i)\right\}$(in a.u.)	Numerator $-\lvert[ia\rvert ia]\rvert^2$ (in a.u.^{2})	Denominator $2(\varepsilon_a-\varepsilon_i)$ (in a.u.)
FULL state	−0.01534	−0.00418	0.27232
Delete-TB state	−0.09792	−0.02197	0.22437
TB contribution (=FULL − delete-TB)	0.08258	0.01779	0.04795

Modified with permission from Ref. [5]. Copyright 2006 American Chemical Society

$(E^{S}_{corr(MP2)}(TB) = 0.135$ a.u.) comes from the HOMO–LUMO component $E^{S,HOMO-LUMO}_{corr(MP2)}(TB)$ (=0.083 a.u.). Thus, the TB interaction prevents the stabilization of $E^{S,HOMO-LUMO}_{corr(MP2)}$. For this reason, the TB contribution results in the relative stabilization of the high-spin triplet state of **1**.

The reduction in $E^{S,HOMO-LUMO}_{corr(MP2)}$ stabilization by the TB interaction (−0.098 a.u. (delete-TB) → −0.015 a.u. (FULL)) can be explained by the following two effects:

1. The TB interaction increases the numerator of Eq. (4.7) by 0.018 a.u.^{2} and reduces the absolute value of the numerator in the FULL state (−0.022 a.u.^{2} (delete-TB) → −0.004 a.u.^{2} (FULL)). Figure 4.6 shows the HOMO and LUMO shapes of the singlet state of **1** in the FULL (upper) and delete-TB (bottom) states. Both the HOMO and LUMO coefficients are delocalized over the whole molecule in the FULL state. However, the coefficients are localized onto the radical centers after deleting the TB interaction. The change in HOMO and LUMO shapes means that the TB interaction through the π-network pathway contributes to the delocalization of the HOMO and LUMO. The orbital shape change is directly related to the change of the numerator in Eq. (4.7), $-|[ia\,|\,ia]|^2$.
2. The TB interaction increases the denominator of Eq. (4.7) by 0.048 a.u. (0.224 a.u. (delete-TB) → 0.272 a.u. (FULL)). This change accelerates the decrease in the absolute value of the HOMO–LUMO component. The deletion of the TB

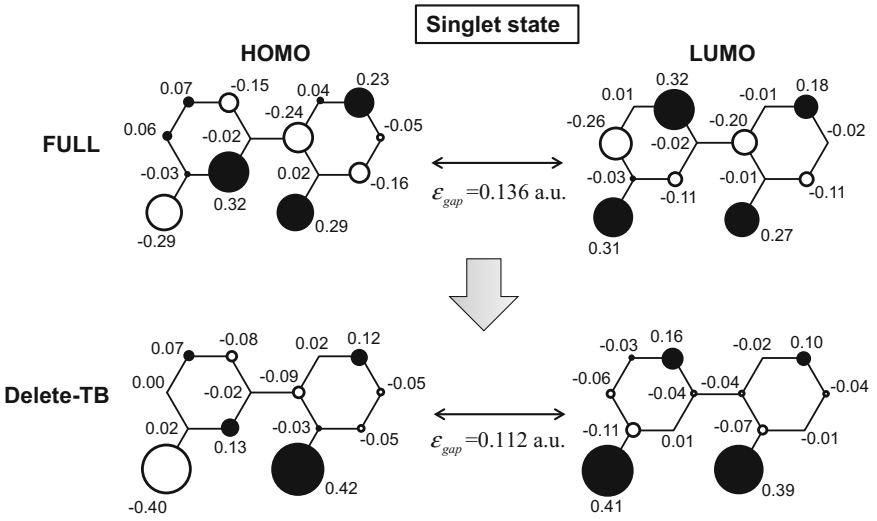

Fig. 4.6 HOMO and LUMO shapes for singlet state of model **1**: FULL (*upper*) and delete-TB (*bottom*) states. For simplicity, only p_Z'' coefficients in triple-zeta basis functions are shown. ε_{gap} indicates HOMO–LUMO energy gap (Modified with permission from Ref. [5]. Copyright 2006 American Chemical Society)

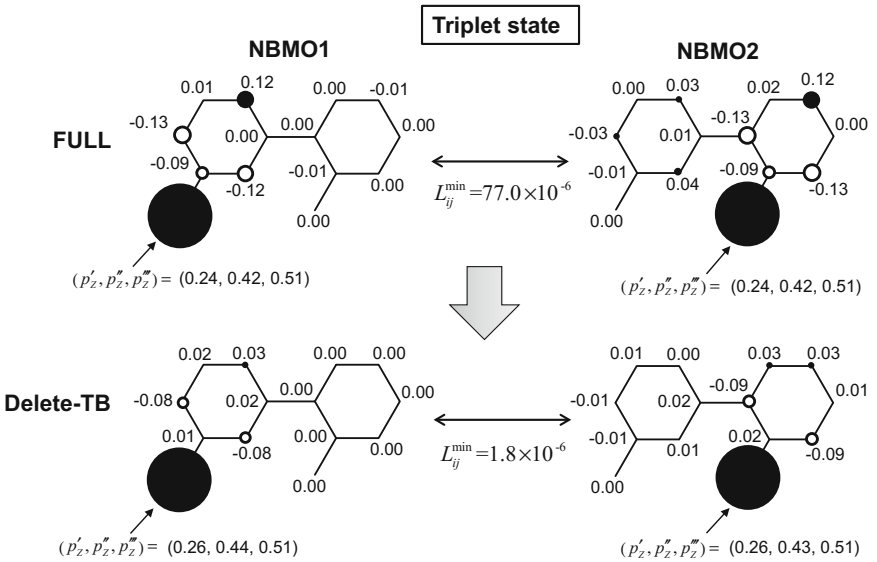

Fig. 4.7 Two NBMOs (NBMO1 and NBMO2) for triplet state of model **1**: FULL (*upper*) and delete-TB (*bottom*) states. For simplicity, only p_Z''' coefficients in triple-zeta basis functions are shown, except for those corresponding to radical center. L_{ij}^{min} shows magnitude of NBMO mixing (Modified with permission from Ref. [5]. Copyright 2006 American Chemical Society)

interaction reduces the HOMO–LUMO orbital energy gap ε_{gap}, as shown in Fig. 4.6 (0.136 a.u. (FULL) → 0.112 a.u. (delete-TB)). That is, the TB interaction increases the HOMO–LUMO energy gap. Here, the ε_{gap} change relates to the change in the denominator of Eq. (4.7), $2(\varepsilon_a - \varepsilon_i)$.

Figure 4.7 shows two NBMOs corresponding to $L_{ij}^{\min}$ after unitary rotations for the triplet state of **1** in the FULL (upper) and delete-TB (bottom) states. In the FULL state, active carbon sites, denoted as "*", have coefficients with finite values in both NBMO1 and NBMO2. The FULL results show that NBMO1 in BR-1 was completely localized on its own unit and was not delocalized over the BR-2 unit. In contrast, NBMO2 in BR-2 was slightly delocalized over the BR-1 unit. This feature highlights the fact that the 0−* linkage between BR-1 and BR-2 produces non-disjoint NBMO mixings.

The deletion of the TB interaction had several consequences. Firstly, the NBMO coefficient at the radical center position increased slightly (see the p_Z' and p_Z'' coefficients), while the NBMO coefficients at the other active carbon sites decreased. In other words, the deletion suppressed the 0–* property of the alternant hydrocarbon. At the same time, the delocalization of the NBMO coefficients into the adjacent BR units was eliminated after deletion and each was localized into each own unit. The localization reduced the NBMO mixing and increased the disjoint property. The decrease of $L_{ij}^{\min}$ (77.0×10^{-6} (FULL) → 1.8×10^{-6} (delete-TB))

supports the reduced NBMO mixing. It can be concluded that the TB interaction contributes to (1) the delocalization of NBMOs into adjacent unit(s) and (2) the increase in NBMO mixing leading to the non-disjoint (0−*) property.

In this subsection, the effects of the TB interactions between radicals were described using two different approaches. One was a direct discussion using the total energy. The other was an indirect but understandable discussion using NBMO shapes and the corresponding $L_{ij}^{\min}$ values. The former energetic treatments firmly supported the reliability of $L_{ij}^{\min}$ for predicting the magnetic properties of a system.

4.3.2 Spacer Size and Number of Radicals: Effects on High-Spin Stability

To gain a deeper understanding of the relationship between inter-radical TB interactions and high-spin stability, we further examined the following issues:

1. The effect of inter-radical spacer size on the high-spin stability.
2. The effect of the number of radicals on the high-spin stability.

We prepared models **2**–**4** as shown in Fig. 4.8a and 4.10a. Single point calculations at the ROMP2(FC)/6-311G level were performed for models **2**–**4** based on their ROHF/6-311G optimized geometries while maintaining their planar structures. The TB interaction was assumed to occur through the shortest TB pathway between radicals, shown as a bold line in the figures. Based on this assumption, **3** has an all-*trans* TB pathway, while **2** and **4** have mixed *cis*–*trans* TB pathways.

Figure 4.8b shows the relationship between the high-spin stability, ΔE_{total}^{S-T}, and spacer size n for models **2** and **3**. ΔE_{total}^{S-T} in model **2** drastically decreases with increasing n compared with that of model **3**. At n = 0 and 1, ΔE_{total}^{S-T} in model **2** is positive, meaning that the high-spin state is stable. When $n \geq 2$, however, ΔE_{total}^{S-T} becomes negative, indicating that the low-spin state is more stable. Figure 4.8c shows the components of ΔE_{total}^{S-T}, i.e., ΔE_{HF}^{S-T} and $\Delta E_{MP2(corr)}^{S-T}$. In model **2**, the positive ΔE_{HF}^{S-T} and negative $\Delta E_{MP2(corr)}^{S-T}$ effectively cancel each other in ΔE_{total}^{S-T}. The negative $\Delta E_{MP2(corr)}^{S-T}$ arises because $\Delta E_{MP2(corr)}^{S-T}$ mainly stabilizes the singlet state. The cancelation results in a smaller absolute magnitude of ΔE_{total}^{S-T}. ΔE_{HF}^{S-T} gradually increases with n and tends to converge to a constant value. In contrast, $\Delta E_{MP2(corr)}^{S-T}$ drastically decreases with n. The decrease in ΔE_{total}^{S-T} can be explained by considering the $\Delta E_{MP2(corr)}^{S-T}$ term, which can be further divided into singlet $(E_{MP2(corr)}^{S})$ and triplet $(E_{MP2(corr)}^{T})$ energies, as shown in Fig. 4.8d. The behavior of $\Delta E_{MP2(corr)}^{S-T}$ can be explained by the fact that $E_{MP2(corr)}^{S}$ stabilizes more quickly than $E_{MP2(corr)}^{T}$ does with an increase in n.

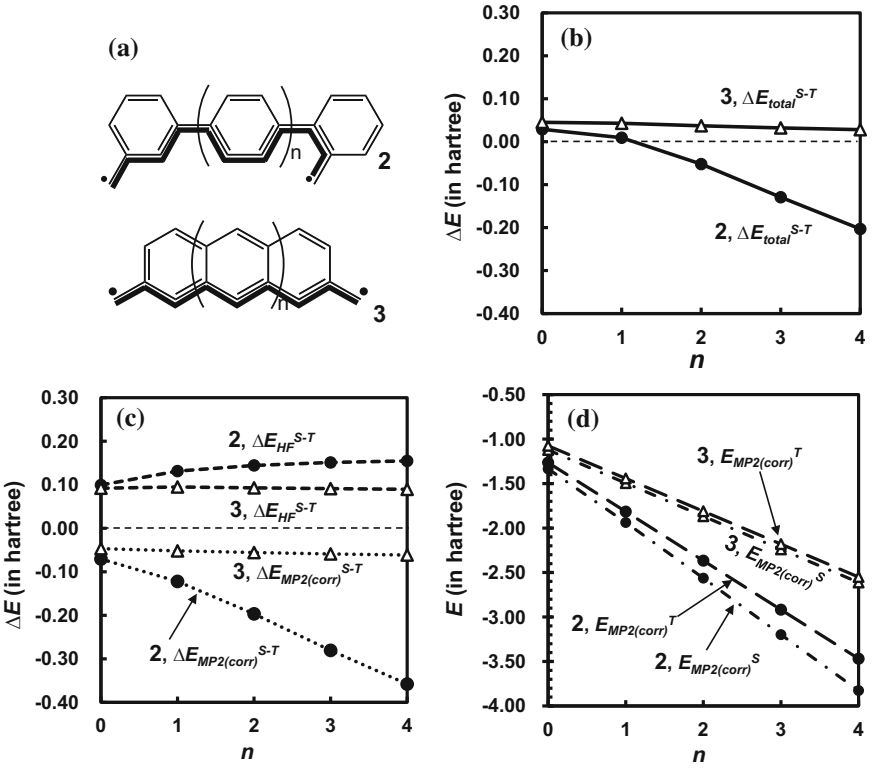

Fig. 4.8 **a** Bi-radical models **2** and **3** for examining inter-radical interaction pathways. *Bold lines* indicate possible shortest TB interaction pathway between radicals. *n* represents number of spacer units. **b** and **c** Relationships between the singlet–triplet energy difference (and its components) and *n* for models **2** and **3**. **d** System size dependence of MP2 correlation energy term for each model (Modified with permission from Ref. [5]. Copyright 2006 American Chemical Society)

In contrast to ΔE_{total}^{S-T} of model **2**, ΔE_{total}^{S-T} of model **3** gradually decreases with *n* and remains positive even at $n = 4$ (see Fig. 4.8b). This result implies that the all-*trans* TB pathway in model **3** is more effective for long-range exchange interactions between radicals than that in model **2**. This behavior can be explained by the fact that ΔE_{HF}^{S-T} remains constant, whereas $\Delta E_{MP2(corr)}^{S-T}$ gradually decreases with *n* (see Fig. 4.8c). The small $\Delta E_{MP2(corr)}^{S-T}$ change in model **3** is quite different from the large $\Delta E_{MP2(corr)}^{S-T}$ change in model **2**. From Fig. 4.8d, it is evident that the small change in $\Delta E_{MP2(corr)}^{S-T}$ for model **3** comes from the stabilization in $E_{MP2(corr)}^{S}$ with *n*, which occurs at almost the same speed as for $E_{MP2(corr)}^{T}$.

The results show that the high-spin stability of these systems is controlled by the electron correlation term $\Delta E_{MP2(corr)}^{S-T}$ rather than the HF term ΔE_{HF}^{S-T}. Moreover, in the correlation term, the energy difference $\Delta E_{MP2(corr)}^{S-T}$ is more important than the

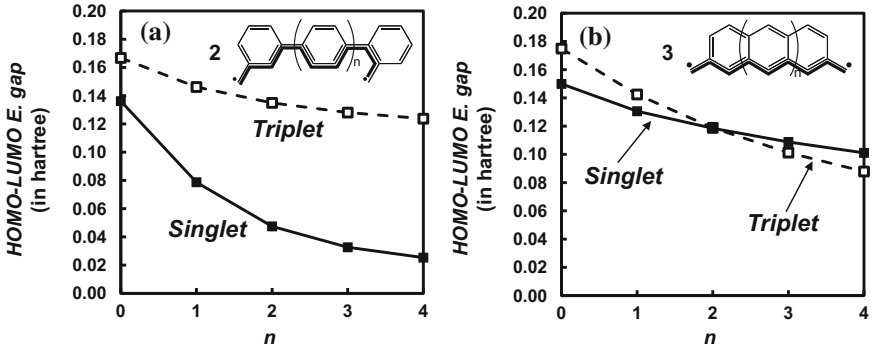

Fig. 4.9 Relationships between HOMO–LUMO (or NBMO–LUMO) energy gap and n for **a** model **2** and **b** model **3** (Modified with permission from Ref. [5]. Copyright 2006 American Chemical Society)

energy of the spin states, $E^{S}_{MP2(corr)}$ and $E^{T}_{MP2(corr)}$. The difference between the behaviors of the correlation terms of models **2** and **3** can be qualitatively explained by the difference between their HOMO–LUMO energy gaps, which corresponds to the denominator of Eq. (4.7). Figure 4.9a, b show the relationships between n and the HOMO–LUMO gaps for models **2** and **3**, respectively. For the triplet state, the energy difference between the highest NBMO and LUMO was used instead of the HOMO–LUMO gap. The energy gap of model **2** rapidly decreases with n in the singlet state, while the gap gradually decreases in the triplet state. By considering the large decrease in the HOMO–LUMO gap, it is expected that the absolute value of the HOMO–LUMO component [Eq. (4.7)] drastically increases with n in the singlet state. The large negative $E^{S}_{MP2(corr)}$ relative to the $E^{T}_{MP2(corr)}$ term results in the large negative $\Delta E^{S-T}_{MP2(corr)}$. In addition, the HOMO–LUMO gap converges to a constant value with increasing n. In contrast, $\Delta E^{S-T}_{MP2(corr)}$ continuously decreases with increasing n. The behavior of the $\Delta E^{S-T}_{MP2(corr)}$ implies that the numerator of the HOMO–LUMO component is more important than the corresponding denominator in the range of larger n. On the other hand, the singlet and triplet states of model **3** show very similar behaviors. The similarity is expected to be the reason for the similar values and behaviors of $E^{S}_{MP2(corr)}$ and $E^{T}_{MP2(corr)}$. The similar energy terms for the singlet and triplet states result in the small absolute value of $\Delta E^{S-T}_{MP2(corr)}$.

Figure 4.10 shows the relationship between the high-spin stability of **4** and the number of radical units m, excluding the terminal two BRs (Fig. 4.10a), and the corresponding components (Fig. 4.10b). m = 0, 2, 4, and 6 were selected. The total numbers of radicals present in the whole system corresponded to (m + 2), i.e., 2, 4, 6, and 8 for m = 0, 2, 4, and 6, respectively. The low-spin (L) and high-spin (H) states of model **4** were the singlet and highest spin states, respectively. For example, for m = 2, the total number of radicals was (m + 2) = 4, and the L and H

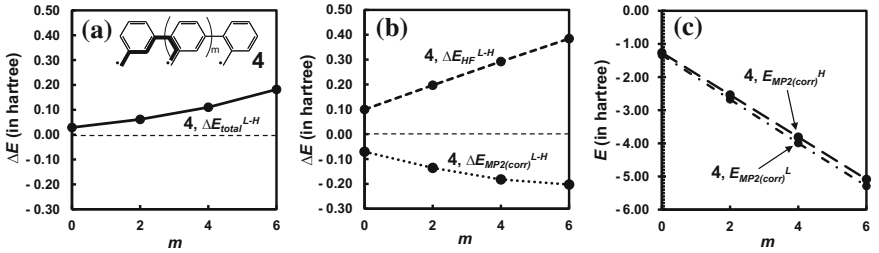

Fig. 4.10 **a** Relationship between high-spin stability and m for poly-radical model **4**, where m corresponds number of radical units excluding terminal two BR units. *Bold line* indicates possible shortest TB interaction path between radicals. **b** HF and MP2 correlation energy components in high-spin stability. **c** System size dependence of MP2 correlation energy term (Modified with permission from Ref. [5]. Copyright 2006 American Chemical Society)

states were the singlet and quintet states, respectively. In this case, ΔE_{total}^{L-H} increases with m. This behavior can be explained by the following two effects: the increment of ΔE_{HF}^{L-H} in proportion to m and the convergence of $\Delta E_{MP2(corr)}^{L-H}$ to a constant value with increasing m. Figure 4.10c shows the details of $\Delta E_{MP2(corr)}^{L-H}$ for model **4**. In the correlation term, the magnitude of the energetic stabilization of $E_{MP2(corr)}^{L}$ is larger than that of $E_{MP2(corr)}^{H}$. However, the correlation energy terms of both spin states decrease in a similar manner with m. This similar decrease resulted in the constant $\Delta E_{MP2(corr)}^{L-H}$. It can be considered that each radical unit in model **4** is connected to the adjacent unit while maintaining the short-range TB path. In such a system, high-spin stability can be expected because the stability increases linearly with the number of radicals.

In this subsection, we have shown that electron correlation effects mainly control the high-spin stability of a system. The design of the correlation term directly leads to the design of ferromagnetism. The relationship between the correlation effects and ferromagnetic properties discussed here is a fundamental but essential factor in the effective design of ferromagnetic materials.

References

1. Glendening, E.D., Badenhoop, J.K., Reed, A.E., Carpenter, J.E., Bohmann, J.A., Morales, C. M., Landis, C.R., Weinhold, F.: NBO 6.0. Theoretical Chemistry Institute. University of Wisconsin, Madison (2013)
2. Imamura, A., Sugiyama, H., Orimoto, Y., Aoki, Y.: Ab initio through space/bond interaction analysis on the stereoelectronic effect by modifying the exponents of the basis set. Int. J. Quant. Chem. **74**, 761–768 (1999)
3. Orimoto, Y., Naka, K., Aoki, Y.: NBO-based CI/MP through-space/bond interaction analysis and its application to stereoelectronic effects in S_N2 reactions. Int. J. Quant. Chem. **104**, 911–918 (2005)

4. Jiang, L., Orimoto, Y., Aoki, Y.: Stereoelectronic effects in Menshutkin-type S_N2 reactions: theoretical study based on through-space/bond orbital interaction analysis. J. Phys. Org. Chem. **26**, 885–891 (2013)
5. Orimoto, Y., Imai, T., Naka, K., Aoki, Y.: Ab Initio MO Analysis of Interaction Paths between Radicals in Ferromagnetic Organic Systems. J. Phys. Chem. A **110**, 5803–5808 (2006)
6. Orimoto, Y., Aoki, Y.: Pure through-bond state in organic molecules for analysis of the relationship between intramolecular interactions and total energy. Int. J. Quant. Chem. **92**, 355–366 (2003)
7. Orimoto, Y., Aoki, Y.: Quantum-chemical approach to the solvatochromic transition in polysilane derivatives. J. Polym. Sci., Part B: Polym. Phys. **44**, 119–133 (2006)
8. Orimoto, Y., Aoki, Y.: Enhanced hyperpolarizability via electron correlations in donor-σ-acceptor systems. Phys. Rev. A **68**, 063808 (2003)
9. Orimoto, Y., Aoki, Y.: Strong electron correlation effects on first- and second-order hyperpolarizabilities in zwitterionic σ-conjugated systems: its dependence on substituents, conformations, spacer size, and basis sets. J. Phys. Chem. A. **111**, 8241–8249 (2007)
10. Orimoto, Y., Aoki, Y.: Ab initio through-space/bond interaction analysis of the long C-C bonds in Bi(anthracene-9,10-dimethylene) photoisomers. Int. J. Quant. Chem. **86**, 456–467 (2002)
11. Orimoto, Y., Naka, K., Takeda, K., Aoki, Y.: Ab initio MO study on [3 + 2] annulation using β-phenylthio-acryloylsilanes with alkyl methyl ketone enolates and its through-space/bond interaction analysis. Org. Biomol. Chem. **3**, 2244–2249 (2005)
12. Jiang, L., Orimoto, Y., Aoki, Y.: Substituent effects on Menshutkin-type reactions in the gas phase and solutions: theoretical approach from the orbital interaction view. J. Chem. Theory Comput. **9**, 4035–4045 (2013)
13. Schmidt, M.W., Baldridge, K.K., Boatz, J.A., Elbert, S.T., Gordon, M.S., Jensen, J.H., Koseki, S., Matsunaga, N., Nguyen, K.A., Su, S., Windus, T.L., Dupuis, M., Montgomery Jr., J.A.: General atomic and molecular electronic structure system. J. Comput. Chem. **14**, 1347–1363 (1993)
14. Frisch, M.J., Trucks, G.W., Schlegel, H.B., Scuseria, G.E., Robb, M.A., Cheeseman, J.R., Montgomery, J.A., Jr., Vreven, T., Kudin, K.N., Burant, J.C., Millam, J.M., Iyengar, S.S., Tomasi, J., Barone, V., Mennucci, B., Cossi, M., Scalmani, G., Rega, N., Petersson, G.A., Nakatsuji, H., Hada, M., Ehara, M., Toyota, K., Fukuda, R., Hasegawa, J., Ishida, M., Nakajima, T., Honda, Y., Kitao, O., Nakai, H., Klene, M., Li, X., Knox, J.E., Hratchian, H.P., Cross, J.B., Adamo, C., Jaramillo, J., Gomperts, R., Stratmann, R.E., Yazyev, O., Austin, A. J., Cammi, R., Pomelli, C., Ochterski, J.W., Ayala, P.Y., Morokuma, K., Voth, G.A., Salvador, P., Dannenberg, J.J., Zakrzewski, V.G., Dapprich, S., Daniels, A.D., Strain, M.C., Farkas, O., Malick, D.K., Rabuck, A.D., Raghavachari, K., Foresman, J.B., Ortiz, J.V., Cui, Q., Baboul, A.G., Clifford, S., Cioslowski, J., Stefanov, B.B., Liu, G., Liashenko, A., Piskorz, P., Komaromi, I., Martin, R.L., Fox, D.J., Keith, T., Al-Laham, M.A., Peng, C.Y., Nanayakkara, A., Challacombe, M., Gill, P.M.W., Johnson, B., Chen, W., Wong, M.W., Gonzalez, C., Pople, J.A.: Gaussian 03, revision C. 02. Gaussian, Inc., Wallingford, CT (2004)

Chapter 5
O(N) Ab Initio Open-Shell MMELG-PCM Method and Its Application to Radical Polymers

Abstract We developed the minimized mixing elongation—polarizable continuum model (MMELG-PCM) method, which implements the elongation method in conjunction with the minimized mixing molecular orbital localization process for non-bonding molecular orbitals under the polarizable continuum model. Besides the highest spin state, the MMELG-PCM method can treat the lowest or even intermediate spin state of open-shell systems, which is either difficult or impossible to implement correctly with the conventional method. The MMELG-PCM method can also be combined with the $L_{\min}$ method, which was described in Chap. 3. The MMELG-PCM-$L_{\min}$ method can predict the high-spin stability of conjugated organic radicals with solvent effects and thus would be useful for designing organic ferromagnets.

5.1 Introduction

Organic radical molecules possess unpaired electron(s), and, as a result of their high reactivities, prefer to combine with other radicals, achieving stability by forming dimers instead of existing as radicals. However, it is now known that stable organic radical molecules maybe synthesized by controlling the time spent at ambient conditions. Stable organic radicals have been extended to their related radical polymers, which can exhibit many useful functions, including conduction, magnetism, photosensitivity, non-linear optics, and charge storage. In particular, π-conjugated high-spin radical alignment has been used in attempts to synthesize organic-based ferromagnetic materials; noteworthy compounds have been prepared by Nishide [1–4], Rajca [5–8], and many other experimentalists in the polymer synthesis field. In addition, molecular magnets based on organic radicals have been investigated as new magnetic materials, and the syntheses of polyradical molecular stacking systems have been significantly developed.

The functional properties of materials are based on their microscopic electronic states, and thus quantum chemistry (QC) that precisely reflects the electronic properties of an individual atom or molecule must be effective. However, the

Y. Aoki et al., *Quantum Chemical Approach for Organic Ferromagnetic Material Design*,
SpringerBriefs in Electrical and Magnetic Properties of Atoms, Molecules, and Clusters,
DOI 10.1007/978-3-319-49829-4_5

computational time required increases as the number of the bases functions is increased: at the Hartree–Fock (HF) level, time requirements scale at N^{3-4} and become N^{5-7} at post-HF levels. Therefore, the application of full post-HF-level methods to cohesion systems and materials remains difficult, even if the most advanced supercomputers, which are not widely available for use, are employed. As was described in Sect. 1.7.1, the DMRG method is expected to become a powerful ab initio QC tool rapidly for the investigation of magnetic properties.

The elongation (ELG) method, an efficient treatment developed in our laboratory since the early 1990s, has also been applied to large systems (for example, [9–21]). It can be supposed that this method, which was developed for large closed-shell systems, especially biological systems, will also be applicable to open-shell systems. Using this method, one can mimic experimental polymerization/copolymerization procedures computationally and determine electronic states efficiently and precisely, including for radical polymerization processes. The ELG method addresses local parts directly (but includes the electronic states of whole systems), and it therefore shows several advantages when we deal with large-scale complex systems, which the conventional (CONV) method cannot handle.

One advantage of the ELG method is its fast computational time on a single computer core because the concept is sequential and local. In other words, parallelization scalability is not linear with respect to the number of cores at the end of the complete ELG, although parallelization efficiency at each SCF step is the same as in CONV calculations. That is, single core calculations are very fast due to the sequential concept that underpins the ELG method; thus, this method does not appear to scale well when applied to multi-core calculations. Therefore, the ELG method can be implemented efficiently even on small laboratory-based cluster systems with less than 100 cores, which have become the most preferable parallel size in conventional *ab initio* QC calculations, because the ELG method is as well parallelized at each ELG step as the CONV method when comparing the same level of theory.

The second advantage is a smoothly converged self-consistent field (SCF) procedure, which results from the small SCF space in the regional localized molecular orbitals (RLMOs) used in the calculations [11]. We already found data that show that the ELG-SCF converges within 20–30 cycles even for complicated systems that include metals, for which conventional SCF methods cannot converge, even after 500 SCF cycles. The fast ELG convergence is because the dimension of the diagonalization in the ELG method maintains a constant size for the whole system from the starting cluster calculation to the end of the ELG, while that used in the CONV method increases with system size; in the latter case, the eigenvalues become too dense, leading to difficulties in SCF convergence.

The third advantage is smoothly converging geometry optimization resulting from the use of a small number of optimized parameters. The process may be undertaken without the loss of necessary optimization in the geometrical parameters because we can remove unnecessary parameters that are already optimized. The optimization routine used by the ELG method can even reach more stable structure that cannot be found using CONV direct optimization methods.

The fourth advantage is that post-HF calculations can be very efficiently implemented based on RLMOs; for example, the second-order local Møller–Plesset (LMP2) or local configuration interaction (LCI) methods can use RLMOs as the basis wavefunctions [15].

The fifth advantage is that the ELG method can perform efficient search of the most preferable energy, sequence, function in large systems, and so on (not only the structure optimization), because the electronic states that have already been obtained can be frozen against any new interaction with the attacking monomer if the effect of the interaction is negligible within the frozen region. The orbital freeze in unnecessary part makes it possible to calculate the necessary part as a partial SCF only in the local space while including all of the effects of the frozen part. In contrast, it is necessary to repeat the calculations for the whole system when using CONV direct methods, even for very slight perturbations. Therefore, to find the most likely spin states, for example, we can search the preferred spin states at each ELG step, and then the system that has been elongated to the desired length must eventually reach the most stable spin state.

Only one disadvantage appears when we use a high-performance computer with one million cores for a single molecular system, because the ELG process is sequential. This disadvantage in scalability can be overcome by simultaneously performing the many independent calculations required for a lot of samplings, because ELG performance across a few cores is very fast as mentioned above, which allows many jobs to be submitted with different conditions using other cores in parallel.

The most important advantage of the ELG method is that no approximations are incorporated, which makes the approach different from other $O(N)$ fragmentation methods. The only step required is to remove some orbitals (frozen orbitals) that are unnecessary in the SCF; however, the frozen orbital removing is not an approximation but simply a manipulation to reduce the dimension diagonalized in the eigenvalue problem to avoid unnecessary calculations. The removal of the frozen orbitals is well-controlled to keep the energy difference between the conventional and ELG methods to less than some threshold (we normally set it to be 10^{-8} hartrees per atom in energy errors). Recently, the ELG method was extended from one-dimensional systems to three-dimensional systems [16, 20, 21].

In this chapter, we describe the application of the ELG method to high-spin systems toward the theoretical design of organic magnetism. Post-HF techniques must be used to deal with magnetic properties because the existing open-shell large active space requires configuration interactions. To facilitate a qualitative prediction of magnetism, the ELG procedure was developed to be applicable to large open-shell systems possessing the highest spin states as the first step (a treatment for intermediate spin states based on RLMOs is in progress), where a fast localization method, called the minimized mixing molecular orbital (MMMO) localization method, was implemented for existing systems containing many non-bonding molecular orbitals (NBMOs) to evaluate the high spin stability.

We named this approach the minimized mixing NBMO (MMNBMO) method. By combining the MMNBMO and ELG methods, a classical index to show high spin stability, described in Chap. 3, was introduced to examine the possibility of magnetism in large organic systems at the ab initio level of theory.

5.2 Method

5.2.1 Elongation Method for Closed-Shell Systems

Using the ELG method, the electronic structure of a polymer is theoretically synthesized step-by-step via a sequential interaction between an oligomer and an attacking fragment, as occurs in a real polymerization reaction. For this purpose, the electronic states of an appropriately sized small oligomer are calculated (starting cluster), and RLMOs are defined at the oligomer terminus that experiences an interaction with the monomer. For this purpose, some of the canonical molecular orbitals (CMOs) in the starting cluster are regionally localized into region B (active RLMOs) near to the attacking monomer and the others are localized into region A (frozen RLMOs) far from the monomer.

Next, we proceed to ELG of the chain during which the oligomer (starting cluster) interacts with the attacking monomer. The HF SCF calculations are performed on the system in which the approaching monomer interacts with one end of cluster part B. The interaction in our treatment means to diagonalize only the RLMO-based Fock matrix of the interactive region until the SCF calculation converges within this small space.

In the subsequent ELG process, the achievement of *linear scaling* is attributed to the efficient treatment of only the necessary interaction between the active RLMOs of the cluster and the attacking monomer, while discarding the unnecessary frozen RLMOs; this leads to $O(N)$ computations for large systems. The working space for the new interaction is then limited by the RLMOs assigned to the B region together with the CMOs of the attacking monomer. The solution yields a set of CMOs in the reduced space of B + C, which can be localized again into a new frozen region (A + B) and a new active region (C). The whole ELG procedure is repeated until the desired length is reached. As the system enlarges, the size of the interaction region is unchanged from that of the starting cluster, and the CPU time required for the ELG-SCF is more or less constant throughout the ELG process. Consequently, SCF convergence is much smoother than that of the CONV direct method due to the limited number of eigenstates (orbital energies in the SCF).

Figure 5.1a shows an illustration that represents the concept of ELG by repeated localization and interaction along the polymer chain, while the Fig. 5.1b shows the schematic orbital shapes of the frozen and active RLMOs during the ELG process. It is evident that the active RLMOs are always concentrated in the area of interaction with the attacking monomer, as are the active atomic orbitals (AOs).

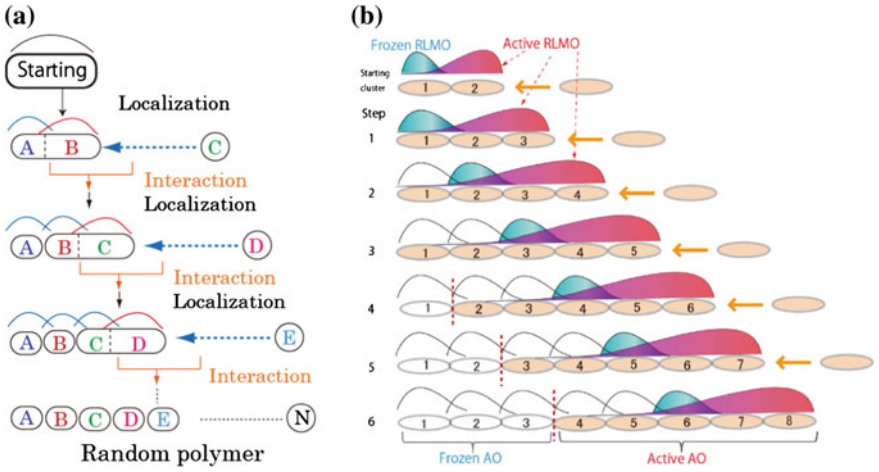

Fig. 5.1 **a** Schematic illustration of ELG method and **b** corresponding RLMOs. (Modified with permission from Ref. [16]. Copyright 2012 Royal Society of Chemistry)

The dotted line between the white and gray zones in the growing units indicates the boundary between the frozen and active AOs. The frozen AOs are removed from the two-electron (2e) integral calculations when constructing the Fock matrix, except for the necessary strong Coulomb interaction integrals that must have some effect on the Fock matrix in the active region. Hereafter, the CPU time required to calculate the 2e-integrals—which makes up around 90% of the time required for a conventional HF calculation—will be much reduced. A detailed explanation of this method and its application to biological systems like DNA or proteins are described in our review (for example, [16]).

5.2.2 *Open-Shell Elongation Method with Polarizable Continuum Model*

The ELG method for closed-shell systems has been extended to include open-shell systems [12]. In this section, a brief outline of the open-shell ELG method is provided. To initiate the ELG method, the eigenvalue problem of the starting cluster A + B is solved using a CONV method with a high-spin state if the purpose of the calculation is to determine highest-spin states of the final system. Here, we suppose that each unit has one unpaired electron in a high-spin system, as shown in Fig. 5.2, and then the system is elongated. In this example, a triplet state is used in the interaction region, although any multiple states calculations are feasible. For simplicity, in the case in which two units are used as a starting cluster, the CMOs of the A + B starting cluster are localized into two different sets using an RLMO method. One set is localized in region A, and the other is localized in region B, each of

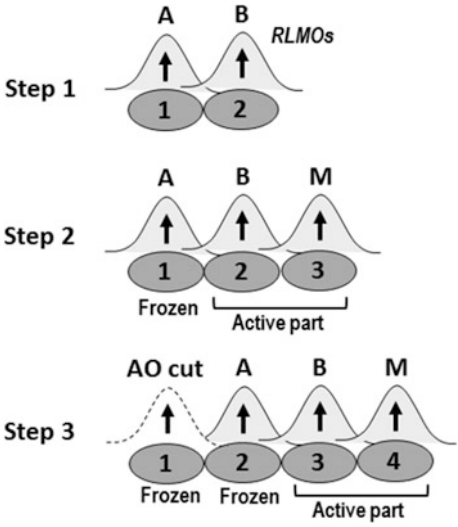

Fig. 5.2 Schematic illustration of open-shell ELG method. (Reproduced with permission from Ref. [27]. Copyright 2016 Walter de Gruyter GmbH)

which has one electron. In the next step, region A is frozen and only region B is active toward a new attacking monomer M, which also has one electron.

The eigenvalue problem of B + M to be solved is

$$\mathbf{F}^{RLMO(B+M)(\omega)}_{RLMO(B+M)}\mathbf{C}^{new(\omega)}_{RLMO(B+M)} = \mathbf{S}^{RLMO(B+M)(\omega)}_{RLMO(B+M)}\mathbf{C}^{new(\omega)}_{RLMO(B+M)}\boldsymbol{\varepsilon}^{new(\omega)}, \tag{5.1}$$

where

$$\mathbf{F}^{RLMO(B+M)(\omega)}_{RLMO(B+M)} = \mathbf{C}^{RLMO(B+M)(\omega)\dagger}_{Active\,AO}\mathbf{F}^{Active\,AO(\omega)}_{Active\,AO}\mathbf{C}^{RLMO(B+M)(\omega)}_{Active\,AO}, \tag{5.2}$$

for each spin (ω), α spin orbital, or β spin orbital. The new coefficients obtained are based on RLMO (B + M) and are transformed back to the original AOs in their basis using AO-based RLMOs, $\mathbf{C}^{RLMO(B+M)(\omega)}_{ActiveAO}$, using the relation

$$\mathbf{C}^{new(\omega)}_{Active\,AO} = \mathbf{C}^{RLMO(B+M)(\omega)}_{Active\,AO}\mathbf{C}^{new(\omega)}_{RLMO(B+M)}. \tag{5.3}$$

It is necessary to solve Eq. (5.1) for each spin state using the unrestricted HF (UHF) method. The new CMOs obtained, $\mathbf{C}^{new(\omega)}_{Active\,AO}$, are again localized onto parts B and C. In each ELG step, a new M is added, and the eigenvalue problem is treated at the desired multiplicity by solving the Fock matrix with a constant dimension of active RLMOs. This process is repeated until the system has been elongated to the desired length.

Open-shell systems have recently been found to contribute to spin batteries, spin-donor conduction, and photonic devices, in addition to ferromagnets, and solvent effects sometimes provide important enhancements of spin transport as well

as functional properties. To be applicable to a solute in solution, we introduced the polarizable continuum model (PCM) method [22] for a simple treatment of solvent effects in the open-shell ELG method. The PCM allows one to treat solvents such as liquid crystals, which have intrinsic dielectric anisotropy. In the ELG method, the Fock matrix for $\omega(\alpha$ or $\beta)$ spin in the working space with the PCM can be described for (A + B) ← M at the first ELG step as follows:

$$F_{\mu\nu}^{(\omega)}(PCM) = F_{\mu\nu}^{(\omega)}(\mathrm{A}\,|\,\mathrm{B}+\mathrm{M}) + \left\langle \mu \left| \int \frac{\sigma(s)}{|r-s|} d^2 s \right| v \right\rangle, \tag{5.4}$$

where $F_{\mu\nu}^{(\omega)}(\mathrm{A}\,|\,\mathrm{B}+\mathrm{M})$ is a matrix element of the solute Fock matrix with ω spin, the second term in the right-hand side is the matrix element of the electrostatic potential, and $\sigma(s)$ is the surface charge distribution. The size of part A (i.e., the frozen region) will become larger and larger as the size of the whole system increases, and the size of B + M (i.e., the active part) used in the SCF remains constant. The ELG calculations under PCM are implemented only as the second term is added to the one-electron Hamiltonian, reflecting the solvent effects on the electronic states in the SCF part at each ELG step.

5.2.3 *Minimized Mixing Molecular Orbital Localization and Minimized Mixing Elongation Methods*

To formulate a reasonable index that should show the possibility of high spin stability, we introduce a special localization treatment, the MMMO localization method, by which we can localize the NBMOs to provide the minimum on-site overlap between two degenerate NBMOs, followed by the process described in Sect. 3.2. This manipulation must provide regionally localized orbitals similar to those prepared using the RLMO procedure of the ELG method, but differs in the conditions used to make the localization. The localized NBMOs thus obtained can be used in the $L_{\min}$ method described in Sect. 3.2. In applying the open-shell ELG method, the MMMO localization procedure is applied to the open-shell part, i.e., the singly occupied molecular orbitals (SOMOs), while the RLMO localization in the ELG method is applied to the other orbitals, either fully occupied or fully unoccupied.

We suppose that a system has plenty of units $(A, B, \ldots)$, each of which has an unpaired electron with an up-spin. The flow chart of MMELG method is shown in Fig. 5.3 where an index to show the mixing between two NBMOs

$$L_{\min} = \sum_{j>i} L_{\mathrm{ij}}^{\min} = \sum_{j>i} \sum_{r} \left(C'_{ri} C'_{rj} \right)^2 \tag{5.5}$$

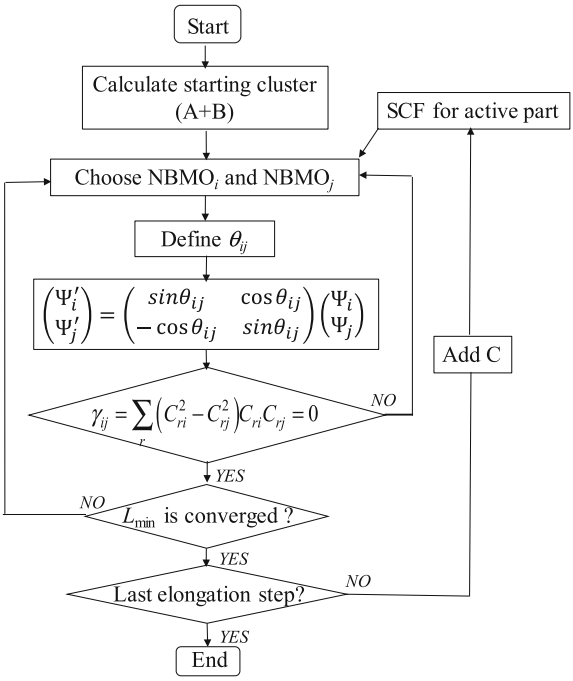

Fig. 5.3 Flow chart for MMELG method

is defined to perform the MMMO localization. The details of the process have been described elsewhere [23]. The treatments described above are also available at the density functional theory (DFT) level of theory.

5.3 Applications and Comparison with the Conventional Method

5.3.1 Application of the Open-Shell Elongation Method

To investigate the accuracy of the open-shell ELG method for high-spin systems at both the HF and DFT levels of theory, test calculations on the polyglycine radical in Fig. 5.4 (Model 1) were performed at the ROHF/6-31G(d), ROB3LYP/6-31G(d) (restricted open-shell Becke's three-parameter, Lee–Yang–Parr exchange-correlation functional), UHF/6-31G(d), and UB3LYP/6-31G(d) (unrestricted B3LYP) levels. The starting cluster size was set to 10 units (N_{st} = 10), in which the number of units in region A was set to two, that in region B was set to eight, and that in M was set to two. Therefore, the number of unpaired electrons present in the whole system at each step N_{se} increases with ELG as N_{se} = 10, 12, …, 38, 40. Figure 5.4 shows that the energy differences between the CONV and ELG

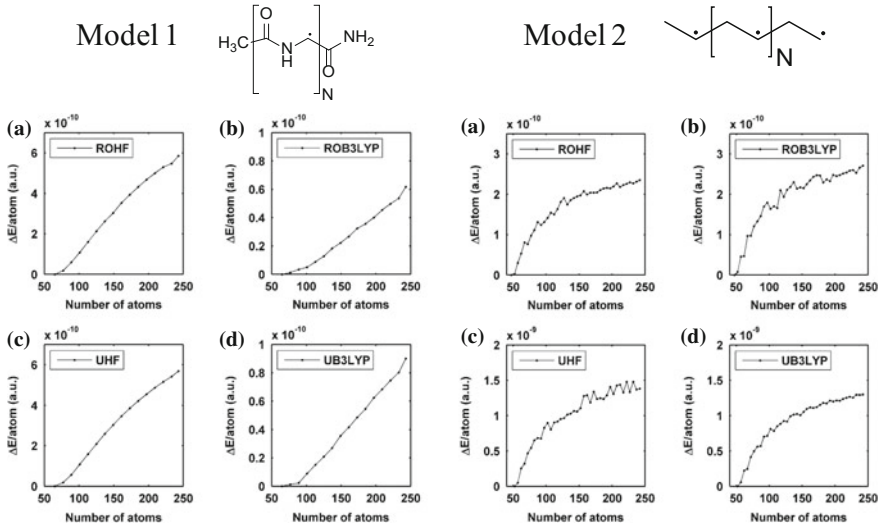

Fig. 5.4 ΔE/atom (a.u.) for polyglycine radical (Model 1) and polyethylene radical (Model 2) calculated at restricted and unrestricted HF and DFT levels with 6-31G(d) basis set

calculations ΔE/atom are almost zero ($\approx 10^{-10}$ a.u. per atom) and increase asymptotically with the number of atoms for both restricted and unrestricted open-shell treatments.

Calculations were also undertaken using the polyethylene (Model 2) radical with the 6-31G(d) basis set (Fig. 5.4, right-hand side). The differences (errors) between the CONV and ELG calculations must become flat at large numbers of atoms for all the panels (a)–(d), which is easily attained when the one unit is small. In the case of Model 2, panels (a) and (b) show the results obtained when the starting cluster size was set to nine units ($N_{st} = 9$), in which the number of region A was set to one, that of region B was set to eight, and that of the monomer was set to one ($N_{se} = 9, 10, \ldots, 48$). Panels (c) and (d) in Model 2 show the results obtained when the starting cluster size was set to 10 units ($N_{st} = 9$), in which the number of units in region A was set to one, that in region B was set to nine, and that in M was set to one ($N_{se} = 10, 11, \ldots, 48$). The results show that the unrestricted treatments yielded total energy differences one order of magnitude smaller than the restricted treatments, even when a longer starting cluster was used. In both cases, ΔE/atom was almost negligible.

5.3.2 *Application of the Minimized Mixing Elongation Method*

To confirm the validity of the MMMO localization method and the L_{min} values obtained as described in Chap. 3 for predicting ferromagnetism, the two methods

were combined with the GAMESS program package [24]. The $L_{\min}$(MMMO) was defined by localizing the coefficients of the canonical NBMOs generated using the CONV method. As a reference, $L_{\min}$(ER) was also calculated directly using the coefficients of the localized NBMOs (LNBMOs) generated using the Edmiston–Rüdenberg (ER) localization method [25]. In the ER localization method, where the unitary transformation U in $\phi_v = \sum_\mu \varphi_\mu U_{\mu v}$ ($\{\varphi_\mu\}$ is the basis) is defined to give the maximum for the 2e integrals, $D(\phi) = \sum_v \left[\phi_v^2 \middle| \phi_v^2\right]$, and then the coefficients of the LNBMOs are generated for calculating $L_{\min}$(ER) [see Chap. 3].

The validity and efficiency of our $L_{\min}$(MMMO) method was examined by comparing the results with $L_{\min}$(ER). Figure 5.5a shows that $L_{\min}$(ER) and $L_{\min}$(MMMO) are the same for the model depicted in the graph with N_{se} = 4, 6, 8, 10, and 12 at the level used for testing (ROHF/STO-3G). It was confirmed that the MMMO localization method works correctly for cases including two NBMOs in a unit. A small basis set was used because the ER localization needs a long CPU time to converge at large system sizes; thus, the MMMO CPU time cannot be distinguished from the zero axis line in Fig. 5.5b. It can be seen that the CPU times for $L_{\min}$(ER) increase dramatically, while the CPU times for $L_{\min}$(MMMO) are kept constantly small. Also, though we don't show the graph here, the memory requirements for the ER localization method increase dramatically with increasing N_{se}. These disadvantages, which are inherent in the ER method, render the ER method impractical for calculations on large systems. The increases in CPU time and memory requirements arise because the ER localization method requires heavy 2e integrals calculations, while the MMMO localization method only needs localization procedure. Therefore, the MMMO localization method can be applied quite efficiently to large open-shell systems during the ELG process. Figure 5.5c shows that K increases with $L_{\min}$(MMMO) for the model at the ROM06-HF/6-31G level. The exchange integral K_{ij} corresponds to the energy difference between the

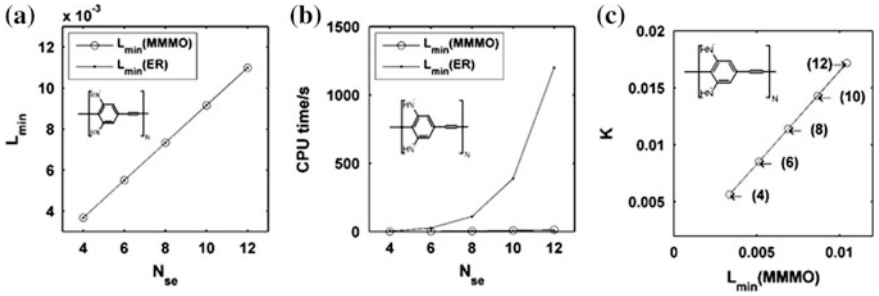

Fig. 5.5 **a** $L_{\min}$ calculated with coefficients of canonical NBMOs and localized NBMOs by ER localization at ROHF/STO-3G level for the model depicted in the graph, **b** CPU times used to compute $L_{\min}$(MMMO) and $L_{\min}$(ER) at ROHF/STO-3G level, **c** relationship between $L_{\min}$(MMMO) and K for N_{se} = 4, 6, 8, 10, and 12 (shown in *parentheses* on each point) at ROM06-HF/6-31G level. (Modified with permission from Ref. [23]. Copyright 2015 John Wiley & Sons, Inc.)

triplet and open-shell singlet states, corresponding to $\Delta E(L\text{-}H)$ in Chap. 3. For simplicity, however, the closed-shell singlet state can also be used in the discussion of $L_{\min}$ in this approach because the CI treatment used to determine the open-shell singlet state in the ELG method is under construction, and the relationship between K and $L_{\min}$ was shown in our previous paper [23].

5.3.3 *Application of the Minimized Mixing Elongation-Polarizable Continuum Model Method*

Figure 5.6 shows the MMELG-PCM method applied to a model of Rajca's compound [8]. The *tert*-butylbenzene substituents present in the experimental system were replaced by hydrogen atoms for simplicity to yield model R. One monomer unit of model R, as shown in Fig. 5.6, was optimized at the UB3LYP/6-31G(d) level. One optimized unit of model R was then used as the repeating unit to construct the whole system.

The values of $\Delta E(L\text{-}H)$ and its increments as functions of N are plotted in Fig. 5.7a, b, respectively. The figure shows results calculated using both the MMELG-PCM and CONV methods at the ROHF/6-31G level. It can be seen that,

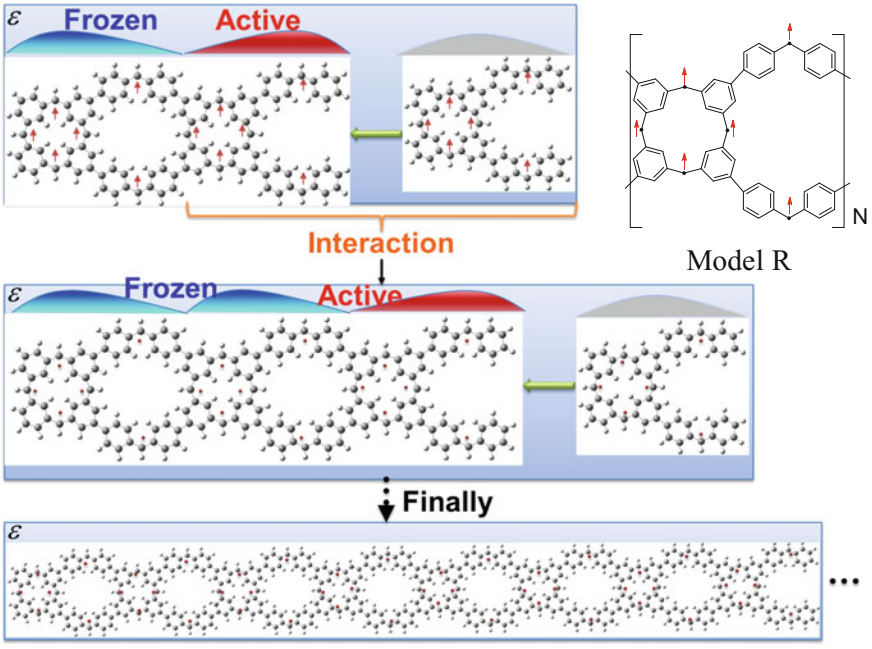

Fig. 5.6 MMELG-PCM method as applied to model of Rajca's high-spin organic polymer. (Modified with permission from Ref. [26]. Copyright 2016 Elsevier B.V.)

in the case of ELG calculations, $\Delta E(L-H)$ increases linearly with N, while for the CONV calculations, $\Delta E(L-H)$ does not linearly depend on N. As model R is a periodic system except for terminal effects, $\Delta E(N) - \Delta E(N-1)$ should change smoothly with almost identical values. In Fig. 5.7b, $\Delta E(N)$ corresponds to $\Delta E(L-H)$ with N units and $\Delta E(N-1)$ corresponds to $\Delta E(L-H)$ with $(N-1)$ units. It is evident that the values of $[\Delta E(N) - \Delta E(N-1)]$ calculated using the MMELG method are almost constant, while those calculated using CONV deviate sharply. Since the lowest spin state is an open-shell singlet in which half of all of the unpaired electrons have up-spins and the remainder have down-spins, the system represents a difficult case for a single-reference method. In one CMO, there are two unpaired electrons arising from two atoms, and the coefficients should be focused on these two atoms. However, in the CONV method, the CMOs are delocalized. With increasing system size, more and more unpaired electrons become involved, which increases the order of complexity of the SCF calculations. In contrast, in the MMELG method, the coefficients of each CMO in each ELG step are localized on the two atoms containing the two unpaired electrons. Since the MMELG method treats a system of constant size during the SCF calculations, the number of unpaired electrons involved remains constant, which reduces the complexity of the SCF calculations. The lowest spin state of the open-shell systems has a multi-reference nature since there are many electronic configurations. The number of electronic configurations possible in the CONV method is proportional to 2^n and thus increases rapidly; in contrast, the number of possible configurations in the MMELG method remains constant during the SCF calculations, even for huge open-shell systems. Therefore, the MMELG method can be useful for calculating the multi-configurational spin state of an open-shell system and can even obtain better results than the CONV method due to its smooth convergence that results from the efficient ELG-SCF method.

Figure 5.7c shows the relationship between the values of $\Delta E(L\text{-}H)$ and $L_{\min}$ for model R that were calculated using the MMELG-PCM-$L_{\min}$ method at the ROHF/6-31G level. It is evident that the high spin stability of conjugated organic

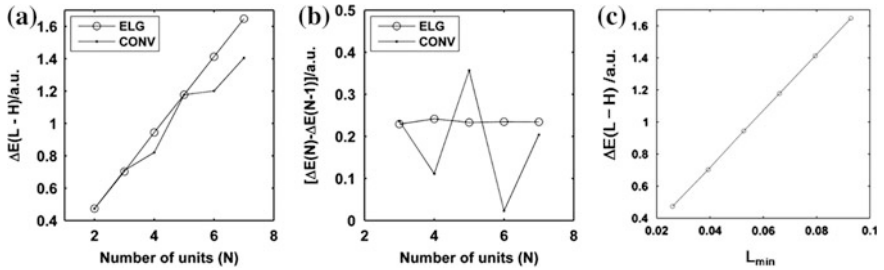

Fig. 5.7 **a** $\Delta E(L\text{-}H)$ and **b** $\Delta E(L\text{-}H)$ per unit for model R calculated using MMELG-PCM and CONV methods at ROHF/6-31G level. **c** Relationship between $L_{\min}$ and $\Delta E(L\text{-}H)$ calculated for model R using MMELG-PCM-$L_{\min}$ method at ROHF/6-31G level. (Modified with permission from Ref. [26]. Copyright 2016 Elsevier B.V.)

radicals, such as model R, in a solvent can be predicted by the simple L_{min} values calculated using the MMELG-PCM-L_{min} method. The MMELG method suggests that the electronic states for open-shell systems thus obtained can be a reliable starting point to proceed further to more precise calculations at post-HF levels of theory.

5.3.4 *Application of the Minimized Mixing Elongation Method to a Dendrimer Model*

To investigate the accuracy of the unrestricted ELG method for high-spin systems, we performed test calculations at the UHF/6-31G(d) and UB3LYP/6-31G(d) levels of theory on the two-dimensional dendrimer model shown in Fig. 5.8. For simplicity, only one ELG step is shown. In the first step, the eigenvalue problem is solved for the (A + B) part and in the second step, the frozen part is defined as A, third step, M is attacked one by one in three directions at a time. The parameters in the calculations were $N_{st} = 5$ (the number of starting cluster units), $N_B = 4$ (the number of units of region B), $N_M = 1$ (the number of monomer units), and $N_{se} = 30, 36, \ldots, 78$ (the number of unpaired electrons of the system at each ELG step). Figure 5.9 shows that ΔE/atom is very small ($\approx 10^{-9}$ a.u.) in the ELG process under all three theoretical conditions. Such a small difference suggests that the unrestricted ELG method is highly accurate and efficient and is therefore also suitable for dendrimer radical systems, which are known to exhibit large Non-Linear Optical (NLO) properties, at the HF and DFT levels and also under PCM conditions. More details on the methodology and its applications are described in the articles [26–28].

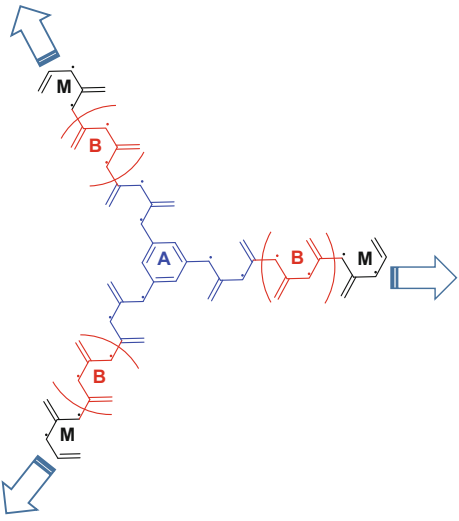

Fig. 5.8 Simple model for open-shell dendrimer. *A*, *B*, and *M* denote frozen region, active region, and monomer, respectively. (Modified with permission from Ref. [27]. Copyright 2016 Walter de Gruyter GmbH)

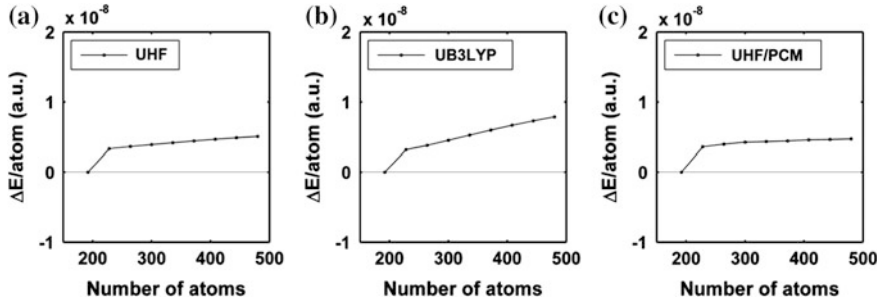

Fig. 5.9 ΔE/atom for calculations on model dendrimer shown in Fig. 5.8 using unrestricted ELG method at **a** UHF/6-31G(d), **b** UB3LYP/6-31G(d), and **c** UHF/6-31G(d) under PCM levels of theory. ELG method was performed with $N_{st} = 5$, $N_B = 4$, $N_M = 1$, and $N_{se} = 30, 36, \ldots, 78$ for all calculations. (Reproduced with permission from Ref. [27]. Copyright 2016 Walter de Gruyter GmbH)

References

1. Takahashi, M., Tsuchida, E., Nishide, H., Yamada, S., Matsuda, H., Nakanishi, H.: Optical nonlinearity of an open-shell and degenerate π-conjugated polymer: poly (4-oxyphenyl-1, 2-phenylenevinylene) radical. Chem. Commun. 1853–1854 (1997)
2. Nishide, H., Ozawa, T., Miyasaka, M., Tsuchida, E.: A nanometer-sized high-spin polyradical: Poly (4-phenoxyl-1, 2-phenylenevinylene) planarily extended in a non-Kekulé fashion and its magnetic force microscopic images. J. Am. Chem. Soc. **123**, 5942–5946 (2001)
3. Kaneko, T., Makino, T., Miyaji, H., Teraguchi, M., Aoki, T., Miyasaka, M., Nishide, H.: Ladderlike ferromagnetic spin coupling network on a π-conjugated pendant polyradical. J. Am. Chem. Soc. **125**, 3554–3557 (2003)
4. Nishide, H., Iwasa, S., Pu, Y.-J., Suga, T., Nakahara, K., Satoh, M.: Organic radical battery: nitroxide polymers as a cathode-active material. Electrochim. Acta **50**, 827–831 (2004)
5. Rajca, A., Wongsriratanakul, J., Rajca, S.: Organic spin clusters: Ferromagnetic spin coupling through a biphenyl unit in polyarylmethyl tri-, penta-, hepta-, and hexadecaradicals. J. Am. Chem. Soc. **119**, 11674–11686 (1997)
6. Rajca, A., Lu, K., Rajca, S.: High-spin polyarylmethyl polyradical: Fragment of a macrocyclic 2-strand based upon calix [4] arene rings. J. Am. Chem. Soc. **119**, 10335–10345 (1997)
7. Rajca, A., Wongsriratanakul, J., Rajca, S., Cerny, R.: A dendritic macrocyclic organic polyradical with a very high spin of *S*=10. Angew. Chem. Int. Ed. **37**, 1229–1232 (1998)
8. Rajca, A., Wongsriratanakul, J., Rajca, S.: Magnetic ordering in an organic polymer. Science **294**, 1503–1505 (2001)
9. Imamura, A., Aoki, Y., Maekawa, K.: A theoretical synthesis of polymers by using uniform localization of molecular orbitals: proposal of an elongation method. J. Chem. Phys. **95**, 5419–5431 (1991)
10. Aoki, Y., Imamura, A.: Local density of states of aperiodic polymers using the localized orbitals from an *ab initio* elongation method. J. Chem. Phys. **97**, 8432–8440 (1992)
11. Gu, F.L., Aoki, Y., Korchowiec, J., Imamura, A., Kirtman, B.: A new localization scheme for the elongation method. J. Chem. Phys. **121**, 10385–10391 (2004)
12. Korchowiec, J., Gu, F.L., Aoki, Y.: Elongation method at restricted open-shell Hartree-Fock level of theory. Int. J. Quant. Chem. **105**, 875–882 (2005)

13. Korchowiec, J., Gu, F.L., Imamura, A., Kirtman, B., Aoki, Y.: Elongation method with cutoff technique for linear SCF scaling. Int. J. Quant. Chem. **102**, 785–794 (2005)
14. Korchowiec, J., Lewandowski, J., Makowski, M., Gu, F.L., Aoki, Y.: Elongation cutoff technique armed with quantum fast multipole method for linear scaling. J. Comput. Chem. **30**, 2515–2525 (2009)
15. Makowski, M., Korchowiec, J., Gu, F.L., Aoki, Y.: Describing electron correlation effects in the framework of the elongation method–elongation-MP2: formalism, implementation and efficiency. J. Comput. Chem. **31**, 1733–1740 (2010)
16. Aoki, Y., Gu, F.L.: An elongation method for large systems toward bio-systems. Phys. Chem. Chem. Phys. **14**, 7640–7668 (2012)
17. Liu, K., Inerbaev, T., Korchowiec, J., Gu, F.L., Aoki, Y.: Geometry optimization for large systems by the elongation method. Theor. Chem. Acc. **131**, 1277 (2012)
18. Liu, K., Korchowiec, J., Aoki, Y.: Intermediate electrostatic field for the generalized elongation method. ChemPhysChem **16**, 1551–1556 (2015)
19. Orimoto, Y., Yamamoto, R., Xie, P., Liu, K., Imamura, A., Aoki, Y.: *Ab initio O*(N) elongation-counterpoise method for BSSE-corrected interaction energy analyses in biosystems. J. Chem. Phys. **142**, 104111 (2015)
20. Liu, K., Peng, L., Gu, F.L., Aoki, Y.: Three dimensional elongation method for large molecular calculations. Chem. Phys. Lett. **560**, 66–70 (2013)
21. Liu, K., Yan, Y.-A., Gu, F.L., Aoki, Y.: A modified localization scheme for the three-dimensional elongation method applied to large systems. Chem. Phys. Lett. **565**, 143–147 (2013)
22. Cancès, E., Mennucci, B., Tomasi, J.: A new integral equation formalism for the polarizable continuum model: theoretical background and applications to isotropic and anisotropic dielectrics. J. Chem. Phys. **107**, 3032 (1997)
23. Zhu, X., Aoki, Y.: Development of minimized mixing molecular orbital method for designing organic ferromagnets. J. Comput. Chem. **36**, 1232–1239 (2015)
24. Schmidt, M.W., Baldridge, K.K., Boatz, J.A., Elbert, S.T., Gordon, M.S., Jensen, J.H., Koseki, S., Matsunaga, N., Nguyen, K.A., Su, S., Windus, T.L., Dupuis, M., Montgomery Jr., J.A.: General atomic and molecular electronic structure system. J. Comput. Chem. **14**, 1347–1363 (1993)
25. Edmiston, C., Ruedenberg, K.: Localized atomic and molecular orbitals. Rev. Mod. Phys. **35**, 457–464 (1963)
26. Zhu, X., Aoki, Y.: Efficient prediction of high spin ground state stability in organic polyradicals under solvent effects. Chem. Phys. Lett. **637**, 143–147 (2015)
27. Zhu, X., Orimoto, Y., Aoki, Y.: An efficient unrestricted PCM-Elongation method for large high-spin polymer/dendrimer systems. Z. Phys. Chem. **230**, 667–680 (2016)
28. Zhu, X.: Development of efficient quantum chemical methods for designing organic ferromagnets. Doctoral thesis, Kyushu University (2015)

Chapter 6
Conclusions and Future Prospects

There are many functional materials of interest that are too huge to be studied by means of quantum chemistry approach. Magnetism is one of these areas, and there is significant interest in the development of functional materials based on novel ferro- or ferrimagnets with high Curie temperatures and the improving the quality and synthetic costs of existing magnets. For the last three decades there have been intense efforts aimed at the discovery of intriguing alternatives to conventional magnets, and thus organic ferromagnets have been a target for their many advantages in a wide range of applications.

Magnetism is based on the interaction between electron spins and can only be properly described by taking into account electron–electron interactions. In many cases though, the systems that display magnetism are huge. Therefore, a direct treatment of total systems that accounts for exact electron–electron interaction is almost impossible; thus, to avoid heavy computations, a simple treatment to evaluate even the qualitative possibility of magnetism was desired. One way to gain an insight into whether a conjugated organic system possesses a stable high-spin state would be to understand the concept of a "disjoint or non-disjoint" system, which is easily inferred from the molecular structure. Therefore, as the first step in the development of a method that makes it possible to predict the magnetic property of a material, we elucidated the "disjoint or non-disjoint" concept using matrix algebra from a mathematical point of view and then constituted several analytical methods to gain an insight into the multiplicity of the system. The reason that even organic compounds can display magnetic properties, however, is still not definitive from a microscopic point of view, and thus not only Hund's rule but also a theoretical investigation that can elucidate the spin multiplicity is required. For this purpose, we have introduced the TS/TB method to analyze the relationship between the orbital interactions and the effect of the inter-radical exchange interaction on the total energy of a system with various multiplicities, which leads to the systematic elucidation of high-spin stability.

In contrast, highly accurate ab initio methods for open-shell systems have been developing in the field of quantum chemistry to better understand the magnitudes of

Y. Aoki et al., *Quantum Chemical Approach for Organic Ferromagnetic Material Design*,
SpringerBriefs in Electrical and Magnetic Properties of Atoms, Molecules, and Clusters,
DOI 10.1007/978-3-319-49829-4_6

exchange integrals, which are very important values in the discussion of molecular spin states. However, the systems for which one can examine the effectiveness of these integrals are still limited to a few molecules (units) unless the periodic boundary condition is imposed. In fact, the magnetic properties of materials are mostly discussed using the Ising model, for which highly accurate computations for the entire system are not needed, although the results obtained strongly depend on the parameters used in the calculations. To overcome the problem that direct ab initio calculations are intractable for large systems, we developed the ELG method at both the HF and post-HF levels. This method is applicable for use in the open-shell electronic state calculations of large random systems for which a periodic boundary condition is not applied. In that regard, more efficient localization treatment of MOs into a specific region where a radical exists should be effective when one focuses on the magnetic properties that come from the presence of degenerate NBMOs. In order to realize cheaper computations, therefore, the MMMO localization scheme is applied to the open-shell part while the ELG method is performed; this approach was also proposed and its application to the prediction of high-spin stability have proved successful for quasi-1D systems at the HF level. The extension to three-dimensional systems is already feasible for closed-shell systems (3D-ELG method) and is under construction for open-shell systems. Geometry optimization using the elongation method is also possible for pseudo-one-dimensional systems and represents a much more efficient style than the use of conventional optimization methods based on canonical MOs; this method is still under construction in our laboratory for three-dimensional systems.

Recently, more sophisticated and highly accurate approaches for open-shell systems have been developed in quantum chemistry with a view towards the theoretical investigation of functional materials like spin-electronics devices, battery materials, optical spin manipulation, and so on. Theoretical approaches both in quantum chemistry and solid state physics, in connection with computer science using parallel supercomputers, will become more and more important because a deeper understanding of the mechanism of spin-related phenomena from a theoretical point of view would help experimental design of novel magnetic materials in the future.